INSTABILITY THRESHOLDS AND DYNAMICS OF MESA PATTERNS IN REACTION-DIFFUSION SYSTEMS

by

Rebecca Charlotte McKay

Submitted in partial fulfilment of the requirements
for the degree of Doctor of Philosophy

at

Dalhousie University
Halifax, Nova Scotia
August 2011

DALHOUSIE UNIVERSITY

DEPARTMENT OF MATHEMATICS AND STATISTICS

The undersigned hereby certify that they have read and recommend to the Faculty of Graduate Studies for acceptance a thesis entitled "INSTABILITY THRESHOLDS AND DYNAMICS OF MESA PATTERNS IN REACTION-DIFFUSION SYSTEMS" by Rebecca Charlotte McKay in partial fulfilment of the requirements for the degree of Doctor of Philosophy.

Dated: August 19, 2011

External Examiner: _____

Research Supervisor: _____

Examining Committee: _____

_____

Departmental Representative: _____

DALHOUSIE UNIVERSITY

DATE: August 19, 2011

AUTHOR: Rebecca Charlotte McKay

TITLE: Instability Thresholds and Dynamics of Mesa Patterns in Reaction-Diffusion Systems

DEPARTMENT OR SCHOOL: Department of Mathematics and Statistics

DEGREE: PhD CONVOCATION: October YEAR: 2011

Signature of Author

To Neil, whose love and support made this possible

Table of Contents

List of Figures

Abstract

We consider reaction-diffusion systems of two variables with Neumann boundary conditions on a finite interval with diffusion rates of different orders. Solutions of these systems can exhibit a variety of patterns and behaviours; one common type is called a mesa pattern; these are solutions that in the spatial domain exhibit highly localized interfaces connected by almost constant regions. The main focus of this thesis is to examine three different mechanisms by which the mesa patterns become unstable. These patterns can become unstable due to the effect of the heterogeneity of the domain, through an oscillatory instability, or through a coarsening effect from the exponentially small interaction with the boundary. We compute instability thresholds such that, as the larger diffusion coefficient is increased past this threshold, the mesa pattern transitions from stable to unstable. As well, the dynamics of the interfaces making up these mesa patterns are determined. This allows us to describe the mechanism leading up to the instabilities as well as what occurs past the instability threshold. For the oscillatory solutions, we determine the amplitude of the oscillations. For the coarsening behaviour, we determine the motion of the interfaces away from the steady state. These calculations are accomplished by using the methods of formal asymptotics and are verified by comparison with numerical computations. Excellent agreement between the asymptotic and the numerical results is found.

List of Abbreviations and Symbols Used

CIMA ..... Chlorite-Iodide-Malonic Acid-starch reaction

BZ ..... Belousov-Zhabotinskii reaction

ODE ..... ordinary differential equation

PDE ..... partial differential equation

Δ ..... Laplacian operator

$\delta(x - x_0)$ ..... Dirac delta function

$\sim$ ..... to leading order

$\gg$, $\ll$ ..... much greater than, much less than

$\approx$ ..... approximately

D ..... diffusion coefficient, $D >> 1$

ε ..... diffusion coefficient, $\varepsilon << 1$

$\mathcal{O}(x)$ ..... order of x

u_x, $u'(x)$, $\frac{du}{dx}$ ..... u differentiated with respect to x

u_{xx} ..... the second derivative of u with respect to x

$\frac{\partial}{\partial n}$ ..... the normal derivative

λ ..... eigenvalue

ψ, ϕ ..... eigenfunctions

∞ ..... infinity

Acknowledgements

I thank my supervisor, Theodore Kolokolnikov, for lending his expertise and for help in completing this thesis. I also thank David Iron, Paul Muir and Thomas Witelski for reading this thesis as well as providing valuable input and thoughtful suggestions.

Chapter 1

Introduction

The study of patterns that form as solutions of reaction-diffusion equations began with Turing's 1952 paper [77] on morphogenesis. Turing showed that for a reaction of two substances with different diffusivities a homogeneous steady state could become unstable and form spatially inhomogeneous patterns. Many years later, these patterns were observed experimentally [64, 63, 4]. Turing's methods are limited to patterns that are close to the homogeneous steady state, but these reaction-diffusion models can also exhibit patterns that are far from the homogeneous steady state. Pearson and others [65, 41] showed, through numerical simulations, that reaction-diffusion models could exhibit many complex spatially localized patterns. Examples of types of patterns are spikes, fronts, stripes, spots, wriggled stripes and labyrinthine patterns [8, 53, 52].

In this thesis, we consider a general class of reaction-diffusion systems

$$\begin{cases} u_t = \varepsilon^2 u_{xx} + f(u,w) \\ \tau w_t = D w_{xx} + g(u,w) \end{cases} \tag{1.1}$$

with Neumann boundary conditions on a bounded interval where ε and D are the diffusion coefficients and τ is a non-negative constant. Let the initial conditions be given by

$$u(x,0) = u_I(x), \quad w(x,0) = w_I(x).$$

Reaction-diffusion systems of the general form (1.1) have been used to model many diverse phenomena. Some examples are:

- Model of the Belousov-Zhabotinskii (BZ) reaction in a water-in-oil microemulsion system [29, 80, 35, 28]. A simplified version of this model is

$$\begin{cases} u_t = \varepsilon^2 u_{xx} - f_0 \dfrac{u-q}{u+q} + wu - u^2 \\ \tau w_t = D w_{xx} + 1 - uw \end{cases}, \tag{1.2}$$

  where f_0 and q are problem dependent constants.

- Model of the Chlorite-Iodide-Malonic Acid-starch (CIMA) reaction [43, 56]. This model, also known as the Lengyel-Epstein model, can be written as

$$\begin{cases} u_t = \varepsilon^2 u_{xx} + a - u - \dfrac{4uw}{1+u^2} \\ \\ \tau w_t = D w_{xx} + u - \dfrac{uw}{1+u^2} \end{cases}, \tag{1.3}$$

  where a is a constant.

- The Brusselator model (a model of an autocatalytic reaction) [67, 34, 37]. After a change of variables the Brusselator may written as

$$\begin{cases} u_t = \varepsilon^2 u_{xx} - u + uw - u^3 \\ \tau w_t = D w_{xx} - \beta_0 u + 1 \end{cases}, \tag{1.4}$$

  where β_0 is a constant.

- The Gierer-Meinhardt model with saturation (a model of stripe patterns on animal hides) [46, 47, 32, 38]. After some rescaling, the model is

$$\begin{cases} u_t = \varepsilon^2 u_{xx} - u + \dfrac{u^2}{w(1+\kappa u^2)} \\ \tau w_t = D w_{xx} - w + u^2 \end{cases}, \tag{1.5}$$

  where κ is a constant.

In addition to modeling chemical reactions and animal stripe patterns, reaction-diffusion systems can model gas discharge dynamics [19, 79], population dynamics [1, 66], vegetation in arid regions [48], coexistence of competing species [49], chemotaxis [23] and phase separation in diblock copolymers [7].

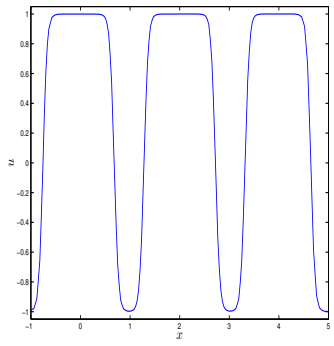

Figure 1.1: A 3-mesa pattern solution

The two dimensional analogue to (1.1) is

$$\begin{cases} u_t = \varepsilon^2 \Delta u + f(u,w) \\ \tau w_t = D\Delta w + g(u,w) \end{cases}. \tag{1.6}$$

The two-dimensional versions of each of the models above have been studied as well; see [28, 80, 29, 56, 36, 38] and references therein. Such a system has also been used to model spreading depressions in the brain which play a major role in strokes [5]. For thin domains (that is, where the length of the domain is much greater than its width), the system (1.6) can be approximated by a one dimensional system with heterogenous diffusion,

$$\begin{cases} u_t = \frac{\varepsilon^2}{h(x)}[h(x)u_x]_x + f(u,w) \\ \tau w_t = \frac{D}{h(x)}[h(x)w_x]_x + g(u,w) \end{cases}, \tag{1.7}$$

where $h(x)$ is a positive function corresponding to the domain height. This reduction is known as an lubrication theory approximation on a slender geometry, see for example [24, 76]. This will be considered in Chapter 3.

A common phenomenon observed in reaction-diffusion systems is the formation of *mesa patterns*. These patterns consist of a sequence of highly localized interfaces that connect regions where the solution is nearly constant. Such a solution can be seen in Figure 1.1. In the limits

$$\varepsilon \ll 1 \quad \text{and} \quad D \gg 1, \tag{1.8}$$

and under some general conditions on the functions f and g (that will be specified in Chapter 2), the system (1.1) admits a solution for u that has the property that u

is either u_+ or u_- for some constants $u_+ \neq u_-$ everywhere except near the interface location, where it has a layer of $\mathcal{O}(\varepsilon)$ connecting the two constant states u_+ and u_-. A single mesa solution consists of two interfaces or fronts, one connecting u_- to u_+ and another connecting u_+ back to u_-. By mirror reflection a single mesa can be extended to a symmetric K mesa solution consisting of $2K$ interfaces. Figure 1.1 has $u_- \approx -1$ and $u_+ \approx 1$ with $K = 3$. These types of solutions have been extensively studied. See, for example, [10, 17, 75, 30, 54, 53, 31, 60, 59, 70, 57] and works cited there.

Patterns of reaction-diffusion systems can exhibit many different types of behaviour. The formations can coarsen as seen in Figure 1.2(a) and as seen in [34]. These patterns can also self-replicate. This is observed experimentally in the self-replication of spots in an experiment involving ferrocyanide-iodide-sulfite [42] or in the splitting of fronts in the BZ reaction [50]. Analytically, this is seen in the self-replication of spots in the Gray-Scott model [69] or of mesas in the one-dimensional Brusselator [37]. The patterns can oscillate, as seen experimentally in [21] or as analyzed in [20] or [34]. Also, these patterns can exhibit spatio-temporal chaos [61]. In this thesis, we examine, in the regime where $D \gg 1$, some of the mechanisms by which mesa patterns can become unstable: through a oscillatory instability, through coarsening or due to domain heterogeneity, in the case of a thin domain.

1.1 Background

The general system (1.1) has been well studied. It is known that there exists a D_c of $\mathcal{O}(1)$, such that for $D > D_c$, under certain conditions on f and g, a K mesa pattern is stable for all K [59, 37]. As $D \to \infty$, the system (1.1) with $\tau = 0$ and $x \in [a, b]$ reduces to

$$\begin{cases} u_t = \varepsilon^2 u_{xx} + f(u, w_0) \\ \int_a^b g(u, w_0) dx = 0 \end{cases}, \tag{1.9}$$

where w_0 is a constant. This is called the *shadow system*. Equation (1.9) also includes many models of phase separation such as the Allen-Cahn equation [70] as a special case. Under the same general conditions on f and g, a single interface of the shadow system is also stable; however, a pattern consisting of more than one interface is known to be unstable [55]. Similar type of analysis has been done for a K-spike

pattern (see for example [40]).

In [73], the authors study internal layer solutions of the generalized Ginzburg-Landau equation, which models the slow propagation of an internal layer in a thin channel

$$u_t = \frac{\varepsilon^2}{A}[Au_x]_x + Q(u) \tag{1.10}$$

where $A = A(x;\varepsilon)$ is the cross-sectional area of the channel. Here the function A is perturbed from the uniform value $A \equiv 1$ by an exponentially small term depending on ε. This equation is similar to the equations in the system (1.7). In [27], the authors consider a spike solution of the shadow Gierer-Meinhardt model (that is, $D \to \infty$) where a weak spatially inhomogeneous diffusivity has been added,

$$\begin{cases} u_t = \frac{\varepsilon^2}{\kappa}[\kappa u_x]_x - u + \frac{u^p}{w^q} \\ \\ w = \left(\frac{\varepsilon^{-1}}{2\mu}\int_{-1}^{1} u^r dx\right)^{1/(s+1)} \end{cases}, \tag{1.11}$$

where $\mu > 0$, the exponents r, s, p, q are assumed to satisfy

$$p > 1,\ q > 0,\ r > 0,\ s \geq 0,\ 0 < \frac{p-1}{q} < \frac{r}{s+1},$$

and where κ is a function of x close to 1. A one spike solution which would be unstable when κ is 1 can become stable for non-constant κ.

Patterns of reaction-diffusion systems can exhibit oscillatory or *breather* type behaviour, such as shown in Figure 1.2(b). Koga and Kuramoto first suggested that a pattern in a reaction-diffusion system could destabilize and oscillate [33]. Since then oscillatory behaviour has been examined in many other reaction-diffusion systems in one and higher dimensions, see for example [6, 15, 19, 79, 20, 21, 26, 25, 74, 84, 22]. The onset of the oscillations for the system (1.1) is well understood in terms of a Hopf bifurcation, see for example [33, 60]. The Hopf bifurcation occurs when τ is increased beyond a critical threshold τ_h. For τ only slightly beyond τ_h, weakly nonlinear analysis is possible [19, 20, 79, 60]. In [20], the Hopf bifurcation structure was determined for a system of the form (1.1). In [79], for a specific three-component gas discharge model, the oscillatory behaviour of fronts was observed from numerical simulations, and, in [11], the authors determined analytically that the Hopf bifurcation leading to this behaviour can either be subcritical (unstable limit cycle) or supercritical (stable limit cycle) depending on the choice of parameter. In [19], the normal form of

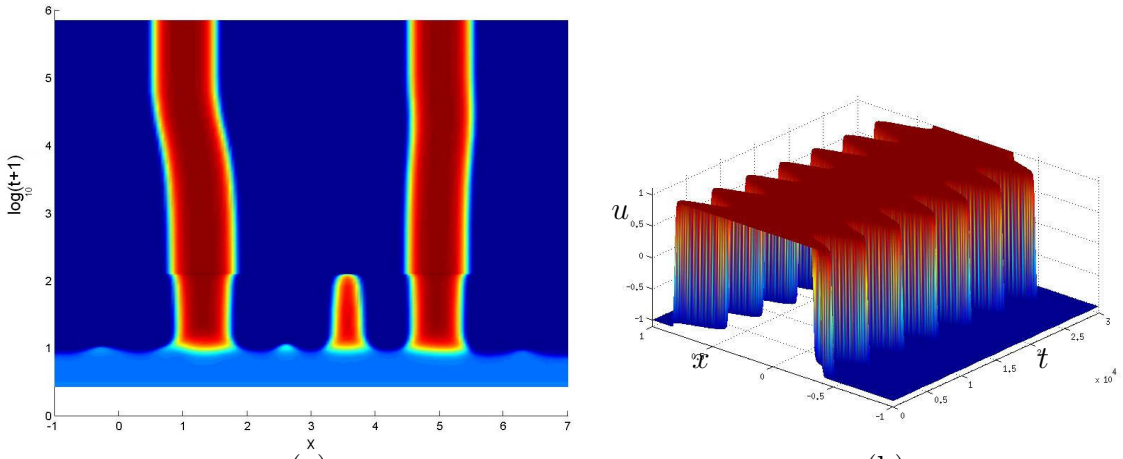

(a) (b)

Figure 1.2: (a) Coarsening process in Lengyel-Epstein model (1.3) (b) An example of an oscillating single mesa pattern

a general reaction-diffusion system for oscillations close to the Hopf bifurcation was determined. However, the constants in this normal form are not easily determined analytically. In [6], the oscillation of spikes in the Gray-Scott model was analyzed. The authors derived a reduced ODE-PDE Stefan problem with a moving source. They rederived the Hopf bifurcation thresholds. Away from the Hopf bifurcation, they solved the Stefan problem numerically.

1.2 Overview of Thesis

The main focus of this thesis is to examine the mechanisms that lead to mesa patterns becoming unstable. In Chapter 2, we consider the system (1.1) with $\tau = 0$. We examine how a K mesa pattern transitions from the stable regime where D is of $\mathcal{O}(1)$ to the unstable regime where $D \to \infty$. For $D = \mathcal{O}(1)$, the stability of the K mesa pattern of u comes from the stabilizing effect of the variable w [59]. As D is increased, this effect is decreased and the pattern eventually becomes unstable. This instability is caused by the exponentially small interaction between the interfaces of the K mesa pattern of u, as D becomes exponentially large. We first construct the steady state consisting of K mesas of the system (1.1). We analyze the eigenvalues of the linearized problem and compute the instability threshold D_K such that a K mesa solution on a fixed domain size is stable if $D < D_K$ and is unstable if $D > D_K$.

The instability thresholds have an ordering

$$D_K : D_1 > D_2 > \ldots > D_K.$$

In addition to considering the stability of the mesa patterns, we also study their dynamics. For a K mesa pattern, we derive $2K$ ODEs that govern the motion of the $2K$ interfaces. These asymptotic results are compared with numerical simulations of specific examples. We apply our results to the Belousov-Zhabotinskii model (1.2) and to a cubic model

$$\begin{cases} u_t = \varepsilon^2 u_{xx} + 2u - 2u^3 + w \\ \tau w_t = D w_{xx} - u + \beta \end{cases}, \tag{1.12}$$

which is a variation on a FitzHugh-Nagumo model used in [17, 52]. This cubic model is one of the simplest systems of the form (1.1) making it a convenient model for assessing our asymptotic results. It is found that the asymptotic results agree closely with the numerical simulations. Note that all the results also generalize to the case where τ is small, $0 < \tau \ll \frac{1}{\varepsilon}$. The results of Chapter 2 can be found in [44].

In Chapter 3, we examine how a K mesa pattern of (1.6) on a thin domain becomes unstable by considering the equivalent one dimensional problem (1.7), for the case where $\tau = 0$. Here the instability comes from effects of the heterogenous domain. We first show how we reduce (1.6) to the one dimensional problem (1.7) in the case of a thin domain. Then, for $\tau = 0$, as was done in Chapter 2, we determine the eigenvalues of the linearized problem and thresholds for the stability of the mesa patterns. These thresholds depend on the function $h(x)$. Again, the results also hold for sufficiently small τ. We use the cubic model (1.12) to verify our asymptotic results against numerical simulations.

In Chapter 4, we examine how a mesa pattern of (1.1) can become unstable as we increase τ, where τ is shown to be of $\mathcal{O}(\frac{D}{\varepsilon})$. Previously, as in [60, 11, 79], this has been done by determining the Hopf bifurcation through spectral analysis. Here, by assuming D is large, we can study the dynamics of the interfaces even far away from the Hopf bifurcation. We begin by considering a single interface, or half-mesa pattern. Similar to what was done in [6], we start by obtaining a reduced ODE-PDE system for the motion of the interfaces. However, since we have assumed that D is large, we can further approximate this reduced system by a weakly-forced harmonic oscillator. Performing a multiple scales analysis, an equation for the amplitude of oscillations

of the interface is obtained. From this amplitude equation, we determine the critical value of τ at which the Hopf bifurcation occurs. Similarly, for one mesa, that is, two interfaces, we determine an equation for the amplitude. We use the cubic model (1.12) to verify our asymptotic results against numerical simulations. The results of Chapter 4 can be found in [45]. We finish in Chapter 5, with our conclusions and suggestions for future work.

Chapter 2

Instability Thresholds and Dynamics of Mesa Patterns

In this chapter, we consider mesa pattern solutions of the system (1.1) with $\tau = 0$

$$\begin{cases} u_t = \varepsilon^2 u_{xx} + f(u,w) \\ 0 = Dw_{xx} + g(u,w) \end{cases}, \tag{2.1}$$

with Neumann boundary conditions. In previous work, a K mesa pattern for D sufficiently large, but of $\mathcal{O}(1)$, has been shown to be stable [59, 37]. For the corresponding shadow system (1.9), a K mesa pattern is unstable for any K [55]. We examine how a K mesa pattern transitions from the stable regime where D is of $\mathcal{O}(1)$ to the unstable regime where $D \to \infty$. This instability is caused by the exponentially small interactions between the interfaces of the K mesa solution of u as D becomes large. Resolving these exponentially small terms is essential to determining how the transition to instability occurs and is the main result of this chapter, given in Principal Result 2.2.1.

Linearizing around the steady state, constructed in Proposition 2.1.1, we obtain an eigenvalue problem with Neumann boundary conditions. To determine these eigenvalues, we start by considering the eigenvalue problem with periodic boundary conditions and then extend the result to the Neumann boundary problem. From these eigenvalues, we determine the stability of the mesa patterns. There exist exponentially large instability thresholds D_K: $D_1 > D_2 > \ldots > D_K$, such that a K mesa solution on a fixed domain size is stable if $D < D_K$ and is unstable if $D > D_K$. We also derive a system of $2K$ ODEs to describe the motion of the interfaces. These results

are verified by comparing the results of numerical computations with the asymptotic results. We begin with the construction of the steady steady state solution having a K mesa pattern.

2.1 Preliminaries: Construction of the $K-$Mesa Steady State

We start by constructing the steady state mesa-type solution to (2.1). The mesa (or box) solution consists of two back-to-back interfaces. Thus we first consider the conditions for existence of a single interface solution and review its construction. A solution with a mesa pattern can then be constructed from a single interface by reflecting and doubling the domain size. Similarly, a K-mesa pattern is then constructed by making K copies of a single mesa. We summarize the construction as follows.

Proposition 2.1.1. *Consider the steady state of the PDE system (2.1) satisfying*

$$\begin{cases} 0 = \varepsilon^2 u_{xx} + f(u,w) \\ 0 = Dw_{xx} + g(u,w) \end{cases} \tag{2.2}$$

with Neumann boundary conditions and in the limit where

$$\varepsilon \ll 1 \quad \textit{and } D \gg 1. \tag{2.3}$$

Suppose that u_+, u_-, w_0 are constants that satisfy

$$\int_{u_-}^{u_+} f(u,w_0)du = 0; \quad f(u_+,w_0) = 0 = f(u_-,w_0), \tag{2.4}$$

with $u_+ \neq u_-$.

Define

$$g_\pm := g\left(u_\pm, w_0\right) \tag{2.5}$$

and suppose in addition that

$$f_u\left(u_\pm, w_0\right) \leq 0; \quad \textit{and} \quad 0 < \frac{g_-}{g_- - g_+} < 1. \tag{2.6}$$

Then a single interface solution, on the interval $[0,L]$ is given by

$$u(x) \sim U_0\left(\frac{x-l}{\varepsilon}\right), \qquad w \sim w_0$$

where U_0 is the heteroclinic connection between u_+ and u_- satisfying

$$\begin{cases} U_{0yy} + f(U_0, w_0) = 0; \\ U_0 \to u_- \text{ as } y \to \infty; \quad U_0 \to u_+ \text{ as } y \to -\infty; \\ f(U_0(0), w_0) = 0 \end{cases} \tag{2.7}$$

and l is the location of the interface so that

$$u \sim \begin{cases} u_+, & 0 < x < l \\ u_-, & l < x < L \end{cases}.$$

Moreover, l satisfies

$$l = l_0 + \varepsilon l_1 + O(\varepsilon^2) \tag{2.8}$$

where

$$l_0 = \frac{g_-}{g_- - g_+} L \tag{2.9}$$

and

$$l_1 = \frac{\int_0^\infty [g(U_0(y), w_0) - g_-]\, dy + \int_{-\infty}^0 [g(U_0(y), w_0) - g_+]\, dy}{g_- - g_+} \tag{2.10}$$

A single mesa solution on the interval $[-L, L]$ is obtained by even reflection of the interface solution on an interval $[0, L]$ around $x = 0$. A K-mesa solution on the interval $[-L, (2K-1)L]$ is then obtained making K copies of the single mesa solution on the interval $[-L, L]$.

The construction of this solution is standard (see for example [37, 58]), but we review the details here. First, consider a single interface located at $x = l$ inside the domain $[0, L]$. We assume that $u \sim u_+$ for $0 < x < l$ and $u \sim u_-$ for $l < x < L$ where $u_\pm$ are constants to be determined. Since we assumed that $D \gg 1$, we expand

$$w = w_0 + \frac{1}{D} w_1 + \cdots$$

so that to leading order $w \sim w_0$ is constant. Near the interface we introduce inner variables

$$x = l + \varepsilon y; \; u(x) \sim U_0\left(\frac{x - l}{\varepsilon}\right), \quad w \sim w_0. \tag{2.11}$$

Then $U_0(y)$ satisfies the system (2.7). Note that the last equation of this system is to define the arbitrary constant of integration. In order for such a solution to exist, $u_\pm$ must both be roots of $f(u, w_0)$ and U_0 must be a heteroclinic orbit connecting

u_+ and u_-. This yields the three algebraic constraints (2.4) which determine $u_\pm$ and w_0. To determine the location l of the interface, we integrate the second equation in (2.2), and using Neumann boundary conditions we obtain

$$\int_0^L g(u, w_0)dx = 0. \tag{2.12}$$

Changing variables $x = l + \varepsilon y$ we estimate the above condition by

$$0 \sim \varepsilon \int_{-l/\varepsilon}^0 g(U_0(y), w_0)dy + \varepsilon \int_0^{(L-l)/\varepsilon} g(U_0(y), w_0)dy;$$
$$0 \sim lg_+ + \varepsilon \int_{-\infty}^0 \left[g(U_0(y), w_0) - g_+\right] dy + (L-l)g_- + \varepsilon \int_0^\infty \left[g(U_0(y), w_0) - g_-\right] dy$$

Expanding l in ε as in (2.8) then yields (2.9) and (2.10). Since we must have $0 < l < L$, this yields an additional constraint, the second equation of (2.6). The first conditions will be necessary below.

2.2 Stability of $K-$Mesa Pattern

Now we consider the stability of a K mesa pattern. We begin by stating the main result

Principal Result 2.2.1. *Consider the steady state consisting of K mesas on the interval $[-L, (2K-1)L]$, with Neumann boundary conditions, as constructed in Proposition 2.1.1. Suppose that*

$$g_w - g_u \frac{f_w}{f_u} < 0 \text{ for all } x, \quad \text{and } \frac{\int_{u_-}^{u_+} f_w du}{g_- - g_+} > 0. \tag{2.13}$$

Let

$$\alpha_+ := \frac{2C_+^2\mu_+^3}{\int_{u_-}^{u_+} f_w du}\frac{1}{\varepsilon}\exp\left(-\frac{2\mu_+}{\varepsilon}l\right); \quad \alpha_- := \frac{2C_-^2\mu_-^3}{\int_{u_-}^{u_+} f_w du}\frac{1}{\varepsilon}\exp\left(-\frac{2\mu_-}{\varepsilon}(L-l)\right) \tag{2.14}$$

where l is defined as in Proposition 2.1.1 and where we also define

$$\mu_\pm := \sqrt{-f_u\left(u_\pm, w_0\right)} \geq 0, \tag{2.15}$$

and define constants $C_\pm$ to be such that

$$\begin{aligned} U_0(y) &\sim u_- + C_- e^{-\mu_- y}, \quad y \to +\infty, \\ U_0(y) &\sim u_+ - C_+ e^{\mu_+ y}, \quad y \to -\infty. \end{aligned} \tag{2.16}$$

Define

$$D_1 \equiv \frac{Lg_-^2}{2\left(g_- - g_+\right)\alpha_-}, \tag{2.17}$$

and for $K \geq 2$, *define*

$$D_K \equiv \begin{cases} \frac{Lg_-^2}{2(g_- - g_+)\alpha_-} & \text{if} \quad \alpha_+ \ll \alpha_- \\ \\ \frac{Lg_+^2}{2(g_- - g_+)\alpha_+} & \text{if} \quad \alpha_- \ll \alpha_+ \\ \\ \frac{L}{2(g_- - g_+)\left(g_+^{-2}\alpha_+ + g_-^{-2}\alpha_-\right)} \left(\frac{1}{2} + \sqrt{\frac{1}{4} - \frac{2\alpha_+\alpha_-(1-\cos\pi/K)g_+^2 g_-^2}{4\left(g_-^2\alpha_+ + g_+^2\alpha_-\right)^2}}\right)^{-1} & \text{if } O(\alpha_+) = O(\alpha_-) \end{cases} \tag{2.18}$$

then the K *mesa pattern is a stable steady state of the time-dependent system (2.1) if* $D < D_K$, *and is unstable if* $D > D_K$.

Principal Result 2.2.1 follows from examining the eigenvalue problem that comes from the linearization. We consider perturbations of the steady state of the form

$$u(x,t) \sim u(x) + \phi(x)e^{\lambda t}, \qquad w(x,t) \sim w(x) + \psi(x)e^{\lambda t}$$

where $u(x), w(x)$ denotes the K-mesa equilibrium solution of (2.2) on the interval of length $2KL$ with Neumann boundary conditions, whose leading order asymptotic profile was constructed in Proposition 2.1.1. For small perturbations ϕ, ψ we get the following eigenvalue problem,

$$\begin{cases} \lambda\phi = \varepsilon^2\phi_{xx} + f_u(u,w)\phi + f_w(u,w)\psi \\ 0 = D\psi_{xx} + g_u(u,w)\phi + g_w(u,w)\psi \end{cases}, \tag{2.19}$$

with Neumann boundary conditions. The sign of the real part of the eigenvalue λ determines the stability: the system is said to be unstable if there exists a solution to (2.19) with $\mathrm{Re}(\lambda) > 0$ and it is stable if $\mathrm{Re}(\lambda) < 0$ for all solutions λ to (2.19).

To analyse the stability for Neumann boundary conditions, the first step is to consider periodic boundary conditions. The eigenvalues for the periodic boundary problem are given in the following lemma.

Lemma 2.2.2. *Consider the steady state consisting of* K *mesas on the interval* $[-L, (2K-1)L]$, *as constructed in Proposition 2.1.1, and consider the linearized problem (2.19) with periodic boundary conditions*

$$\phi\left(-L\right) = \phi((2K-1)L)$$

The linearized problem admits $2K$ eigenvalues. Of these, $2K-2$ are given asymptotically by

$$\lambda_\theta^{\pm} \sim (a \pm |b|)\, \frac{\int_{u_-}^{u_+} f_w du}{\int_{-L}^{0} u_x^2 dx} \tag{2.20}$$

where

$$a = \alpha_+ + \alpha_- + \frac{(g_+ - g_-)}{D}\frac{L}{1-\cos\theta} - \frac{g_+ l}{D} \tag{2.21}$$

$$|b|^2 = \alpha_+^2 + \alpha_-^2 + 2\alpha_+\alpha_-\cos\theta + \frac{2\,(g_+ - g_-)}{D}\left[\frac{L\,(\alpha_+ + \alpha_-)}{1-\cos\theta} - l\alpha_+ - (L-l)\alpha_-\right] + \frac{(g_+ - g_-)^2}{D^2\,(1-\cos\theta)^2}\left[L^2 - 2\,(1-\cos\theta)\,l(L-l)\right] \tag{2.22}$$

with

$$\alpha_+ = \frac{2C_+^2\mu_+^3}{\int_{u_-}^{u_+} f_w du}\frac{1}{\varepsilon}\exp\left(-\frac{2\mu_+}{\varepsilon}l\right), \quad \alpha_- = \frac{2C_-^2\mu_-^3}{\int_{u_-}^{u_+} f_w du}\frac{1}{\varepsilon}\exp\left(-\frac{2\mu_-}{\varepsilon}(L-l)\right) \tag{2.23}$$

and

$$\theta = 2\pi j/K; \quad j = 1, \ldots, K-1. \tag{2.24}$$

The other two eigenvalues are $\lambda = 0$ and

$$\lambda_{even} \sim -\frac{g_- - g_+}{\sigma_+ l + \sigma_-(L-l)}\frac{\int_{u_-}^{u_+} f_w du}{\int_{-L}^{0} u_x^2 dx} \tag{2.25}$$

where $\sigma_\pm$ are given in (2.35). In the case $\theta = \pi$, the formula (2.20) simplifies to

$$\lambda_\pi^- = \left(2\alpha_- - \frac{g_-^2 L}{D(g_- - g_+)}\right)\frac{\int_{u_-}^{u_+} f_w du}{\int_{-L}^{0} u_x^2 dx}; \lambda_\pi^+ = \left(2\alpha_+ - \frac{g_+^2 L}{D(g_- - g_+)}\right)\frac{\int_{u_-}^{u_+} f_w du}{\int_{-L}^{0} u_x^2 dx} \tag{2.26}$$

The eigenvalues given here are the *critical eigenvalues* [59]. There may exist non-critical eigenvalues, but they all have negative real parts and thus do not affect the stability of the mesa pattern solutions. For further reference, see [59].

Derivation of Lemma 2.2.2. The idea is to make use of Floquet theory. For further discussion on Floquet exponents, see [18]. That is, instead of considering (2.19) with periodic boundary conditions on $[-L, (2K-1)L]$, we consider (2.19) on the interval $[-L, L]$ with the boundary conditions

$$\phi(L) = z\phi(-L), \quad \phi'(L) = z\phi'(-L); \qquad \psi(L) = z\psi(-L), \quad \psi'(L) = z\psi'(-L), \tag{2.27}$$

for some z. We then extend such solution to the interval $[L, 3L]$ by defining $\phi(x) \equiv z\phi(x - 2L)$ for $x \in [L, 3L]$ and similarly for ψ. This extension ensures the continuity of ϕ, ψ and ϕ_x, ψ_x at L. Since u, w are periodic with period $2L$, it is clear that ϕ, ψ extended in this way satisfies (2.19) on $[-L, 3L]$ and moreover $\phi(3L) = z^2\phi(-L)$. Repeating this process, we obtain the solution of (2.19) on the whole interval $[-L, 2KL - L]$ with $\phi(2KL - L) = \phi(-L)z^K$. Thus, by choosing

$$z = \exp\left(2\pi ij/K\right), \quad j = 0, \ldots, K - 1,$$

we have obtained a periodic solution to (2.19) on $[-L, 2KL - L]$.

To solve (2.19) subject to (2.27), we estimate the eigenfunctions as

$$\phi \sim c_\pm u_x; \quad \psi \sim \psi\left(\pm l\right) \quad \text{when } x \sim \pm l, \tag{2.28}$$

where $c_\pm$ are unknown constants. Note that

$$0 = \varepsilon^2 u_{xxx} + f_u u_x + f_w w_x.$$

Multiplying (2.19) by u_x and integrating by parts on $[-L, 0]$ we then obtain

$$\lambda c_- \int_{-L}^{0} u_x^2 dx \sim \varepsilon^2 \left(\phi_x u_x - \phi u_{xx}\right)_{-L}^{0} + \int_{-L}^{0} f_w \left(\psi u_x - \phi w_x\right) dx.$$

We note that the integral term on the right hand side is dominated by the contribution from $x = -l$. Using (2.28) we then obtain

$$\lambda c_- \int_{-L}^{0} u_x^2 dx \sim \varepsilon^2 \left(\phi_x u_x - \phi u_{xx}\right)_{-L}^{0} + \left(\psi(-l) - c_- w_x\left(-l\right)\right) \int_{u_-}^{u_+} f_w du. \tag{2.29}$$

Similarly on the interval $[0, L]$ we get

$$\lambda c_+ \int_{0}^{L} u_x^2 dx \sim \varepsilon^2 \left(\phi_x u_x - \phi u_{xx}\right)_{0}^{L} - \left(\psi(+l) - c_{+.} w_x(-l)\right) \int_{u_-}^{u_+} f_w du \tag{2.30}$$

In matrix form, equations (2.29) and (2.30) become

$$\lambda\kappa_0 \begin{pmatrix} c_+ \\ c_- \end{pmatrix} = \begin{pmatrix} \kappa_1 \left(-\phi u_{xx}\right)_0^L - \psi(+l) + c_- w_x(+l) \\ \kappa_1 \left(-\phi u_{xx}\right)_{-L}^0 + \psi(-l) - c_- w_x(-l) \end{pmatrix} \tag{2.31}$$

where

$$\kappa_0 = \frac{\int_{-L}^{0} u_x^2 dx}{\int_{u_-}^{u_+} f_w du}; \quad \kappa_1 = \frac{\varepsilon^2}{\int_{u_-}^{u_+} f_w du}.$$

We now transform (2.31) into an matrix eigenvalue problem. To do so, we will express the boundary terms as well as $\psi(\pm l)$ in terms of $c_\pm$.

First, we determine $\psi(\pm l)$. We start by estimating

$$\int_{u_-}^{u+} g_u du \sim g_+ - g_-;$$
$$\int_{u_+}^{u-} g_u du \sim g_- - g_+$$

where $g_\pm = g(u_\pm, w_0)$. On the other hand, ϕ is dominated by the contribution from the interfaces. Hence we estimate

$$g_u \phi \sim c_- (g_+ - g_-) \delta(x+l) + c_+ (g_- - g_+) \delta(x-l) \tag{2.32}$$

where δ is the delta function. Therefore we write

$$\psi(x) \sim -\frac{(g_+ - g_-)}{D} (c_- \eta(x; -l) - c_+ \eta(x; l))$$

where $\eta(x; x_0)$ is a Green's function which satisfies

$$\eta'' + \frac{\sigma(x)}{D}\eta = \delta(x - x_0) \tag{2.33}$$

with boundary conditions

$$\eta(L) = z\eta(-L), \quad \eta'(L) = z\eta'(-L), \quad z = \exp(2\pi i j/K), \quad j = 0 \ldots K-1 \tag{2.34}$$

where

$$\sigma(x) \equiv \begin{cases} \sigma_+, & |x| < l \\ \sigma_-, & l < |x| < L \end{cases} \quad ; \quad \sigma_\pm \equiv \left(g_w - g_u \frac{f_w}{f_u} \right) \Big|_{u=u_\pm, w=w_0}. \tag{2.35}$$

As will become evident, $z = 1$ is a special case and will be considered later. For now, assume $z \neq 1$. Then to leading order, η must satisfiy

$$\eta_{xx} = 0; \quad \eta\left(x_0^-; x_0\right) = \eta\left(x_0^+; x_0\right); \quad \eta'\left(x_0^+; x_0\right) - \eta'\left(x_0^-; x_0\right) = 1.$$

so that

$$\eta \sim \begin{cases} A + (x+L)B, & x < x_0 \\ A + (L+x_0)B + (1+B)(x-x_0), & x > x_0 \end{cases}.$$

The constants A and B are to be chosen so that the boundary conditions (2.27) are satisfied, which gives

$$A + 2BL + L - x_0 = zA, \qquad 1 + B = zB.$$

We then obtain

$$B = \frac{z-1}{(z-1)^2}, \quad A = \frac{2L + (L - x_0)(z-1)}{(z-1)^2},$$

$$\eta(l;l) = \eta(-l;-l) = \frac{2Lz}{(z-1)^2}, \tag{2.36}$$

$$\eta(l;-l) = \frac{2Lz + 2zl(z-1)}{(z-1)^2}, \tag{2.37}$$

$$\eta(-l;l) = \frac{2Lz + 2l(1-z)}{(z-1)^2} = \overline{\eta(l;-l)}.$$

In summary, we obtain

$$\begin{pmatrix} \psi(l) \\ -\psi(-l) \end{pmatrix} \sim \frac{(g_+ - g_-)}{D} \begin{pmatrix} \eta(l;l) & -\eta(l;-l) \\ -\overline{\eta(l;-l)} & \eta(l;l) \end{pmatrix} \begin{pmatrix} c_+ \\ c_- \end{pmatrix} \tag{2.38}$$

where $\eta(l;l),\ \eta(l;-l)$ are given by (2.36) and (2.37).

Next we compute the boundary terms. We start by estimating the behaviour of u_x and ϕ near $-L$. Since $u'(-L) = 0$, we have

$$u \sim u_- + A\left[\exp(\mu_- z) + \exp(-\mu_- z)\right], \quad z = \frac{x+L}{\varepsilon}. \tag{2.39}$$

The constant A is found by matching u to the heteroclinic solution as $x \to -L$

$$\begin{aligned} &U(y) \sim u_- + C_- \exp(\mu_- y); \\ &u(x) \sim U\left(\frac{x+l}{\varepsilon}\right) \sim u_- + C_- \exp\left(\mu_- \frac{x+l}{\varepsilon}\right). \end{aligned} \tag{2.40}$$

Matching (2.39) and (2.40) we then obtain

$$A = C_- \exp\left(-\frac{\mu_-}{\varepsilon}(L-l)\right).$$

Performing a similar analysis at $x = 0$ and at $x = L$ we get:

$$u''(\pm L) = 2C_- \frac{\mu_-^2}{\varepsilon^2} \exp\left(-\frac{\mu_-}{\varepsilon}(L-l)\right); \qquad u''(0) = -2C_+ \frac{\mu_+^2}{\varepsilon^2} \exp\left(-\frac{\mu_+}{\varepsilon} l\right).$$

Next we estimate $\phi(-L)$. Near $x \sim -L$ we write

$$\phi = C_1 \exp\left(\frac{\mu_-}{\varepsilon}(x+L)\right) + C_2 \exp\left(-\frac{\mu_+}{\varepsilon}(x+L)\right)$$

where C_1 and C_2 are to be determined. Away from $-L$, we have $\phi \sim c_- u'$. Matching, we then obtain

$$C_1 = c_- C_- \frac{\mu_-}{\varepsilon} \exp\left(-\frac{\mu_-}{\varepsilon}(L-l)\right).$$

On the other hand, near $x \sim +L$ we write

$$\phi = C_3 \exp\left(\frac{\mu_-}{\varepsilon}(x+L)\right) + C_4 \exp\left(-\frac{\mu_+}{\varepsilon}(x+L)\right);$$

as before, we get

$$C_4 = -c_+ C_+ \frac{\mu_+}{\varepsilon} \exp\left(-\frac{\mu_+}{\varepsilon}(L-l)\right).$$

The constants C_2 and C_3 are determined by using the boundary condtions (2.34), which yields

$$C_3 = zC_1 \quad \text{and} \quad C_4 = zC_2$$

In summary, we get

$$\phi(-L) \sim C_- \frac{\mu_-}{\varepsilon} \exp\left(-\frac{\mu_-}{\varepsilon}(L-l)\right)\left[c_- - \frac{1}{z}c_+\right];$$
$$\phi(L) \sim C_- \frac{\mu_-}{\varepsilon} \exp\left(-\frac{\mu_-}{\varepsilon}(L-l)\right)\left[zc_- - c_+\right].$$

Performing a similar analysis at $x \sim 0$, we obtain

$$\phi(0) \sim C_+ \frac{\mu_+}{\varepsilon} \exp\left(-\frac{\mu_+}{\varepsilon}l\right)\left[c_- - c_+\right].$$

We thus obtain

$$(\phi u_{xx})_0^L = 2C_-^2 \frac{\mu_-^3}{\varepsilon^3} \exp\left(-\frac{2\mu_-}{\varepsilon}(L-l)\right)\left[zc_- - c_+\right] + 2C_+^2 \frac{\mu_+^3}{\varepsilon^3} \exp\left(-\frac{2\mu_+}{\varepsilon}l\right)\left[c_- - c_+\right],$$
$$(\phi u_{xx})_{-L}^0 = -2C_-^2 \frac{\mu_-^3}{\varepsilon^3} \exp\left(-\frac{2\mu_-}{\varepsilon}(L-l)\right)\left[c_- - \frac{1}{z}c_+\right] - 2C_+^2 \frac{\mu_+^3}{\varepsilon^3} \exp\left(-\frac{2\mu_+}{\varepsilon}l\right)\left[c_- - c_+\right],$$

so that

$$\begin{bmatrix} \kappa_1 \left(\phi_x u_x - \phi u_{xx}\right)_0^L \\ \kappa_1 \left(\phi_x u_x - \phi u_{xx}\right)_{-L}^0 \end{bmatrix} = \begin{bmatrix} \alpha_+ + \alpha_- & -\alpha_+ - z\alpha_- \\ -\alpha_+ - \frac{1}{z}\alpha_- & \alpha_+ + \alpha_- \end{bmatrix} \begin{bmatrix} c_+ \\ c_- \end{bmatrix} \tag{2.41}$$

where $\alpha_\pm$ are given by (2.14).

Finally, we estimate

$$w'(l) \sim -\frac{g_+ l}{D} \sim -w'(-l). \tag{2.42}$$

Substituting (2.41), (2.42) and (2.38) into (2.31) we obtain

$$\lambda\kappa_0 \begin{pmatrix} c_+ \\ c_- \end{pmatrix} = \begin{pmatrix} a & b \\ \bar{b} & a \end{pmatrix} \begin{pmatrix} c_+ \\ c_- \end{pmatrix}$$

where

$$a = \alpha_+ + \alpha_- + \frac{(g_- - g_+)}{D}\eta(l;l) - \frac{g_+ l}{D}; \quad b = -\alpha_+ - z\alpha_- - \frac{(g_- - g_+)}{D}\eta(l;-l).$$

It follows that

$$\lambda\kappa_0 = a \pm |b|\,.$$

Next we compute

$$\begin{aligned}
a &= \alpha_+ + \alpha_- + \frac{2\,(g_- - g_+)}{D}\frac{Lz}{(z-1)^2} - \frac{g_+ l}{D} \\
b &= -\alpha_+ - z\alpha_- - \frac{2\,(g_- - g_+)}{D}\frac{Lz + zl(z-1)}{(z-1)^2} \\
\bar{b} &= -\alpha_+ - \frac{1}{z}\alpha_- - \frac{2\,(g_- - g_+)}{D}\frac{Lz - l(z-1)}{(z-1)^2} \\
|b|^2 &= \alpha_+^2 + \alpha_-^2 + \alpha_+\alpha_-\,(z + \bar{z}) + \alpha_+\frac{2\,(g_- - g_+)}{D}\left(\frac{2Lz}{(z-1)^2} + l\right) \\
&\quad + \alpha_-\frac{2\,(g_- - g_+)}{D}\left(\frac{L\,(z^2+1)}{(z-1)^2} - l\right) + \frac{4\,(g_- - g_+)^2}{D^2}\left(\frac{z^2L^2}{(z-1)^4} + \frac{zl(L-l)}{(z-1)^2}\right)
\end{aligned}$$

We write

$$z = e^{i\theta}, \quad \theta = 2\pi j/K, \quad j = 0, \ldots, K-1$$

and note that

$$\frac{2z}{(z-1)^2} = \frac{1}{\cos\theta - 1}; \quad \frac{(z^2+1)}{(z-1)^2} = \frac{\cos\theta}{\cos\theta - 1}.$$

Combining these computations, we obtain (2.20), (2.21), (2.22), provided that $z \neq 1$.

Next we consider (2.27) with $z = 1$, which corresponds to periodic boundary conditions on $[-L, L]$. This admits two solutions. One is $\lambda = 0$ corresponding the odd eigenfunction $\phi = u_x, \psi = w_x$. The other eigenfunctions look like the derivative $\phi = u_x, \psi = w_x$ near the interfaces, that is, in the inner variables, but this is not the

case outside the interfaces. The other eigenfunction corresponding to $z = 1$ is even. This corresponds to imposing the boundary conditions

$$\phi'(0) = 0 = \phi'(L); \quad \psi'(0) = 0 = \psi'(L).$$

As before, we assume

$$\phi \sim u_x; \quad \psi \sim \psi(l) \quad \text{when } x \sim l. \tag{2.43}$$

and obtain

$$\lambda \int_0^L u_x^2 dx \sim \varepsilon^2 (\phi_x u_x - \phi u_{xx})_0^L - (\psi(l) - w_x(l)) \int_{u_-}^{u_+} f_w du. \tag{2.44}$$

As before, we obtain

$$\psi(x) \sim \frac{(g_+ - g_-)}{D} \eta(x; l)$$

where $\eta(x; x_0)$ satisfies (2.33) with boundary conditions $\eta'(0) = 0 = \eta'(L)$. We then obtain

$$\eta \sim \frac{1}{\int_0^L \sigma(x) dx} \sim \frac{1}{\sigma_+ l + \sigma_-(L - l)}.$$

The boundary term is evaluated as previously, but is of smaller order. This yields the formula (2.25) for the even eigenvalue.

At this juncture, we note that these results also hold provided τ is sufficiently small, not just when $\tau = 0$. The expression that changes from the addition of a non-zero τ, that is, the addition of the τw_t term, is

$$\sigma_\pm = -\lambda\tau + \left(g_w - g_u \frac{f_w}{f_u} \right) \Bigg|_{u=u_\pm, w=w_0}. \tag{2.45}$$

To leading order, this is equal to (2.35) as long as $\lambda\tau \ll 1$. Provided that $0 < \tau \ll \mathcal{O}(\frac{1}{\varepsilon})$, the results remain unchanged.

We now use Lemma 2.2.2 to determine the stability of the problem with Neumann boundary conditions as follows. Suppose that ϕ satisfies Neumann boundary conditions on $[0, a]$. Then we may extend ϕ by even reflection around the origin and then ϕ becomes periodic on $[-a, a]$. From this principle, it follows that the eigenvalues of a K mesa steady state solution satisfying Neumann boundary conditions form a subset of the eigenvalues of $2K$ mesas with periodic boundary conditions. On the other hand, if ϕ is an eigenfunction on $[-a, a]$ with periodic boundary conditions then so is $\phi(-x)$ and hence $\hat{\phi}(x) = \phi(x) + \phi(-x)$ is an eigenfunction on $[0, a]$ with Neumann boundary

conditions, provided that $\hat{\phi}(x) \neq 0$. Since $\hat{\phi}'(0) = 0$ and ϕ satisfies a 2nd order ODE, $\hat{\phi} \neq 0$ if and only if $\hat{\phi}(0) \neq 0$ which only holds if $\phi(0) \neq 0$. Verifying this condition (and the same condition on ψ), we obtain the following result.

Lemma 2.2.3. *Consider the steady state consisting of K mesas on the interval $[-L, (2K-1)L]$, with Neumann boundary conditions. The linearized problem admits $2K$ eigenvalues. Of these, $2K-2$ are given asymptotically by (2.20) to (2.23) of Lemma 2.2.2, but with*

$$\theta = \pi j/K, \quad j = 1 \dots K-1. \tag{2.46}$$

The additional two eigenvalues correspond to an even and odd eigenfunction with Neumann boundary conditions on $[-L, +L]$. They are

$$\lambda_{odd} = \left(2\alpha_- - \frac{g_-^2 L}{D(g_- - g_+)}\right) \frac{\int_{u_-}^{u_+} f_w du}{\int_{-L}^{0} u_x^2 dx}, \tag{2.47}$$

and

$$\lambda_{even} = -\frac{g_- - g_+}{\sigma_+ l + \sigma_-(L-l)} \frac{\int_{u_-}^{u_+} f_w du}{\int_{-L}^{0} u_x^2 dx}, \tag{2.48}$$

with all the symbols as defined in Lemma 2.2.2.

Consider λ_{odd} given in (2.47). Note that α_- is exponentially small with respect to ε. So, as $\varepsilon \to 0$, this term goes to zero and $\lambda_{odd} < 0$. For ε larger (although still small), as D is increased, the second term becomes very small, and λ_{odd} becomes positive. Thus, we obtain a threshold for the instability of the mesa pattern. In a similar way, $\lambda_\theta^\pm$ can become positive for sufficiently large D. The even eigenvalue λ_{even} does not depend on D. It is $\mathcal{O}(\varepsilon)$, and, thus, $|\lambda_{even}|$ is much larger than the other eigenvalues. The conditions (2.13) guarantee that a single interface will be stable for any $D \gg 1$. These conditions imply that $\lambda_{even} < 0$. The second part of (2.13) guarantees that $\lambda_{odd} < 0$ whenever $1 \ll \ln D \ll \frac{1}{\varepsilon}$. Therefore, if (2.13) holds, a single mesa will be stable whenever $1 \ll \ln D \ll \frac{1}{\varepsilon}$.

Critical Thresholds. To obtain instability thresholds, we set $\lambda_\theta^\pm = 0$ in Lemma 2.2.2; we then obtain $a^2 - |b|^2 = 0$. Using $l = \frac{g_- L}{g_- - g_+}$ and after some algebra we obtain:

$$0 = 2\alpha_+\alpha_- (1 - \cos\theta) D^2 - 2L \frac{g_-^2\alpha_+ + g_+^2\alpha_-}{g_- - g_+} D + L^2 \frac{g_+^2 g_-^2}{(g_- - g_+)^2} \tag{2.49}$$

which implies that $\lambda_\theta^+ = 0$ if and only if $D > D(\theta)$ where

$$D(\theta) \sim \begin{cases} \dfrac{Lg_+^2}{2\left(g_- - g_+\right)\alpha_-} & \text{if} \quad \alpha_+ \ll \alpha_- \\ \\ \dfrac{Lg_-^2}{2\left(g_- - g_+\right)\alpha_+} & \text{if} \quad \alpha_- \ll \alpha_+ \end{cases}$$

and more generally, without any assumptions on α_- and α_+,

$$D(\theta) = \frac{L}{2\left(g_- - g_+\right)\left(g_-^{-2}\alpha_- + g_+^{-2}\alpha_+\right)} \left(\frac{1}{2} + \sqrt{\frac{1}{4} - \frac{2\alpha_+\alpha_-\left(1-\cos\theta\right)g_+^2 g_-^2}{4\left(g_-^2\alpha_+ + g_+^2\alpha_-\right)^2}} \right)^{-1}.$$

It is clear that $D(\theta)$ is an increasing function of θ. It is also easy to verify that $\lambda_\theta^\pm < 0$ if $\alpha_\pm$ is decreased sufficiently, or equivalently, if D is sufficiently small. In this case the formula (2.20) reduces to

$$\lambda_\theta^\pm \kappa_0 \sim \frac{\left(g_+ - g_-\right)L}{D^2\left(1-\cos\theta\right)} \left(1 \pm \sqrt{\left[1 - 2\left(1-\cos\theta\right)\frac{ld}{L^2} \right]} \right) - \frac{g_+ l}{D}. \tag{2.50}$$

On the other hand, when $K = 1$, the eigenvalues are λ_{odd} and λ_{even}, given by (2.47), (2.48). It is clear that $\lambda_{even} < 0$ for all D; on the other hand setting $\lambda_{odd} = 0$ yields the threshold (2.17). This completes the derivation of Principal Result 2.2.1.

2.3 Dynamics

We now derive the equations of motion of the interfaces of the mesa patterns allowing us to describe the dynamics of the fronts that are not necessarily in a symmetric pattern.

We assume that the pattern consists of K mesas on the interval $[-L, (2K-1)L]$. Each mesa is bounded by two interfaces located at x_{li} and x_{ri} and we assume the ordering

$$-L < x_{l1} < x_{r1} < x_{l2} < x_{r2} < \cdots < x_{lK} < x_{rK} < (2K-1)L.$$

Moreover to leading order we assume

$$u \sim \begin{cases} u_+, \text{ if } x \in (x_{li}, x_{ri}) \text{ for some } i \in (1, K) \\ u_-, \quad \text{otherwise} \end{cases}$$

and near each interface,

$$u\left(x_{li}+\varepsilon y\right)\sim U(-y),\quad u\left(x_{ri}+\varepsilon y\right)\sim U(y),\quad y=O(1),\quad i=1\ldots K,$$

where U is the heteroclinic orbit given in (2.7), with $U(y)\to u_{\pm}$ as $y\to\mp\infty$. We also suppose that x_{li}, x_{ri} are slowly changing with time. In addition we define:

$$\begin{aligned}
x_{ci} &\equiv \frac{x_{li}+x_{ri}}{2},\quad i=1\ldots K,\\
x_{di} &\equiv \frac{x_{ri}+x_{l(i+1)}}{2},\quad i=1\ldots K-1,\\
x_{d0} &\equiv -L,\\
x_{dK} &\equiv (2K-1)L.
\end{aligned}$$

The equations of motions are derived from $2K$ solvability conditions about each interface.

First consider the interface x_{l1}. We expand

$$u(x,t)=u_0(z)+\frac{1}{D}u_1,\quad w(x,t)=w_0+\frac{1}{D}w_1$$

where w_0 is given by (2.4) and

$$z=x-x_{l1}(t);\quad u_0(z)=U\left(-z/\varepsilon\right).$$

Expanding in terms of $\frac{1}{D}$ we obtain

$$0=\varepsilon u_{0zz}+f(u_0,w_0), \tag{2.51}$$

$$-x'_{l1}(t)Du'_0=\varepsilon^2u_{1zz}+f_u(u_0,w_0)u_1+f_w(u_0,w_0)w_1, \tag{2.52}$$

$$0=w_{1xx}+g(w_0,u_0). \tag{2.53}$$

It will become evident later that $x'_{l1}=O(\frac{1}{D})$ so the above expansion is indeed consistent. We multiply (2.52) by u'_0 and integrate on $x\in(-L,x_{c1})$. Upon integrating by parts we obtain:

$$-x'_{l1}(t)D\int_{-L}^{x_{c1}}\left(u_{0x}\right)^2dx\sim\varepsilon^2\left(u_{1z}u_{0z}-u_1u_{0zz}\right)_{x=-L}^{x=x_{c1}}+\int_{-L}^{x_{c1}}f_ww_1dx.$$

The boundary term is evaluated similarly as in §2.2 and we obtain

$$\begin{aligned}
\varepsilon^2\left(u_{1z}u_{0z}-u_1u_{0zz}\right)_{x=-L}^{x=x_{c1}} =& 2D\left(-C_+\mu_+^2\exp\left(-\frac{\mu_+}{\varepsilon}\left(x_{r1}-x_{l1}\right)\right)\right.\\
&\left.+C_-\mu_-^2\exp\left(-\frac{2\mu_-}{\varepsilon}\left(L+x_{l1}\right)\right)\right).
\end{aligned}$$

The integral terms are estimated as

$$\int_{-L}^{x_{c1}} (u_{0x})^2\, dx \sim \frac{1}{\varepsilon}\int_{-\infty}^{\infty}\left(\frac{dU}{dy}\right)^2 dy; \qquad \int_{-L}^{x_{c1}} f_w w_1 dx \sim w_1(x_{l1})\int_{u_-}^{u_+} f_w(w_{0,}u)du.$$

Similar analysis is performed at each of the remaining interfaces. In this way, we obtain the following system:

$$\begin{cases} x'_{li}(t) \sim \dfrac{\varepsilon}{\int_{-\infty}^{\infty}\left(\frac{dU}{dy}\right)^2 dy}\left((BT)_{li} - \frac{1}{D}w_1(x_{li})\int_{u_-}^{u_+} f_w(w_{0,}u)du\right) \\ x'_{ri}(t) \sim \dfrac{\varepsilon}{\int_{-\infty}^{\infty}\left(\frac{dU}{dy}\right)^2 dy}\left((BT)_{ri} + \frac{1}{D}w_1(x_{ri})\int_{u_-}^{u_+} f_w(w_{0,}u)du\right) \end{cases}, \; i = 1\ldots K \tag{2.54}$$

where

$$(BT)_{l1} = -2C_-\mu_-^2 \exp\left(-\frac{2\mu_-}{\varepsilon}(L + x_{l1})\right) + 2C_+\mu_+^2 \exp\left(-\frac{\mu_+}{\varepsilon}(x_{r1} - x_{l1})\right) \tag{2.55}$$

$$(BT)_{li} = -2C_-\mu_-^2 \exp\left(-\frac{\mu_-}{\varepsilon}\left(x_{l1} - x_{r(i-1)}\right)\right) + 2C_+\mu_+^2 \exp\left(-\frac{\mu_+}{\varepsilon}(x_{ri} - x_{li})\right), \quad i = 2\ldots K-1 \tag{2.56}$$

$$(BT)_{ri} = -2C_-\mu_-^2 \exp\left(-\frac{\mu_-}{\varepsilon}(x_{ri} - x_{li})\right) + 2C_+\mu_+^2 \exp\left(-\frac{\mu_+}{\varepsilon}\left(x_{l(i+1)} - x_{ri}\right)\right), \quad i = 2\ldots K-1 \tag{2.57}$$

$$(BT)_{rK} = -2C_-\mu_-^2 \exp\left(-\frac{\mu_-}{\varepsilon}(x_{rK} - x_{lK})\right) + 2C_+\mu_+^2 \exp\left(-\frac{2\mu_+}{\varepsilon}((2K-1)L - x_{rK})\right), \tag{2.58}$$

The constants $w_1(x_{li})$ and $w_1(x_{ri})$ are obtained by recursively solving for w_1 which satisfies:

$$w_1'' = \begin{cases} g_+, & x \in [x_{li}, x_{ri}], \quad i = 1\ldots K \\ g_- & \text{otherwise} \end{cases}$$
$$w_1'(-L) = 0 = w_1'((2K-1)L).$$

To simplify the expression for w_1, we first define the interdistances

$$m_i = \begin{cases} x_{l1} + L, & i = 0 \\ x_{l(i+1)} - x_{ri}, & i = 1\ldots K-1 \\ (2K-1)L - x_{ri}, & i = K \end{cases}; \qquad p_i = x_{ri} - x_{li}, \quad i = 1...K.$$

We obtain the following expressions:

$$w'(x_{li}) = \begin{cases} -g_- m_0, & i = 1 \\ w'(x_{r(i-1)}) - g_- m_i, & i = 2 \dots K \end{cases}$$

$$w'(x_{ri}) = w'(x_{li}) - g_+ p_i, \quad i = 1 \dots K;$$

$$w\left(x_{li}\right) = \begin{cases} w(-L) - g_- \frac{m_0^2}{2}, & i = 1 \\ w\left(x_{r(i-1)}\right) + w'(x_{r(i-1)}) m_i - g_- \frac{m_i^2}{2}, & i = 2 \dots K \end{cases}$$

$$w(x_{ri}) = w(x_{li}) + w'(x_{li}) p_i - g_+ \frac{p_i^2}{2}, \ i = 1 \dots K.$$

Expanding, we obtain

$$\begin{aligned} w_1(x_{l1}) =& w(-L) - g_- \frac{m_0^2}{2}, \\ w_1(x_{r1}) =& w(-L) - g_- \left(\frac{m_0^2}{2} + m_0 p_1 \right) - g_+ \frac{p_1^2}{2}, \\ w_1(x_{l2}) =& w(-L) - g_- \left(\frac{m_0^2}{2} + m_0 p_1 + m_0 m_1 + \frac{m_1^2}{2} \right) - g_+ \left(\frac{p_1^2}{2} + p_1 m_1 \right), \\ w_1(x_{r2}) =& w(-L) - g_- \left(\frac{m_0^2}{2} + m_0 p_1 + m_0 m_1 + \frac{m_1^2}{2} + m_0 p_2 + m_1 p_2 \right) \\ & - g_+ \left(\frac{p_1^2}{2} + p_1 m_1 + p_1 p_2 + \frac{p_2^2}{2} \right), \end{aligned}$$

and so on. The general expressions for x_{li} and x_{ri} are

$$\begin{aligned} w(x_{li}) =& w_1(-L) - g_- \left(\sum_{j=0}^{i-1} \sum_{k=j+1}^{i-1} m_j m_k + \sum_{j=0}^{i-1} \sum_{k=j+1}^{i-1} m_j p_k + \sum_{j=0}^{i-1} \frac{m_j^2}{2} \right) \\ & - g_+ \left(\sum_{j=1}^{i-1} \sum_{k=j+1}^{i} p_j p_k + \sum_{j=1}^{i-1} \sum_{k=j}^{i-1} p_j m_k + \sum_{j=1}^{i-1} \frac{p_j^2}{2} \right) \qquad (2.59) \\ w(x_{ri}) =& w_1(-L) - g_- \left(\sum_{j=0}^{i-1} \sum_{k=j+1}^{i-1} m_j m_k + \sum_{j=0}^{i-1} \sum_{k=j+1}^{i} m_j p_k + \sum_{j=0}^{i-1} \frac{m_j^2}{2} \right) \\ & - g_+ \left(\sum_{j=1}^{i} \sum_{k=j+1}^{i} p_j p_k + \sum_{j=1}^{i} \sum_{k=j}^{i-1} p_j m_k + \sum_{j=1}^{i} \frac{p_j^2}{2} \right). \qquad (2.60) \end{aligned}$$

It remains to determine the constant $w_1(-L)$. This is done by considering the conservation of mass (from (2.12)). Integrating the equation for w in (2.1) we obtain that for all time t,

$$g_- \sum m_j + g_+ \sum p_j = 0;$$

moreover $\sum m_j = 2KL - \sum p_j$ so that

$$\sum (x_{ri} - x_{li}) = \frac{2KLg_-}{g_- - g_+}. \tag{2.61}$$

Differentiating (2.61) with respect to t and substituting into (2.54) we then obtain,

$$\sum_{i=1}^{K} (BT)_{ri} - (BT)_{li} + \frac{1}{D}\left[w_1(x_{ri}) + w_1(x_{li})\right] \int_{u_-}^{u_+} f_w(w_{0,}u)du = 0. \tag{2.62}$$

Substituting (2.55)-(2.58), and (2.59)-(2.60) into (2.62) then determines the constant $w_1(-L)$.

Dynamics of a Single Mesa. For a single mesa, we define $x_0 = \frac{x_{l1}+x_{r1}}{2}$ to be the midpoint of the mesa. Due to mass conservation, we have

$$x_{l1} = x_0 - l, \quad x_{r1} = x_0 + l; \qquad l = \frac{g_-}{g_- - g_+}L. \tag{2.63}$$

Substituting (2.63) and $x_0' = (x_{l1}' + x_{r1}')/2$ into (2.54) and after some algebra we then obtain,

$$\begin{aligned}\frac{dx_0}{dt} =& \frac{\varepsilon}{2\int_{-\infty}^{\infty}\left(\frac{dU}{dy}\right)^2 dy}\left(-2C_-\mu_-^2 \exp\left(-\frac{2\mu_-}{\varepsilon}\left(L - l + x_0\right)\right)\right. \\ &\left. +2C_+\mu_+^2 \exp\left(-\frac{2\mu_+}{\varepsilon}\left(L - l - x_0\right)\right) - \frac{2}{D}\frac{g_-^2\int_{u_-}^{u_+} f_w(w_{0,}u)du}{g_- - g_+}x_0\right)\end{aligned}$$

Note that for the special case where $C_\pm = C_0;\ \mu_\pm = \mu_0$ the formula further simplifies to

$$\begin{aligned}\frac{dx_0}{dt} =& \frac{\varepsilon}{2\int_{-\infty}^{\infty}\left(\frac{dU}{dy}\right)^2 dy}\left(C_0\mu_0^2 \exp\left(-\frac{2\mu_0}{\varepsilon}\left(L - l\right)\right)\sinh\left(\frac{2\mu_0}{\varepsilon}\left(x_0\right)\right)\right. \\ &\left. -\frac{2}{D}\frac{g_-^2\int_{u_-}^{u_+} f_w(w_{0,}u)du}{g_- - g_+}x_0\right).\end{aligned}$$

2.4 Numerical Simulations

In this section we compare our asymptotic results with a numerical simulation of (2.1), as well as the linearized equations (2.19) for a specific choice of f and g. Let us first describe the numerical methods used.

To perform the numerical simulation of the PDE system (2.1) we used the software FlexPDE [72] with the default error tolerance of 10^{-5}. To determine the solution to

the linear problem (2.19), we have reformulated it as a boundary value problem by adding an extra equation $\frac{d\lambda}{dx} = 0$ as well as an extra boundary condition such as $\psi(-L) = 1$. We used the asymptotic solution derived in §2.2 as our initial guess. Maple's dsolve/numeric/bvp routine was then used to solve the resulting boundary value problem with the default error tolerance of 10^{-6}.

2.4.1 The Cubic Model

We now specialize our results to the cubic model (1.12),

$$f = 2(u - u^3) + w; \quad g = \beta - u$$

where β is a parameter. Let us first consider a symmetric single mesa solution on interval $[-L, L]$, with its maximum at $x = 0$. For such a solution, we find

$$w_0 = 0; \quad u_- = -1,\ u_+ = +1; \quad U(y) = -\tanh(y); \tag{2.64}$$

$$g_+ = \beta - 1, \quad g_- = \beta + 1; \tag{2.65}$$

$$\int_{-\infty}^{\infty} U_y^2 dy = \frac{4}{3}; \quad \int_{u_-}^{u_+} f_w du = 2; \tag{2.66}$$

$$l_0 = \frac{\beta + 1}{2} L; \quad l_1 = 0; \tag{2.67}$$

$$\mu_\pm = 2; \quad C_\pm = 2; \quad \alpha_\pm = 32 \frac{1}{\varepsilon} \exp\left(-\frac{2}{\varepsilon}(1 \pm \beta) L\right). \tag{2.68}$$

One of the advantages of using the cubic model as a test case is that due to symmetry, $l_1 = 0$. This means that the asymptotic results are expected to be very accurate for small ε.

We obtain the following expressions for λ_{odd} and λ_{even}:

$$\lambda_{even} \sim -12\varepsilon, \tag{2.69}$$

$$\lambda_{odd} \sim -\frac{3(\beta + 1)^2}{4} \frac{L\varepsilon}{D} + 96 \exp\left(-\frac{2L}{\varepsilon}(1 - \beta)\right). \tag{2.70}$$

The even eigenvalue λ_{even} is always negative whereas the odd eigenvalue λ_{odd} becomes positive as D is increased past the critical threshold D_1 given by

$$D_1 = \frac{(\beta + 1)^2 L\varepsilon}{128} \exp\left(\frac{2L}{\varepsilon}(1 - \beta)\right), \tag{2.71}$$

with $\lambda_{odd} < 0$ when $D < D_1$ and with $\lambda_{odd} > 0$ when $D > D_1$. In terms of D_1, we have

$$\lambda_{odd} \sim -\frac{3\left(\beta+1\right)^2 L\varepsilon}{4}\left(\frac{1}{D}-\frac{1}{D_1}\right).$$

The equation of motion for a single mesa becomes

$$\frac{dx_0}{dt} = \frac{3\left(\beta+1\right)^2}{4} L\varepsilon\left(\frac{1}{D_1}\frac{\varepsilon}{4}\sinh\left(\frac{4x_0}{\varepsilon}\right)-\frac{1}{D}x_0\right), \tag{2.72}$$

where $x_0 = \frac{x_{l1}+x_{r1}}{2}$ is the center of the mesa. Note that

$$\frac{\partial}{\partial x_0}\left(\frac{dx_0}{dt}\right)\Big|_{x_0=0} = \lambda_{odd}$$

so that the linearization of the equation of motion around the symmetric equilibrium agrees with the linearization of the original PDE. That is, the results obtained from the dynamics agrees with the results obtained from the eigenvalue problem. The equilibrium $x_0 = 0$ undergoes a pitchfork bifurcation and becomes unstable as D increases past D_1.

For K symmetric mesas on the interval $[-L, (2K-1)L]$, the thresholds (2.18) become:

$$D_K \sim \begin{cases} \frac{(1-\beta)^2 L\varepsilon}{128}\exp\left(2L\left(1+\beta\right)\right), & \text{if } \beta \le 0; \\ \frac{(1+\beta)^2 L\varepsilon}{128}\exp\left(2L\left(1-\beta\right)\right), & \text{if } \beta > 0 \end{cases}; \quad K \ge 2 \tag{2.73}$$

Finally, if we take the "inverted" mesa with $u \sim +1$ near the boundaries, by changing the variables $u \to -u,\ w \to -w$, the model remains the same except β is replaced by $-\beta$. Thus the stability thresholds for the inverted mesa are

$$D_1^i = \frac{\left(1-\beta\right)^2 L\varepsilon}{128}\exp\left(\frac{2L}{\varepsilon}\left(1+\beta\right)\right) \tag{2.74}$$

$$D_K^i \sim \begin{cases} \frac{\left(1-\beta\right)^2 L\varepsilon}{128}\exp\left(2L\left(1+\beta\right)\right), & \text{if } \beta < 0; \\ \frac{\left(1+\beta\right)^2 L\varepsilon}{128}\exp\left(2L\left(1-\beta\right)\right), & \text{if } \beta > 0 \end{cases}; \quad K \ge 2 \tag{2.75}$$

We now numerically validate our asymptotic results by comparison with a numerical simulation of (1.12) with $\tau = 0$.

Experiment 2.1: A Single Mesa.

First, we consider the dynamics (as in §2.3) of a single mesa. Choose $L = 1, \varepsilon = 0.22$ and $\beta = -0.2$. From (2.71) we then get $D_c = 60.138$. Now suppose that $D = 20$.

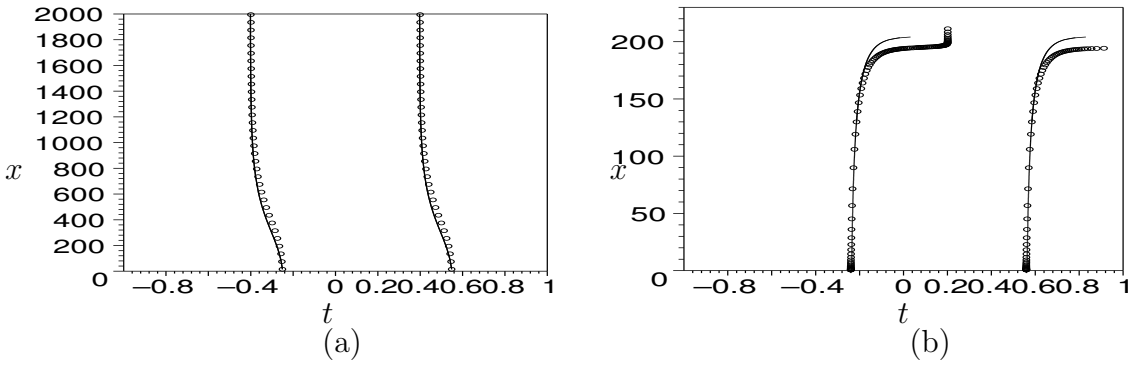

Figure 2.1: (a) Dynamics of a single mesa for the cubic model (1.12) with $\tau = 0$ and with $\beta = -0.2$; $\varepsilon = 0.22$, $D = 20$, $L = 1$. Vertical axis is time, horizontal axis is space. The contour $u = 0$ is shown. Solid lines are the asymptotic results derived in §2.3. Dots represent the output of the numerical simulation of (1.12) with $\tau = 0$ using FlexPDE. The initial conditions are given by (2.76) with $x_0 = 0.15$. The solution moves to the left and converges to a symmetric one-mesa pattern. (b) Same as in (a), but $x_0 = 0.16$. The solution moves to the right until it merges with the boundary.

Then the ODE (2.72) admits three equilibria: $x_e = 0$ (stable) and $x_\pm = \pm 0.156$ (both unstable). We now solve (1.12) with $\tau = 0$. We take initial conditions to be

$$u(x,0) = \tanh\left(\frac{(x-x_0)+l}{\varepsilon}\right) - \tanh\left(\frac{(x-x_0)-l}{\varepsilon}\right) - 1; \quad w(x,0) = 0. \tag{2.76}$$

This corresponds to a mesa solution of length l centered at x_0. If $x_0 \in (-0.156, 0.156)$ then we expect the mesa to move to the center and stabilize there. On the other hand, if $x_0 > 0.156$ then the mesa will move to the right until it merges with the right boundary. In Figure 2.1, we plot the numerical simulations for $x_0 = 0.150$ and $x_0 = 0.160$. The observed behaviour agrees with the above predictions.

Experiment 2.2: Two Mesas.

Here we consider a two-mesa solution. We take the domain $x \in [0, 4]$ (i.e. $L = 1, K = 2$) and take $\beta = -0.3$, $\varepsilon = 0.13$. From (2.67), we get $l = 0.35$ so that the symmetric equilibrium location of the interfaces are 1 ± 0.35 and 3 ± 0.35 which yields $0.65, 1.35, 2.65, 3.35$. According to (2.73), the two-mesa symmetric configuration is stable provided that $D < 82$, and is unstable otherwise. To verify this, we solve the

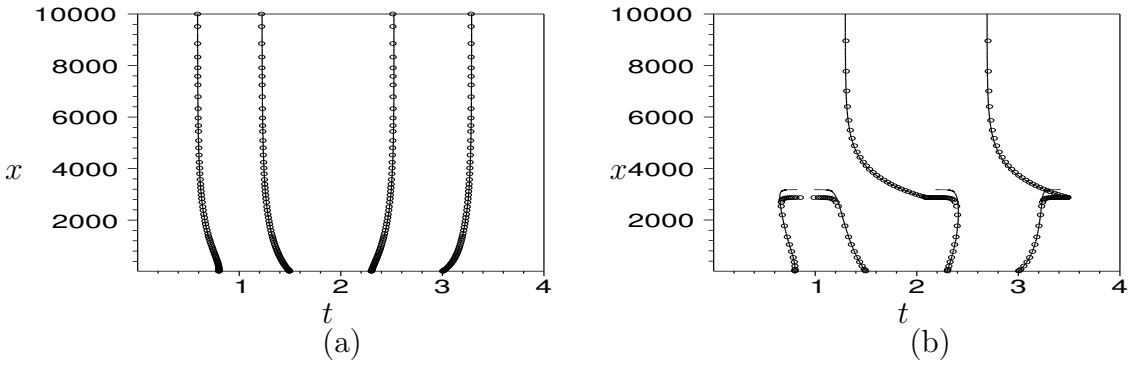

Figure 2.2: Similar to the Figure 2.1, we now consider two mesas. (a) Dynamics of two mesas. The parameters are $K = 2, L = 1$ ($x \in [0, 4]$); $\beta = -0.3,\ \varepsilon = 0.13,\ D = 70$. Initial interface locations are $0.8, 1.5, 2.3, 3.0$. The solution converges to the symmetric two-mesa solution. (b) Same as (a) except that $D = 85$. The two-mesa solution is unstable; the right mesa absorbs the left, eventually resulting in a stable one-mesa pattern which slowly moves to the center.

system with initial conditions

$$u(x,0) = \tanh\left(\frac{x-0.8}{\varepsilon}\right) - \tanh\left(\frac{x-1.5}{\varepsilon}\right)\tanh\left(\frac{x-2.3}{\varepsilon}\right) - \tanh\left(\frac{x-3.0}{\varepsilon}\right) - 1,$$

$$w(x,0) = 0.001.$$

These are relatively close to the symmetric equilibrium. We found that when $D < 80$, such configuration converges to the symmetric two-mesa equilibrium; however it is unstable if $D > 80$ – see Figure 2.2(a, b). This is in good agreement with the the theoretical threshold $D_2 = 82$.

Next we also compute the four eigenvalues for several values of D, and compare them to asymptotic results, shown in Figure 2.3. An excellent agreement is once again observed, including the crossing of zero for $\lambda^+_{\pi/2}$ at $D = 82$.

Experiment 2.3: Eigenvalues.

Figure 2.4 shows the numerical computation (using Maple) of the four distinct eigenvalues and eigenfunctions for the cubic model (1.12) with $\tau = 0$ with $K = 2$. Note that ϕ is localized at the interfaces and is nearly constant elsewhere; whereas ψ has a global variation. An excellent agreement between the asymptotic results and numerical computations is observed.

Experiment 2.4: Transitional Case of $\beta = 0$.

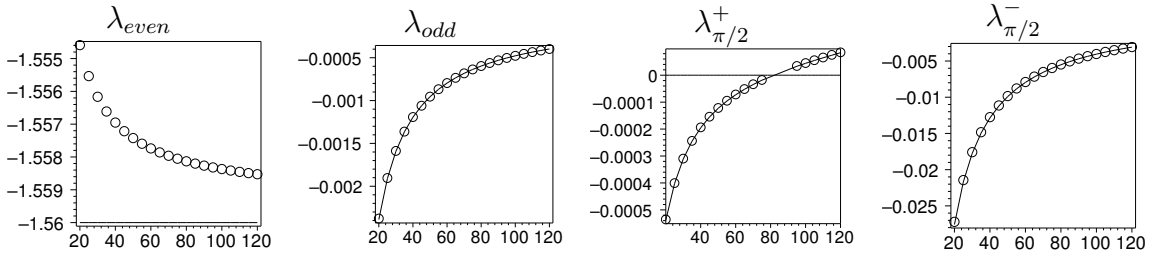

Figure 2.3: The four eigenvalues of the two-mesa pattern of (1.12) as a function of D. Other parameters are as in Figure 2.1(c,d). Circles represent numerical computations of (2.19); lines are the asymptotic results given by (2.20). Excellent agreement is observed, including the crossing of $\lambda^+_{\pi/2}$ at $D = D_2 = 82$.

This is the degenerate case for which the formula (2.73) does not apply. In this case, $\alpha_+ = \alpha_-$ and the formula (2.18) reduces to

$$D_K \sim \frac{L}{256\cos^2\left(\frac{\pi}{4K}\right)}\varepsilon\exp(2L/\varepsilon); \qquad \beta = 0, \quad K \geq 1. \tag{2.77}$$

(this formula is also valid when $K = 1$, as can be verified by comparing it to (2.71)). Note that this is also qualitatively different from $\beta \neq 0$, in that D_K clearly depends on K when $\beta = 0$. To validate (2.77) numerically, we set $\varepsilon = 0.17$, $L = 1, \beta_0 = 0$. Equation (2.77) then yields the asymptotic thresholds $D_1 = 170.8$, $D_2 = 100.1$, $D_3 = 91$. Next, we have computed the eigenvalues λ_{odd} and $\lambda^+_{\pi/K}$ explicitly using the formulation (2.19) for $K = 1, 2, 3$ several different D values and for ε, L as above; these are shown in Figure 2.5. An excellent agreement can be observed with the predicted threshold values.

Experiment 2.5: Boundary Mesas versus Interior Mesas.

Let us now compare the stability properties of interior mesas versus patterns with half-mesas attached to the boundary. The latter are equivalent to an "inverted mesa" patterns. This situation is shown in the Figure 2.6.

Fix $\varepsilon = 0.15$, $L = 1$. Moreover choose $\beta = -0.1 < 0$ so that the roof of the mesa occupies more space than its floor ($l = 0.45 < 1/2$). In this case, the instability threshold for a single mesa given by (2.71), $D_1 \sim 2223$ and for the inverted mesa it is given by (2.74), $D_1^i = 230$. Moreover the instability thresholds for K interior mesas on the interval $2LK$ with $K > 1$ is also (2.73) $D_K \sim 230$. This threshold is also the same for two boundary mesas or K inverted mesas as given by (2.75).

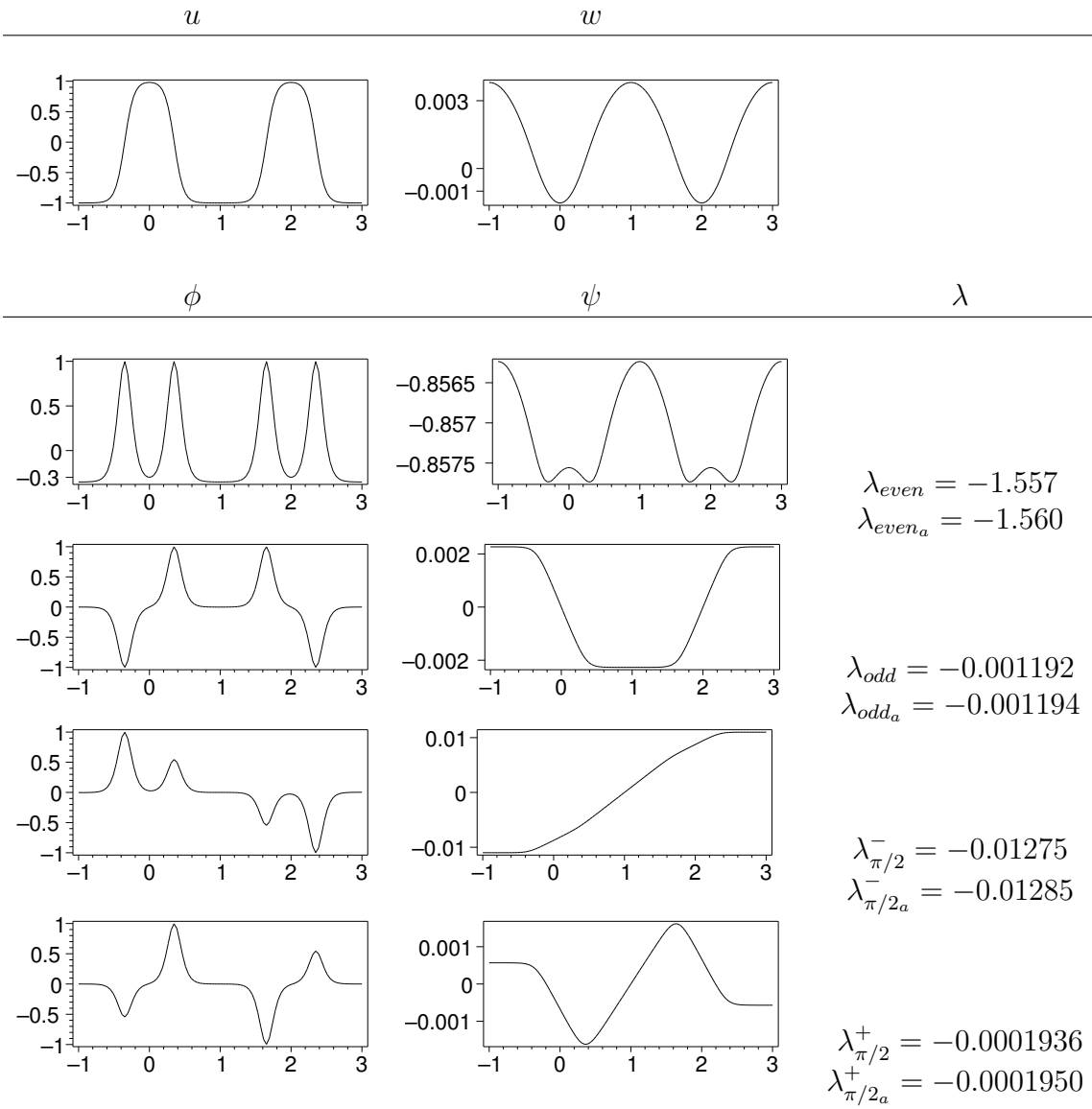

Figure 2.4: Top row: steady-state with two mesas. The cubic model (1.12) was used with $L = 1, \varepsilon = 0.13, D = 40, \beta = -0.3$. Bottom four rows: the four possible eigenfunctions and the corresponding eigenvalues computed using Maple. Asymptotic values (labeled with subscript a) are computed using (2.20). Excellent agreement is observed.

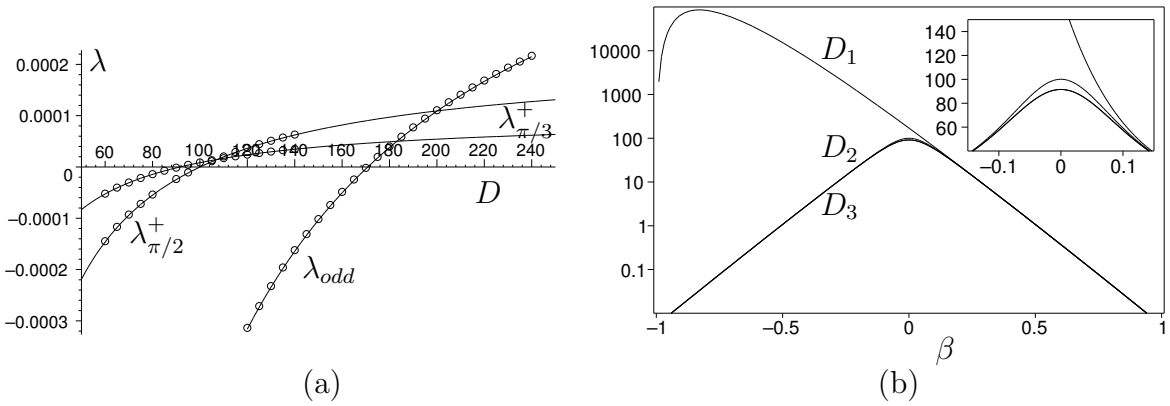

Figure 2.5: Instability thresholds of the K-mesa pattern in the cubic model with $K = 1, 2$ and 3. (a) $L = 1, \varepsilon = 0.17, \beta = 0$. Circles show λ as computed by numerically solving (2.19) for different values of D and the three different modes, as indicated. Solid curves are the asymptotic approximations for λ as given by (2.20). The K-mesa pattern is unstable for $D > D_K$ where $D_1 = 171,\ D_2 = 100,\ D_3 = 91$. (b) The graph of D_K versus β with $L = 1, \varepsilon = 0.17$, as given by Principal Result 2.2.1.The insert shows the zoom near $\beta = 0$.

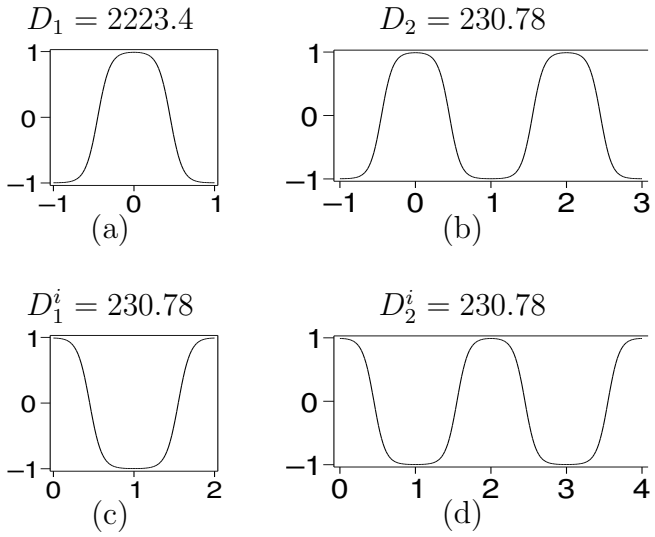

Figure 2.6: (a) Single Interior mesa (b) Two interior mesas (c) Double boundary half-mesas, or an inverted single interior mesa (d) Two half-mesas at the boundaries and one interior mesa, or an inverted two-mesa pattern. In all four cases, $\beta = -0.1$ and $\varepsilon = 0.15$. The instability threshold for D is given above the graph. The case (a) has the biggest stability range here since $l < L/2$.

2.4.2 Model of B-Z Reaction in Water-in-oil Microemulsion

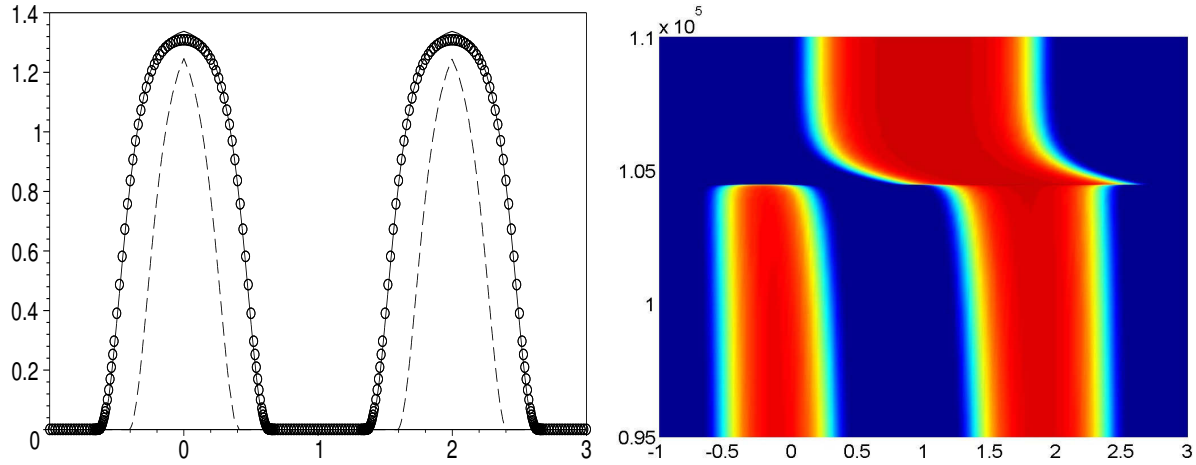

(a) (b)

Figure 2.7: (a) A stable two-mesa solutions to Belouzov-Zhabotinskii model (1.2). Parameter values are $D = 100$, $\varepsilon = 0.1$, $q = 0.001$ and $f_0 = 0.61$. Circles show the numerical solution. The solid line shows the asymptotic approximation as computed in Proposition 2.1.1, with the mesa half-length l computed to two orders. The dashed line is the same approximation, except l_1 is set to zero. (b) Time evolution in the BZ model. Parameter values are the same as in (a), except for $f_0 = 0.63$. Initial conditions were given in the form of a two-mesa asymptotic solution, but shifted to the left by 0.1. The two-mesa equilibrium is unstable, though the instability is very slow and the two-mesa solution persists until about $t \sim 10^5$. This is in good agreement with the theoretical instability threshold of $f_0 \sim 0.612$.

The cubic model is unusual in the sense that due to the symmetry of the interface, the correction to interface length l_1 of Proposition 2.1.1 is zero. To see the more usual case when it is not, we consider the Belousov-Zhabotinskii model (1.2):

$$f(u,w) = -f_0\frac{u-q}{u+q} + wu - u^2; \qquad g(u,w) = 1 - uw; \qquad q \ll 1. \tag{2.78}$$

As was done in [36], in the limit $q \ll 1$, the condition (2.4) reduces to

$$\int_0^{u_+} \left(-f_0 + w_0 u - u^2\right) du \sim 0 \sim -f_0 + w_0 u_+ - u_+^2$$

and we obtain to leading order,

$$u_- \sim 0; \quad u_+ \sim \sqrt{3f_0}; \quad w_0 \sim 4\sqrt{f_0/3} \quad \text{as } q \to 0.$$

(in fact, $u_- = O(q) \ll 1$). To leading order, the profile U_0 then solves $U_0'' - f_0 + 4\sqrt{f_0/3}U_0 - U_0^2 = 0$ for $y < 0$; with $U_0(0) = 0 = U_0'(0)$ and $U_0(y) = 0$ for $y > 0$ and $U_0 \to u_+$ as $y \to -\infty$. We then obtain

$$U_0 \sim \begin{cases} \sqrt{3f_0}\tanh^2\left(3^{-1/4}f_0^{1/4}2^{-1/2}y\right), & y < 0 \\ 0, \ y > 0 \end{cases}.$$

and

$$g_- = 1, \quad g_+ \sim 1 - 4f_0$$
$$l_0 = \frac{L}{4f_0}.$$

Next we compute l_1 using (2.10). We have

$$\begin{aligned} &\int_{-\infty}^{0} [g(U_0(y), w_0) - g_+] \\ &= \int_{-\infty}^{0} 4f_0 - 4f_0 \tanh^2\left(3^{-1/4}f_0^{1/4}2^{-1/2}y\right) \\ &= 4f_0 \int_0^{\infty} \operatorname{sech}^2\left(3^{-1/4}f_0^{1/4}2^{-1/2}y\right) = 3^{1/4}2^{1/2}4f_0^{3/4} \end{aligned}$$

so that

$$l_1 = 3^{1/4}2^{1/2}f_0^{-1/4}.$$

Finally, we have

$$U_0 \sim \sqrt{3f_0}\tanh^2\left(3^{-1/4}f_0^{1/4}2^{-1/2}y\right) \sim \sqrt{3f_0}\left(1 - 4\exp(3^{-1/4}f_0^{1/4}2^{1/2}y)\right) \text{ as } y \to -\infty$$

so that

$$\begin{aligned} C_+ &= 4\sqrt{3f_0}; \quad \mu_+ = 3^{-1/4}f_0^{1/4}2^{1/2}; \\ \int_{u_-}^{u_+} f_w &= \frac{u_+^2}{2} = \frac{3f_0}{2}; \\ \alpha_+ &= 64 \cdot 3^{-3/4}f_0^{3/4}2^{3/2}\exp(-2\mu_+ l_1)\frac{1}{\varepsilon}\exp\left(-\frac{2\mu_+}{\varepsilon}l_0\right) \\ &= 64 \cdot 3^{-3/4}f_0^{3/4}2^{3/2}\exp(-4)\frac{1}{\varepsilon}\exp\left(-\frac{2^{-0.5}3^{-0.25}}{\varepsilon f_0^{0.75}}L\right) \end{aligned}$$

On the other hand, $\mu_- = O(1/q) \gg \mu_+$, so that the critical threshold given by (2.18) becomes

$$\begin{aligned} D_K =& C_0\varepsilon(1 - 4f_0)^2 f_0^{-1.75}\exp\left(\frac{2^{-0.5}3^{-0.25}}{\varepsilon f_0^{0.75}}L\right), \\ C_0 \equiv& e^4 3^{0.75}2^{-10.5} = 0.085942, \quad K \geq 2 \end{aligned} \tag{2.79}$$

To verify this formula numerically, we set $D = 100$, $\varepsilon = 0.1$, $q = 0.001$, $L = 1$ and $K = 2$. Next we solved (2.1) for several different values of f_0, with initial conditions given by the two-mesa steady state approximation on the interval $[-1, 3]$, perturbed by a small shift of size 0.1. We found the two-mesa state was unstable with $f_0 = 0.62$ or higher but became stable when we took $f_0 = 0.61$ or lower. This is seen in Figure 2.7. On the other hand, the threshold value as predicted by (2.79) with above parameter values and $D_K = D$ is $f_0 = 0.6124$. Thus we obtain an excellent agreement between the asymptotic theory and direct numerical simulations.

In Figure 2.7(a), the approximation with and without l_1 to the steady state is shown. We remark that it was essential to compute the correction l_1 to the mesa width; if we were to set $l_1 = 0$ the constant $C_0 = 0.085942$ in (2.79) would be replaced by 0.00157.

2.5 Discussion

We have examined in detail the route to instability of the K-mesa pattern of (2.1) as the diffusion coefficient D is increased. The onset of instability occurs for exponentially large D; it is well known that such solution is unstable for the shadow system case $D \to \infty$ [55]. We have computed instability thresholds D_K given by Principal Result 2.2.1. We have also determined the mesa dynamics when D is large.

The instability thresholds are closely related to the *coarsening* phenomenon. An example of this type of phenomenon can be observed in the Lengyel-Epstein model (1.3) and is seen in Figure 1.2(a). The time evolution of u is shown; with parameters $\varepsilon = 0.06$, $a = 10$, $D = 500$, $\tau = 0.1$, and domain size is 8. Starting with random initial conditions, Turing instability leads to a formation of a three-mesa pattern at $t \sim 10$. However such pattern is unstable, even though this only becomes apparent much later (at $t \sim 100$). The resulting two-mesa pattern then drifts towards a symmetric position where it eventually settles. A similar phenomenon for the Belousov-Zhabotinskii model (1.2) is illustrated in Figure 2.7(b). It shows the time-evolution a two mesa solution to (1.2) with $D > D_2$, starting with initial conditions that consist of a slightly perturbed two-mesa pattern. After a very long time, one of the mesas absorbs the mass of the other, then moves towards the center of the domain where it remains as a stable pattern.

The coarsening phenomenon has been analyzed for the Brusselator model in [34]. The authors conjectured a formula for D_K (for $K > 1$) which was given in Principal Result 2.2.1. This was done without computing the eigenvalues, by constructing the asymmetric patterns. When $O(\alpha_+) \neq O(\alpha_-)$, D_K does not depend on K, and so the instability thresholds can be determined from the asymmetric patterns. In the case $\mu_+ l = \mu_-(L - l)$, D_K depends on K, and, thus, the calculation of the eigenvalues is needed. The coarsening phenomenon observed in reaction-diffusion systems is also similar of Ostwald ripening in thin fluids – see for example [16], [62] and references therein.

There are some similarities between the instability thresholds for mesa patterns computed here, and instability thresholds for Gierer-Meinhardt system computed in [27], [78]. Note that in [27], a singular perturbation and matrix algebra approach was used whereas in [78] an approach using Evans functions and Floquet exponents was used. In the analysis here we used both singular perturbations and Floquet exponents.

We remark that the GM model with saturation (1.5) exhibits mesa patterns when the saturation is sufficiently large, but exhibits spikes when saturation is small. It is an interesting open question to examine the mechanism by which a mesa can become a spike and how the various instability thresholds change from being exponentially large to algebraically large as saturation is decreased.

Chapter 3

Mesa Patterns on a Thin Domain

In this chapter, we consider the following two-dimensional system

$$\begin{cases} u_t = \varepsilon^2 \Delta u + f(u, w) \\ \tau w_t = D\Delta w + g(u, w) \end{cases} \tag{3.1}$$

on the domain

$$\Omega = \{(x, y) : a \leq x \leq b, 0 \leq y \leq H(x)\} \tag{3.2}$$

with Neumann boundary conditions

$$\frac{\partial u}{\partial n} = 0, \ \frac{\partial w}{\partial n} = 0 \ \text{ on } \ \partial\Omega \tag{3.3}$$

where $\frac{\partial}{\partial n}$ is the normal derivative. We assume that the domain is thin, that is,

$$H(x) = \delta h(x) \ \text{ where } \ 0 < \delta \ll \varepsilon \ \text{ and } \ h(x) = \mathcal{O}(1). \tag{3.4}$$

We approximate this problem to a one-dimensional problem with a dependence on $h(x)$.

Linearizing around the steady state, we obtain an eigenvalue problem with Neumann boundary conditions. Using the same techniques as used in Chapter 2, we determine the eigenvalues of this linearized problem: first by considering the eigenvalue problem with periodic boundary conditions and then extending the result to the Neumann boundary problem. From these eigenvalues, we determine the stability of the mesa patterns. For a particular $h(x)$, there exists a large threshold value, D_c, of $\mathcal{O}(\frac{1}{\varepsilon})$, such that the mesa patterns become unstable if $D > D_c$. Here we assume that the effect of the boundary terms and interactions between interfaces is negligible. In order for this assumption to be valid, we require $\ln D \ll \mathcal{O}(\frac{1}{\varepsilon})$. The instability

studied in this chapter arises from effects of the domain, whereas, in Chapter 2, the instability arises from the exponentially small interactions between the interfaces and the boundary.

3.1 Reducing the 2D Problem to 1D

Now we demonstrate how the two dimensional problem above can be approximated by a one dimensional problem. This is a common lubrication theory approach; see [24, 76]. The boundary conditions (3.3) can be written as

$$\text{at } y = \delta h(x): \ \delta h'(x) u_x = u_y, \ \ \delta h'(x) w_x = w_y, \tag{3.5}$$

$$\text{at } y = 0: \qquad u_y = 0, \ \ w_y = 0. \tag{3.6}$$

Let

$$\bar{y} = \frac{y}{\delta}. \tag{3.7}$$

Then (3.1) can be written as

$$u_t = \varepsilon^2 \left(u_{xx} + \frac{1}{\delta^2} u_{\bar{y}\bar{y}} \right) + f(u, w), \tag{3.8}$$

$$w_t = D \left(w_{xx} + \frac{1}{\delta^2} w_{\bar{y}\bar{y}} \right) + g(u, w) \tag{3.9}$$

and the domain Ω can be rewritten as

$$\Omega = \{(x, \bar{y}) : a \leq x \leq b, 0 \leq \bar{y} \leq h(x)\}. \tag{3.10}$$

We expand u and w in terms of δ^2 (where δ is small)

$$u = u_0 + \delta^2 u_1 + \ldots, \ \ w = w_0 + \delta^2 w_1 + \ldots \tag{3.11}$$

so that, substituting these expansions for u and w into (3.8), we have

$$\varepsilon^2 u_{0\bar{y}\bar{y}} = 0, \tag{3.12}$$

$$u_{0t} = \varepsilon^2 u_{0xx} + \varepsilon^2 u_{1\bar{y}\bar{y}} + f(u_0, w_0). \tag{3.13}$$

From the expansion of u, the boundary conditions (3.5) and (3.6) yield

$$\text{at } \bar{y} = 0: \qquad u_{0\bar{y}} = 0, \quad u_{1\bar{y}} = 0, \tag{3.14}$$

$$\text{at } \bar{y} = h(x): \ u_{0\bar{y}} = 0, \quad u_{1\bar{y}} = h'(x) u_{0x}. \tag{3.15}$$

Note that (3.12) implies that u_0 does not depend on $\bar{y}$, so $u_0 \sim u_0(x)$. Integrating (3.13) with respect to $\bar{y}$ from 0 to $h(x)$, we obtain

$$\begin{aligned} -\varepsilon^2 \int_0^{h(x)} u_{1\bar{y}\bar{y}} d\bar{y} &= \int_0^{h(x)} \left(\varepsilon^2 u_{0xx} + f(u_0, w_0) - u_{0t}\right) d\bar{y} \\ \Longrightarrow -\varepsilon^2 h'(x) u_{0x} &= \left(\varepsilon^2 u_{0xx} + f(u_0, w_0) - u_{0t}\right) h(x). \end{aligned}$$

Dividing by $h(x)$ and simplifying, we obtain

$$u_{0t} = \frac{\varepsilon^2}{h(x)} \left[h(x) u_{0x}\right]_x + f(u_0, w_0). \tag{3.16}$$

In a similar way, we obtain

$$\tau w_{0t} = \frac{D}{h(x)} \left[h(x) w_{0x}\right]_x + g(u_0, w_0). \tag{3.17}$$

Dropping the subscripts and letting $\tau = 0$, we obtain the one-dimensional system

$$\begin{cases} u_t = \frac{\varepsilon^2}{h(x)} \left[h(x) u_x\right]_x + f(u, w) \\ 0 = \frac{D}{h(x)} \left[h(x) w_x\right]_x + g(u, w) \end{cases} \tag{3.18}$$

with $x \in [a, b]$ and Neumann boundary conditions.

3.2 Eigenvalue Problem for a Single Mesa Solution

As we did in Chapter 2, we consider mesa pattern solutions of (3.18). We begin by considering a one interface solution of u, that is, a half mesa pattern of (3.18) on $[0, L]$. As before we assume that $D \gg 1$.

For a single interface solution, we determine the location of the interface by integrating the equation for w of (3.18)

$$0 = \frac{D}{h(x)} \left[h(x) w_x\right]_x + g(u, w) \tag{3.19}$$

over the domain $[0, L]$. Then the interface l is defined implicitly by

$$-g_+ \int_0^l h(x) dx - g_- \int_l^L h(x) dx = 0 \tag{3.20}$$

where $g_+ = g(u_+, w_0)$ and $g_- = g(u_-, w_0)$. To show that such an l exists, we consider the function

$$F(l) \equiv -g_+ \int_0^l h(x) dx - g_- \int_l^L h(x) dx.$$

Since $h(x)$ is positive and continuous, we have that $F(l)$ is continuous on $[0, L]$. We have

$$F(0) = -g_- \int_0^L h(x)dx, \quad F(L) = -g_+ \int_0^L h(x)dx$$

where $\int_0^L h(x)dx$ is a positive constant. Thus, if g_- and g_+ are opposite signs, that is, $g_+g_- < 0$, by the Intermediate Value Theorem, $F(l) = 0$ at some $x = l$. Therefore the interface l defined by (3.20) exists. Note that $F'(l) = -g_+h(l) + g_-h(l)$. Since $-g_+$, g_- have the same sign and $h(l) > 0$, $F(l)$ is monotonic on $[0, L]$ and, thus, l is unique.

Let (u, w) be the equilibrium solution. Linearizing around the steady state

$$\begin{cases} u(x,t) \sim u(x) + e^{\lambda t}\phi(x) \\ w(x,t) \sim w(x) + e^{\lambda t}\psi(x) \end{cases} \tag{3.21}$$

and substituting this into the system (3.18), we obtain

$$\begin{cases} \lambda\phi = \frac{\varepsilon}{h(x)}[h(x)\phi_x]_x + \phi f_u(u_0, w_0) + \psi f_w(u_0, w_0) \\ 0 = \frac{D}{h(x)}[h(x)\psi_x]_x + \phi g_u(u_0, w_0) + \psi g_w(u_0, w_0) \end{cases}. \tag{3.22}$$

For a symmetric single mesa solution, consisting of two interfaces located at $\pm l$, we now determine the eigenvalues of this linearized problem.

Principal Result 3.2.1. *Consider a single mesa solution u of (3.18) in the limit*

$$\varepsilon \ll 1, D \gg 1 \tag{3.23}$$

on the interval $[-L, L]$ with Neumann boundary conditions. Assume $h(x)$ is positive, differentiable and symmetric about $x = 0$. Also, assume

$$g_+ \cdot g_- < 0, \quad g_w - g_u\frac{f_w}{f_u} < 0, \quad \text{and } \frac{\int_{u_-}^{u_+} f_w du}{g_- - g_+} > 0. \tag{3.24}$$

Then eigenvalues corresponding to the even and odd eigenfunctions of (3.22) are

$$\lambda_{even} \sim -\frac{\varepsilon}{\kappa_0}(g_+ - g_-)\frac{h(l)}{\int_0^L h(x)\sigma(x)dx} \tag{3.25}$$

and

$$\lambda_{odd} \sim \frac{\varepsilon}{D}\frac{1}{\kappa_0}(g_+ - g_-)\left(\frac{g_-}{g_+ - g_-}\int_l^L \frac{h(x)}{h(l)}dx - \int_0^l \frac{h(l)}{h(x)}dx\right) - \varepsilon^2 G'(l) \tag{3.26}$$

where l and $-l$ are the locations of the interfaces and l is implicitly defined by

$$-g_+\int_0^l h(x)dx - g_-\int_l^L h(x)dx = 0 \tag{3.27}$$

and

$$G(x) = \frac{h'(x)}{h(x)}. \tag{3.28}$$

Also, as in Chapter 2, we define

$$\sigma(x) = g_w - \frac{f_w}{f_u}g_u = \begin{cases}\sigma_+, & |x| < l\\ \sigma_-, & l < |x| < L\end{cases}, \tag{3.29}$$

$$\kappa_0 = \frac{\int_{-\infty}^{\infty} U_{0y}^2 dy}{\int_{u_-}^{u_+} f_w(u_0, w_0)du}, \tag{3.30}$$

$g_\pm = g(u_\pm, w_0)$ and U_0 is given by (2.7).

Derivation of Result 3.2.1.

First, consider the steady state equations

$$\begin{cases} 0 = \frac{\varepsilon^2}{h(x)}\left[h(x)u_x\right]_x + f(u,w)\\ 0 = \frac{D}{h(x)}\left[h(x)w_x\right]_x + g(u,w)\end{cases}. \tag{3.31}$$

From the steady state equations, we expand u and w in terms of $\frac{1}{D}$ as follows

$$u = u_0 + \frac{1}{D}u_1 + \ldots, \quad w = w_0 + \frac{1}{D}w_1 + \ldots. \tag{3.32}$$

Then substituting (3.32) into (3.31), we obtain

$$0 = \frac{\varepsilon^2}{h(x)}[h(x)u_{0x}]_x + f(u_0, w_0), \tag{3.33}$$

$$0 = \frac{\varepsilon^2}{h(x)}[h(x)u_{1x}]_x + u_1 f_u(u_0, w_0) + w_1 f_w(u_0, w_0,) \tag{3.34}$$

$$0 = \frac{1}{h(x)}[h(x)w_{0x}]_x, \tag{3.35}$$

$$0 = \frac{1}{h(x)}[h(x)w_{1x}]_x + g(u_0, w_0). \tag{3.36}$$

Let l be the location of the interface. We expand x as $x = l + \varepsilon y$ and write

$$\frac{h'(x)}{h(x)} \sim \frac{h'(l)}{h(l)} + \left[\frac{h''(l)}{h(l)} - \left(\frac{h'(l)}{h(l)}\right)^2\right]\varepsilon y. \tag{3.37}$$

Let $G(x)$ be as in (3.28), so that $G(x) \sim G(l) + G'(l)\varepsilon y$. Then (3.33) becomes

$$0 = u_{0yy} + \varepsilon \left(G(l) + G'(l)\varepsilon y\right) u_{0y} + f(u_0, w_0) \tag{3.38}$$

and (3.34) becomes

$$0 = u_{1yy} + \varepsilon \left(G(l) + G'(l)\varepsilon y\right) u_{1y} + u_1 f_u(u_0, w_0) + w_1 f_w(u_0, w_0). \tag{3.39}$$

Near the interface $x = l$, we estimate

$$\phi \sim c u_{0_x}, \quad \psi \sim \psi(l). \tag{3.40}$$

Note that $\psi(l)$ is of $\mathcal{O}(\frac{1}{D})$. Away from the interface, the diffusion term is negligible, so we estimate

$$\phi \sim -\frac{f_w(u_0, w_0)}{f_u(u_0, w_0)}\psi. \tag{3.41}$$

Expanding as before in (3.32), the equation for ϕ becomes

$$\begin{aligned}\lambda\phi =& \varepsilon^2\phi_{xx} + \varepsilon^2 G(x)\phi_x + \psi f_w(u_0, w_0) \\ &+ \phi\left(f_u(u_0, w_0) + \frac{1}{D}(f_{uu}(u_0, w_0)u_1 + f_{uw}(u_0, w_0)w_1)\right).\end{aligned} \tag{3.42}$$

We multiply by u_{0x} and integrate over the domain $[0, L]$ to obtain

$$\begin{aligned}\int_0^L \lambda c u_{0x}^2 dx = &\int_0^L \varepsilon^2\phi_{xx}u_{0x}dx + \int_0^L \varepsilon^2 G(x)\phi_x u_{0x}dx + \int_0^L u_{0x}\psi f_w(u_0, w_0)dx \\ &+ \int_0^L u_0'\phi\left(f_u(u_0, w_0) + \frac{1}{D}(f_{uu}(u_0, w_0)u_1 + f_{uw}(u_0, w_0)w_1)\right)dx\end{aligned} \tag{3.43}$$

where we have replaced ϕ in the first integral as in (3.40). As before, we make a change of variables: x as $x = l + \varepsilon y$. After simplifying, we obtain

$$\begin{aligned}\lambda c\frac{1}{\varepsilon}\int_{-\infty}^{\infty} u_{0y}^2 dy = &\int_{-\infty}^{\infty}\phi_{yy}u_{0y}dy + \int_{-\infty}^{\infty}\phi u_{0y}f_u(u_0, w_0)dy + \int_{-\infty}^{\infty}\psi u_{0y}f_w(u_0, w_0)dy \\ &+ \int_{-\infty}^{\infty}\frac{1}{D}\phi u_{0y}(f_{uu}(u_0, w_0)u_1 + f_{uw}(u_0, w_0)w_1)\,dy \\ &+ \int_{-\infty}^{\infty}\varepsilon\left(G(l) + G'(l)\varepsilon y\right)\phi_y u_{0y}dy.\end{aligned} \tag{3.44}$$

Integrating by parts, we obtain

$$\int_{-\infty}^{\infty}\phi_{yy}u_{0y}dy \sim \int_{-\infty}^{\infty}\phi u_{0yyy}dy \tag{3.45}$$

where it has been assumed that the boundary terms that arise from integrating by parts are sufficiently small that they are negligible.

Differentiating (3.33) with respect to y, we obtain

$$u_{0yyy} + f_u(u_0, w_0)u_{0y} = -\varepsilon\left(G(l) + G'(l)\varepsilon y\right)u_{0y} - \varepsilon^2 G'(l)u_{0y}. \tag{3.46}$$

Similarly, differentiating (3.34), we obtain

$$\begin{aligned} u_{0y}\left(u_1 f_{uu}(u_0, w_0) + w_1 fuw(u_0, w_0)\right) = &- u_{1yyy} - \varepsilon\left(G(l) + G'(l)\varepsilon y\right)u_{1y} - \varepsilon^2 G'(l)u_{1y} \\ &- u_{1y}f_u(u_0, w_0) - w_{1y}f_w(u_0, w_0). \end{aligned} \tag{3.47}$$

Writing $\phi \sim c\frac{1}{\varepsilon}u_{0y}$, $\phi_y \sim c\frac{1}{\varepsilon}u_{0yy}$ and using the expressions above, the equation for the eigenvalue becomes

$$\begin{aligned} \lambda c\frac{1}{\varepsilon}\int_{-\infty}^{\infty} u_{0y}^2 dy \sim &\int_{-\infty}^{\infty} c\frac{1}{\varepsilon}u_{0y}\left(-\varepsilon\left(G(l) + G'(l)\varepsilon y\right)u_{0y} - \varepsilon^2 G'(l)u_{0y}\right)dy \\ &+ \int_{-\infty}^{\infty}\psi f_w(u_0, w_0)u_{0y}dy + \int_{-\infty}^{\infty} c\frac{1}{\varepsilon}u_{0yy}\left(G(l) + G'(l)\varepsilon y\right)u_{0y}dy \\ &+ \int_{-\infty}^{\infty} c\frac{1}{\varepsilon}\frac{1}{D}u_{0y}\left[-u_{1yyy} - \varepsilon\left(G(l) + G'(l)\varepsilon y\right)u_{1y} - \varepsilon^2 G'(l)u_{1y}\right. \\ &\left.-u_{1y}f_u(u_0, w_0) - w_{1y}f_w(u_0, w_0)\right]dy \end{aligned} \tag{3.48}$$

Simplifying, as we did in Chapter 2, in the derivation of Principal Result 2.2.1, we write $\int_{-\infty}^{\infty} u_{0y}f_w dy = -\int_{u_-}^{u_+} f_w du$, then we have

$$\lambda c\frac{\int_{-\infty}^{\infty} u_{0y}^2 dy}{\int_{u_-}^{u_+} f_w du} = \varepsilon\left(c\frac{1}{D}w_{1x}(l) - \psi(l)\right) - \varepsilon^2 cG'(l)\frac{\int_{-\infty}^{\infty} u_{0y}^2 dy}{\int_{u_-}^{u_+} f_w du}. \tag{3.49}$$

Define κ_0 as in (3.30). Then

$$\lambda\kappa_0 = \varepsilon\left[\frac{1}{D}w_{1x}(l) - \psi(l)\right] - \varepsilon^2 G'(l)\kappa_0. \tag{3.50}$$

Next, we determine the terms in the square brackets above. For the term $w_{1x}(l)$, we integrate (3.36) from 0 to x

$$h(x)w_{1x} = \int_0^x -g(u_0, w_0)h(x)dx, \tag{3.51}$$

from which we obtain

$$w_{1x}(l) = -g_+\int_0^l \frac{h(x)}{h(l)}dx. \tag{3.52}$$

Next, let us determine $\psi(l)$. From the equation for ψ in (3.22), we have

$$\frac{D}{h(x)}\left[h(x)\psi_x\right]_x + g_u(u_0, w_0)\phi + g_w(u_0, w_0)\psi = 0. \tag{3.53}$$

Then we have

$$\psi(x) \sim -(g_- - g_+)\eta(x; l) \tag{3.54}$$

where $\eta(x; l)$ is the solution of

$$\frac{D}{h(x)}\left[h(x)\eta_x\right]_x + \sigma(x)\eta = \delta(x - l) \tag{3.55}$$

where

$$\sigma(x) = g_w - g_u\frac{f_w}{f_u} = \begin{cases} \sigma_+, & |x| < l \\ \sigma_-, & |x| > l \end{cases}.$$

Note that this is obtained in the same way as in Chapter 2 in equation (2.33).

Consider the odd eigenfunction corresponding to the boundary conditions

$$\eta(0) = 0, \quad \eta'(L) = 0. \tag{3.56}$$

Since D is large, (3.55) to leading order is

$$\frac{D}{h(x)}\left[h(x)\eta_x\right]_x \sim \delta(x - l). \tag{3.57}$$

On the interval $[l, L]$, $\eta \sim \eta_0$ where η_0 is a constant. On the interval $[0, l]$, $\eta(x) \sim \int_0^x \frac{A}{h(x)}dx$ where A is a constant to be determined. The function η must be continuous at the interface l which gives the condition $\eta(l^+) = \eta(l^-)$. The jump condition at the interface gives

$$\eta'(l^+) - \eta'(l^-) = \frac{1}{D}. \tag{3.58}$$

Solving we obtain

$$A = -\frac{h(l)}{D}. \tag{3.59}$$

Then, we have

$$\psi(l) \sim -(g_- - g_+)\eta(l; l) = (g_- - g_+)\int_0^l -\frac{1}{D}\frac{h(l)}{h(x)}dx. \tag{3.60}$$

Thus, we obtain (3.26) in Principal Result 3.2.1.

Next, consider the even eigenfunction corresponding to the boundary conditions

$$\eta'(0) = 0, \quad \eta'(L) = 0. \tag{3.61}$$

Integrating (3.55) over the domain $[0, L]$

$$\eta(l) \sim \frac{h(l)}{\int_0^L h(x)\sigma(x)dx}. \tag{3.62}$$

Therefore,

$$\psi(l) \sim (g_+ - g_-)\frac{h(l)}{\int_0^L h(x)\sigma(x)dx} \tag{3.63}$$

Note that $\psi(l)$ is of $\mathcal{O}(1)$, so that, to leading order, (3.50) gives (3.25) in Principal Result 3.2.1.

3.3 Eigenvalue Problem for Multiple Mesa Solution

Next we consider the stability of a K mesa pattern of (3.18), using the methods of Chapter 2. The K mesa pattern is defined as before on the domain $[-L, (2K-1)L]$, with the interfaces of one mesa located at $\pm l$ where the other $K-1$ mesas are obtained by extending the single mesa symmetrically. We assume that $h(x)$ is positive, differentiable and symmetric around $x = 0$ on the interval $[-L, L]$. Then, in order to construct a symmetric K mesa solution, we assume that $h(x)$ is extended periodically to the entire domain $[-L, (2K-1)L]$.

Principal Result 3.3.1. *Consider the steady state of (3.18) consisting of K mesas on the interval $[-L, (2K-1)L]$ with Neumann boundary conditions. Assume that the assumptions (3.24) hold. Assume that $h(x)$ is positive, differentiable and symmetric around $x = 0$ on the interval $[-L, L]$. Also, assume that $h(x)$ is extended periodically to the entire domain $[-L, (2K-1)L]$. The linearized problem (3.22) admits $2K$ eigenvalues given by λ_{even} and λ_{odd} in Principal Result 3.2.1 , and the other $2K-2$ eigenvalues given by*

$$\lambda_\theta^{\pm} = a \pm |b| \tag{3.64}$$

where

$$a = \frac{\varepsilon}{\kappa_0}\frac{g_-}{D}\int_l^L \frac{h(x)}{h(l)}dx - \varepsilon^2 G'(l) + \frac{\varepsilon}{\kappa_0}\frac{g_+ - g_-}{D}\frac{1}{1-\cos\theta}\int_0^L \frac{h(l)}{h(x)}dx, \tag{3.65}$$

$$\begin{aligned}|b|^2 =& \frac{\varepsilon^2}{\kappa_0^2}\frac{1}{1-\cos\theta}\left(\frac{g_+ - g_-}{D}\right)^2\left\{2\left(\int_0^l \frac{h(l)}{h(x)}dx\right)^2 - 2\left(\int_0^l \frac{h(l)}{h(x)}dx\right)\left(\int_0^L \frac{h(l)}{h(x)}dx\right)\right.\\ &\left. + \left(\frac{1}{1-\cos\theta}\right)\left(\int_0^L \frac{h(l)}{h(x)}dx\right)^2\right\}\end{aligned} \tag{3.66}$$

where l is implicitly defined by (3.27) and where

$$\theta = \frac{j\pi}{K}, \quad j = 1, \ldots, K-1. \tag{3.67}$$

Also $G(x)$ is given in (3.28), $\sigma(x)$ in (3.29), κ_0 in (3.30) and U_0 in (2.7).

Derivation of Result 3.3.1.

As we did in Chapter 2, instead of considering (3.22) with Neumann boundary conditions directly, we consider the linearized problem on the interval $[-L, L]$ with the boundary conditions

$$\phi(L) = z\phi(-L), \quad \phi'(L) = z\phi'(-L), \quad \psi(L) = z\psi(-L), \quad \psi'(L) = z\psi'(-L), \tag{3.68}$$

where, by choosing

$$z = \exp(2\pi ij/K), \; j = 0, \ldots, K-1, \tag{3.69}$$

we obtain a periodic solution to the eigenvalue problem on $[-L, (2K-1)L]$. This result is extended to the case with Neumann boundary conditions, which then gives Principal Result 3.3.1.

We begin by estimating

$$\phi \sim c_{\pm} u_{0x}, \; \psi \sim \psi(\pm l) \text{ when } x \sim \pm l. \tag{3.70}$$

We proceed in a similar manner as we did for one mesa. We multiply the equation for ϕ in (3.22) by u_{0x} and integrate on $[0, L]$, as we did in the derivation of Result 3.2.1, and as before, we obtain

$$\lambda c_+ \kappa_0 = \varepsilon \left[c_+ \frac{1}{D} w_{1x}(l) - \psi(l) \right] - \varepsilon^2 G'(l) c_+ \kappa_0. \tag{3.71}$$

Similarly, by multiplying the equation for ϕ in (3.22) by u_{0x} and integrating on $[-L, 0]$, we obtain

$$\lambda c_- \kappa_0 = \varepsilon \left[\psi(-l) - \frac{1}{D} c_- w_{1x}(-l) \right] - \varepsilon^2 G'(-l) c_- \kappa_0. \tag{3.72}$$

Now we determine the terms inside the square brackets. Integrating (3.36), we estimate

$$w_{1x}(l) \sim \frac{1}{h(l)} g_- \int_l^L h(x)dx \sim -w_{1x}(-l) \tag{3.73}$$

Next, we determine the terms $\psi(\pm l)$. As in §3.2 we have the following equation for ψ

$$\frac{D}{h(x)} \left[h(x)\psi_x \right]_x + g_u(u_0, w_0)\phi + g_w(u_0, w_0)\psi = \delta(x-l) + \delta(x+l), \tag{3.74}$$

so that

$$\psi(x) \sim \frac{-(g_+ - g_-)}{D} h(x) \left(c_- \eta(x; -l) - c_+ \eta(x; l) \right) \tag{3.75}$$

where $\eta(x; x_0)$ is the solution to

$$\frac{D}{h(x)} \left[h(x) \eta_x \right]_x + \sigma(x) \eta = \delta(x - x_0) \tag{3.76}$$

with $\sigma(x)$ as given in (3.29).

For $z \neq 1$, to leading order, we have the following problem

$$\begin{cases} \left[h(x) \eta_x \right]_x = 0 \\ \eta(x_0^-; x_0) = \eta(x_0^+, x_0) \\ \eta'(x_0^+; x_0) - \eta'(x_0^-; x_0) = \frac{1}{h(l)} \end{cases}$$

Solving this, we obtain

$$\eta \sim \begin{cases} A + Bh(-L) \int_{-L}^{x} \frac{1}{h(x)} dx, & x < x_0 \\ A + Bh(-L) \int_{-L}^{x_0} \frac{1}{h(x)} dx + (1 + Bh(-L)) \int_{x_0}^{x} \frac{1}{h(x)} dx, & x > x_0 \end{cases}. \tag{3.77}$$

Now, from the boundary conditions (3.68), we determine the constants A and B to be

$$B = \frac{1}{h(-L)} \frac{1}{z - \frac{h(-L)}{h(L)}}, \tag{3.78}$$

$$A = \frac{1}{z-1} \left(\int_{x_0}^{L} \frac{1}{h(x)} dx + \frac{h(-L)}{h(L)} \left(\frac{1}{z - \frac{h(-L)}{h(L)}} \right) \int_{-L}^{L} \frac{1}{h(x)} dx \right). \tag{3.79}$$

Recall that $h(x)$ is symmetric which allows us to simplify and we obtain

$$\eta(l; l) = \frac{z}{(z-1)^2} \int_{-L}^{L} \frac{1}{h(x)} dx \tag{3.80}$$

$$\eta(-l; -l) = \frac{z}{(z-1)^2} \int_{-L}^{L} \frac{1}{h(x)} dx \tag{3.81}$$

$$\eta(l; -l) = \left(\frac{z}{z-1} \right) \int_{-l}^{l} \frac{1}{h(x)} dx + \left(\frac{z}{(z-1)^2} \right) \int_{-L}^{L} \frac{1}{h(x)} dx \tag{3.82}$$

$$\eta(-l; l) = \overline{\eta(l; -l)} \tag{3.83}$$

Then, in matrix form,

$$\begin{pmatrix} \psi(l) \\ -\psi(-l) \end{pmatrix} = \frac{(g_+ - g_-)}{D} h(l) \begin{pmatrix} \eta(l; l) & -\eta(l; -l) \\ -\overline{\eta(l; -l)} & \eta(-l; -l) \end{pmatrix} \begin{pmatrix} c_+ \\ c_- \end{pmatrix}. \tag{3.84}$$

Therefore, we obtain

$$\lambda \begin{pmatrix} c_+ \\ c_- \end{pmatrix} = \begin{pmatrix} a & b \\ \overline{b} & a \end{pmatrix} \begin{pmatrix} c_+ \\ c_- \end{pmatrix}. \tag{3.85}$$

where a and b are given by

$$\begin{aligned}
a =& \frac{\varepsilon}{\kappa_0}\frac{g_-}{D}\int_l^L \frac{h(x)}{h(l)}dx - \varepsilon^2 G'(l) - \frac{\varepsilon}{\kappa_0}\frac{(g_+ - g_-)}{D}\frac{z}{(z-1)^2}\int_{-L}^L \frac{h(l)}{h(x)}dx, \\
b =& -\frac{\varepsilon}{\kappa_0}\left(\frac{g_+ - g_-}{D}\right)\left(\frac{z}{(z-1)^2}(z-1)\int_{-l}^l \frac{h(l)}{h(x)}dx + \frac{z}{(z-1)^2}\int_{-L}^L \frac{h(l)}{h(x)}dx\right), \\
\overline{b} =& -\frac{\varepsilon}{\kappa_0}\left(\frac{g_+ - g_-}{D}\right)\left(\frac{z}{(z-1)^2}\left(\frac{1}{z}-1\right)\int_{-l}^l \frac{h(l)}{h(x)}dx + \frac{z}{(z-1)^2}\int_{-L}^L \frac{h(l)}{h(x)}dx\right).
\end{aligned}$$

Then we obtain $\lambda = a \pm |b|$ where

$$\begin{aligned}
|b|^2 =& \frac{\varepsilon^2}{\kappa_0^2}\left(\frac{g_+ - g_-}{D}\right)^2 \left\{\frac{z}{(z-1)^2}\left(\int_{-l}^l \frac{h(l)}{h(x)}dx\right)\left(\int_{-L}^L \frac{h(l)}{h(x)}dx\right)\right. \\
& \left. - \frac{z}{(z-1)^2}\left(\int_{-l}^l \frac{h(l)}{h(x)}dx\right)^2 + \left(\frac{z}{(z-1)^2}\right)^2 \left(\int_{-L}^L \frac{h(l)}{h(x)}dx\right)^2\right\}.
\end{aligned}$$

Let $z = e^{i\theta}$. Then

$$\frac{z}{(z-1)^2} = \frac{1}{z + \frac{1}{z} - 2} = \frac{1}{2\cos\theta - 2}.$$

Thus,

$$\lambda_\theta^{\pm} = a \pm |b| \tag{3.86}$$

where

$$a = \frac{\varepsilon}{\kappa_0}\frac{g_-}{D}\int_l^L \frac{h(x)}{h(l)}dx - \varepsilon^2 G'(l) + \frac{\varepsilon}{\kappa_0}\frac{g_+ - g_-}{D}\frac{1}{2-2\cos\theta}\int_{-L}^L \frac{h(l)}{h(x)}dx, \tag{3.87}$$

$$\begin{aligned}
|b|^2 =& \frac{\varepsilon^2}{\kappa_0^2}\left(\frac{g_+ - g_-}{D}\right)^2 \left(\frac{1}{1-\cos\theta}\right)\left\{2\left(\int_0^l \frac{h(l)}{h(x)}dx\right)^2 - 2\left(\int_0^l \frac{h(l)}{h(x)}dx\right)\left(\int_0^L \frac{h(l)}{h(x)}dx\right)\right. \\
& \left. + \left(\frac{1}{1-\cos\theta}\right)\left(\int_0^L \frac{h(l)}{h(x)}dx\right)^2\right\}.
\end{aligned} \tag{3.88}$$

Note that the above does not hold when $z = 1$. For $z = 1$, we have

$$\eta(-L) = \eta(L), \quad \eta'(-L) = \eta'(L).$$

Integrating (3.76) from $-L$ to L

$$\eta(x_0) \sim \frac{h(x_0)}{\int_{-L}^L \sigma(x)h(x)dx}. \tag{3.89}$$

Thus, we have

$$\eta(l;l) = \eta(-l;-l) = \eta(l;-l) = \eta(-l;l) = \frac{h(x_0)}{\int_{-L}^{L} \sigma(x)h(x)dx} = \eta_0.$$

Therefore,

$$\begin{pmatrix} \psi(l) \\ -\psi(-l) \end{pmatrix} = (g_+ - g_-) \begin{pmatrix} \eta_0 & -\eta_0 \\ -\eta_0 & \eta_0 \end{pmatrix} \begin{pmatrix} c_+ \\ c_- \end{pmatrix}. \tag{3.90}$$

Note that the ψ terms are of $\mathcal{O}(1)$, so that, to leading order,

$$\lambda \begin{pmatrix} c_+ \\ c_- \end{pmatrix} = -\frac{\varepsilon}{\kappa_0}(g_+ - g_-) \begin{pmatrix} \eta_0 & -\eta_0 \\ -\eta_0 & \eta_0 \end{pmatrix} \begin{pmatrix} c_+ \\ c_- \end{pmatrix} \tag{3.91}$$

where the eigenvalues are

$$\lambda \sim 0, \quad \lambda \sim -2\frac{\varepsilon}{\kappa_0}(g_+ - g_-)\frac{h(l)}{\int_{-L}^{L} \sigma(x)h(x)dx} = \lambda_{even}. \tag{3.92}$$

As was done in Chapter 2, we can extend these results with periodic boundary conditions to that of Neumann boundary conditions. This problem admits $2K$ eigenvalues with $2K-2$ eigenvalues given by (3.86)-(3.88) but with

$$\theta = \frac{\pi j}{K}, \quad j = 1, \ldots, K-1.$$

To determine the other two eigenvalues, we consider $z = 1$ and $z = -1$. Note that $\lambda = 0$ does not satisfy the condition that $\phi(L) \not\equiv 0$, given in §2.2. Next, consider $z = -1$, that is, $\theta = \pi$, for which we have the two eigenvalues

$$\lambda_{odd} = -\varepsilon^2 G'(l) + \frac{\varepsilon}{D}\frac{1}{\kappa_0}(g_+ - g_-)\left\{\frac{g_-}{g_+ - g_-}\int_l^L \frac{h(x)}{h(l)}dx + \int_0^l \frac{h(l)}{h(x)}dx\right\} \tag{3.93}$$

and

$$\lambda_{\pi} = -\varepsilon^2 G'(l) + \frac{\varepsilon}{D}\frac{1}{\kappa_0}(g_+ - g_-)\left\{\frac{g_-}{g_+ - g_-}\int_l^L \frac{h(x)}{h(l)}dx + \int_l^L \frac{h(l)}{h(x)}dx\right\} \tag{3.94}$$

Again, checking the condition that $\phi(L) \not\equiv 0$, we have that λ_π does not form one of the $2K$ eigenvalues. Thus, we have

$$\lambda_{even} = -2\frac{\varepsilon}{\kappa_0}(g_+ - g_-)\frac{h(l)}{\int_{-L}^{L} \sigma(x)h(x)dx} \tag{3.95}$$

$$\lambda_{odd} = \frac{\varepsilon}{D}\frac{1}{\kappa_0}(g_+ - g_-)\left(\frac{g_-}{g_+ - g_-}\int_l^L \frac{h(x)}{h(l)}dx + \int_0^l \frac{h(l)}{h(x)}dx\right) - \varepsilon^2 G'(l) \tag{3.96}$$

which gives Principal Result 3.3.1.

3.4 Stability of K Mesa Pattern

Now that we have determined the eigenvalues of (3.22), we consider the stability of the mesa patterns. We know that a K mesa pattern is stable if and only if the real part of each of the eigenvalues is negative. We note that λ_{even} does not depend on D. Thus, $\lambda_{even} < 0$ assuming that (3.24) holds. The other eigenvalues can be written as, for $\theta = \frac{\pi}{K}, \ldots, \frac{(K-1)\pi}{K}$,

$$\lambda_\theta^\pm = -\varepsilon^2 G'(l) + \frac{1}{D} F^\pm(\theta) \tag{3.97}$$

where

$$\begin{aligned} F^\pm(\theta) =& \frac{\varepsilon}{\kappa_0}(g_+ - g_-)\left\{ \frac{g_-}{g_+ - g_-}\int_l^L \frac{h(x)}{h(l)}dx + \frac{1}{1-\cos\theta}\left[\int_0^L \frac{h(l)}{h(x)}dx \left(\left(\int_0^L \frac{h(l)}{h(x)}dx\right)^2\right.\right.\right. \\ & \left.\left.\left. \pm\ -2(1-\cos\theta)\int_0^l \frac{h(l)}{h(x)}dx\left(\int_0^L \frac{h(l)}{h(x)}dx - \int_0^l \frac{h(l)}{h(x)}dx\right)\right)^{1/2}\right]\right\}, \end{aligned} \tag{3.98}$$

and

$$\lambda_{odd} = -\varepsilon^2 G'(l) + \frac{\varepsilon}{D}\frac{1}{\kappa_0}(g_+ - g_-)\left\{ \frac{g_-}{g_+ - g_-}\int_l^L \frac{h(x)}{h(l)}dx + \int_0^l \frac{h(l)}{h(x)}dx \right\}.$$

To determine whether the eigenvalues are negative, we first demonstrate that $F^+(\theta)$ is monotonically increasing and $F^-(\theta)$ is monotonically decreasing on $(0,\pi)$, and then show the ordering of the eigenvalues. From this, we determine the stability of a K mesa pattern, which will be given in Principal Result 3.4.1.

To show the monotonicity of $F^\pm$, we begin by noting that on the interval $(0,\pi)$, since $1-\cos\theta$ is increasing, we have that the term under the square root is positive, that is,

$$\left(\int_0^L \frac{h(l)}{h(x)}dx\right)^2 - 2(1-\cos\theta)\int_0^l \frac{h(l)}{h(x)}dx\left(\int_0^L \frac{h(l)}{h(x)}dx - \int_0^l \frac{h(l)}{h(x)}dx\right) > 0.$$

Also, since $g_+ \cdot g_- < 0$, we have

$$\frac{g_-}{g_+ - g_-}\int_l^L \frac{h(x)}{h(l)}dx < 0.$$

Then, differentiating $F^+(\theta)$ with respect to θ, we see that $\frac{dF^+}{d\theta} > 0$ for all $\theta \in (0,\pi)$. Similarly, differentiating $F^-(\theta)$, we find that $\frac{dF^-}{d\theta} < 0$ for all $\theta \in (0,\pi)$. Thus, $F^+(\theta)$

and $F^-(\theta)$ are increasing and decreasing, respectively. Since F^+ is increasing, we have the ordering

$$F^+\left(\frac{\pi}{K}\right) < F^+\left(\frac{2\pi}{K}\right) < \ldots < F^+\left(\frac{(K-1)\pi}{K}\right) < F^+(\pi). \tag{3.99}$$

Similarly, since F^- is decreasing, we have

$$F^-\left(\frac{\pi}{K}\right) > F^-\left(\frac{2\pi}{K}\right) > \ldots > F^-\left(\frac{(K-1)\pi}{K}\right) > F^-(\pi). \tag{3.100}$$

Next, consider $F^{\pm}(\theta)$ at the end points of the interval. It is easy to see that $F^+(0) \to -\infty$. Using l'Hopital's rule, as $\theta \to 0$, we have

$$F^-(0) \to \varepsilon\frac{(g_+ - g_-)}{\kappa_0}\left\{\frac{g_-}{g_+ - g_-}\int_l^L \frac{h(x)}{h(l)}dx + \frac{\int_0^l \frac{h(l)}{h(x)}dx}{\int_0^L \frac{h(l)}{h(x)}dx}\left(\int_0^L \frac{h(l)}{h(x)}dx - \int_0^l \frac{h(l)}{h(x)}dx\right)\right\}. \tag{3.101}$$

Then, at $\theta = \pi$, we obtain

$$\begin{aligned} F^+(\pi) =& \varepsilon\frac{(g_+ - g_-)}{\kappa_0}\left\{\frac{g_-}{g_+ - g_-}\int_l^L \frac{h(x)}{h(l)}dx + \frac{1}{2}\int_0^L \frac{h(l)}{h(x)}dx \right. \\ & \left. + \frac{1}{2}\left|\int_0^L \frac{h(l)}{h(x)}dx - 2\int_0^l \frac{h(l)}{h(x)}dx\right|\right\}, \\ \text{and } F^-(\pi) =& \varepsilon\frac{(g_+ - g_-)}{\kappa_0}\left\{\frac{g_-}{g_+ - g_-}\int_l^L \frac{h(x)}{h(l)}dx + \frac{1}{2}\int_0^L \frac{h(l)}{h(x)}dx \right. \\ & \left. - \frac{1}{2}\left|\int_0^L \frac{h(l)}{h(x)}dx - 2\int_0^l \frac{h(l)}{h(x)}dx\right|\right\}. \end{aligned}$$

Note that one of these gives λ_{odd}. We can see that $F^-(\pi) > F^+(\pi)$. Then, from (3.99) and (3.100), we have

$$\lambda^-_{\pi/K} > \ldots > \lambda^-_{(K-1)\pi/K} > \lambda_{odd} > \lambda^+_{(K-1)\pi/K} > \ldots > \lambda^+_{\pi/K}. \tag{3.102}$$

Using this ordering, we can determine the stability of a symmetric K mesa pattern. This is given in Principal Result 3.4.1.

Principal Result 3.4.1. *Let $F^+(\theta)$ and $F^-(\theta)$ be defined on $(0,\pi)$ as given in (3.98). Under the assumptions given in Principal Result 3.3.1, the behaviour of a K mesa pattern is given by the following three cases:*

(a) if $G'(l) \geq 0$ and $\lim_{\theta\to 0} F^-(\theta) < 0$, where $\lim_{\theta\to 0} F^-(\theta)$ is given by (3.101), then a K mesa pattern is always stable for all D.

(b) if $G'(l) < 0$ and $F^+(\pi) > 0$, then a K mesa pattern is always unstable for all D.

(c) if $G'(l) < 0$ and $F^+(\pi) < 0$, then there exists a critical D value, D_K, given by

$$D_K = \frac{1}{\varepsilon^2 G'(l)} F^- \left(\frac{\pi}{K}\right), \tag{3.103}$$

such that for $D < D_K$, a K mesa pattern is stable and for $D > D_K$ is unstable..

Derivation of Result 3.4.1.

If $G'(l) \geq 0$ and $\lim_{\theta \to 0} F^-(\theta) < 0$, then $F^-(\pi/K) < 0$, and thus $\lambda^-_{\pi/K}$ is always negative. From (3.102), it follows that all other eigenvalues are negative. Thus we obtain case (a). If $G'(l) < 0$ and $F^+(\pi) > 0$, then $\lambda_{odd} > 0$. Therefore, for all K, there is a positive eigenvalue and thus, we obtain case (b). If $G'(l) < 0$ and $F^+(\pi) < 0$, then, as D becomes sufficiently large, $\frac{1}{D}F^+(\theta)$ becomes small. If this term becomes small enough, the eigenvalue becomes positive. From the ordering (3.102), we see that $\lambda^-_{\pi/K}$ is the first to become positive. Setting the expression for $\lambda^-_{\pi/K}$ to zero and solving for D, we obtain the critical value of D. Thus, we obtain the result in case (c).

3.5 Numerical Simulations of the Cubic Model

We now apply these results to the cubic model (1.12),except now in the form (3.18),

$$\begin{cases} u_t = \frac{\varepsilon^2}{h(x)} \left[h(x)u_x\right]_x + 2(u - u^3) + w \\ 0 = \frac{D}{h(x)} \left[h(x)w_x\right]_x + \beta - u \end{cases}. \tag{3.104}$$

For this system, we have

$$u_+ = 1,\ u_- = -1,\ g_+ = \beta - 1,\ g_- = \beta + 1$$

and $\kappa_0 = 2/3$. From (3.37), l is defined by

$$(\beta - 1) \int_0^l h(x)dx + (\beta + 1) \int_l^L h(x)dx = 0. \tag{3.105}$$

First consider the case when $h(x)$ is constant. The system (3.104) becomes the system studied in Chapter 2. From (3.105), we obtain $l = \frac{\beta+1}{2}L$. Since $h'(x) = 0$ which implies that $G'(l) = 0$, we have

$$\lambda_{odd} \sim -\frac{3}{4}\frac{\varepsilon}{D}(\beta + 1)^2 L$$

and Principal Result 3.4 gives that a K mesa pattern is stable for all values of D. This is consistent with the results of Chapter 2, assuming the effect of the boundary terms is negligible, i.e. $\ln(D) \ll \mathcal{O}(\frac{1}{\varepsilon})$.

Now, we examine the behaviour that can be exhibited when $h(x)$ is a non-constant function and $G'(l) \neq 0$.

Experiment 3.1: A Single Mesa.

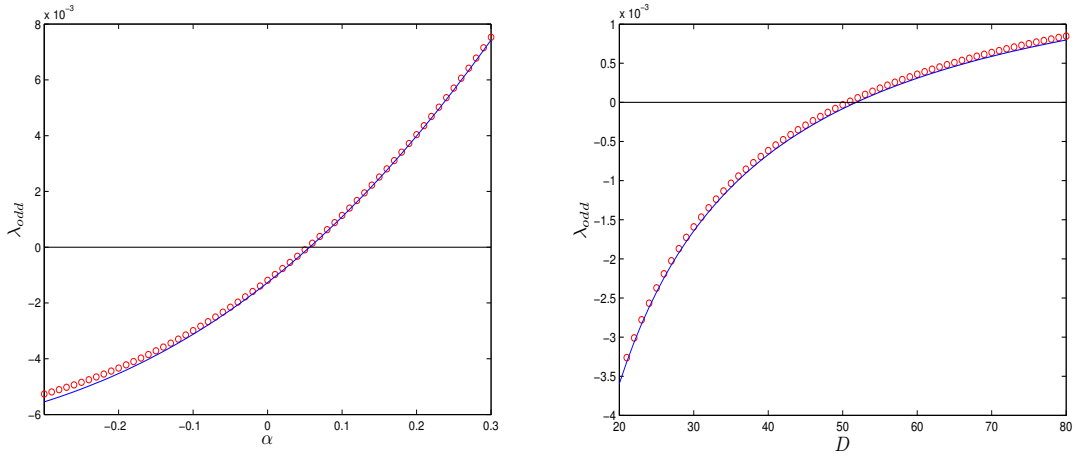

(a) (b)

Figure 3.1: (a) The odd eigenvalue λ_{odd} of a single mesa for the cubic model where $h(x) = 1 - \alpha x^2$, for varying α. Here $D = 100$, $\varepsilon = 0.1$, $\beta = 0.3$. The circles are the numerical solution and the solid line is the solution from the asymptotic formula (3.106). (b) The odd eigenvalue λ_{odd} of a single mesa for the cubic model for varying D. Here $h(x) = 1 - 0.1x^2$, $\varepsilon = 0.1$, $\beta = 0.3$. The circles are the numerical solution and the solid line is the solution from the asymptotic equation (3.106).

In §3.2, we examined a single mesa solution of (3.18) which has two eigenvalues corresponding to the even and odd eigenfunctions. For the cubic model, we consider a single mesa solution of u on $[-1, 1]$ where $h(x) = 1 - \alpha x^2$ and α is a parameter. Here we have

$$\lambda_{odd} \sim -3\frac{\varepsilon}{D}\left\{-\left(\frac{\beta+1}{2}\right)\int_l^L \frac{h(x)}{h(l)}dx\right\} - \varepsilon^2 G'(l) \tag{3.106}$$

where

$$G'(l) = \frac{h''(l)}{h(l)} - \left(\frac{h'(l)}{h(l)}\right)^2 = \frac{-2\alpha}{1-\alpha x^2} - \left(\frac{-2\alpha x}{1-\alpha x^2}\right)^2 = \frac{-2\alpha(1+\alpha x^2)}{1-\alpha x^2}.$$

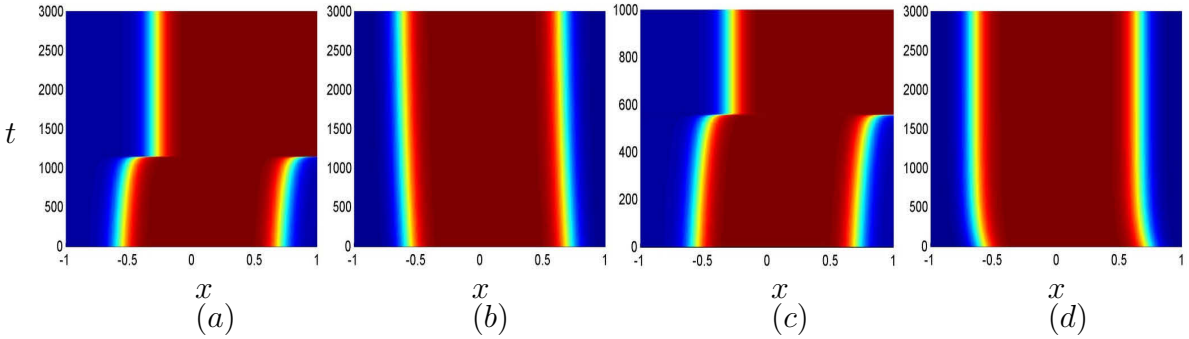

Figure 3.2: Contour plots of u for the cubic model with $\varepsilon = 0.1$, $\beta = 0.3$ and $h(x) = 1 - \alpha x^2$ for (a)$D = 60$, $\alpha = 0.1$ (b) $D = 40$, $\alpha = 0.1$ (c) $D = 100$, $\alpha = 0.1$ (d) $D = 100$, $\alpha = -0.1$

Note that $h(x)$ is symmetric about $x = 0$ on $[-1, 1]$. As was discussed at the beginning of §2.4, Maple is used to solve a boundary value problem that has come from the reformulation of the linearized problem. We compare the results of the numerical computation of λ_{odd} with that of the asymptotic formula of λ_{odd} given in (3.106). In Figure 3.1(a), the value of α is varied while β, ε and D are held fixed. For this D value, $D = 100$, we see that, for $\alpha \sim 0.05$, λ_{odd} becomes positive which implies that the single mesa becomes unstable. We see that the λ_{odd} value from the asymptotic formula agrees with the numerically computed value of λ_{odd}. In Figure 3.1(b), the value of D is varied, while β, ε and α are held fixed. We can see that, as D is increased past $D \approx 52$, λ_{odd} becomes positive, and, thus, the mesa pattern becomes unstable.

From Figure 3.1(b), we have that, for $\alpha = 0.1$, $\lambda_{odd} < 0$ for $D < 52$ and $\lambda_{odd} > 0$ for $D > 52$. Using FlexPDE [72] to simulate (3.104), for $\alpha = 0.1$ and $D = 40$, in Figure 3.2(b), we observe that the one mesa solution is stable, moving to the steady state. For $\alpha = 0.1$ and $D = 60$, in Figure 3.2(a), we observe that the one mesa solution is unstable, with one interface moving to the boundary.

Similarly, from Figure 3.1(a), we have that, for $D = 100$, $\lambda_{odd} < 0$ for $\alpha < 0.05$ and $\lambda_{odd} > 0$ for $\alpha > 0.05$. For $D = 100$ and $\alpha = -0.1$, in Figure 3.2(d), we observe that the one mesa solution is stable, moving to the steady state. For $D = 100$ and $\alpha = 0.1$, in Figure 3.2(c), we observe that the one mesa solution is unstable, with one interface moving to the boundary.

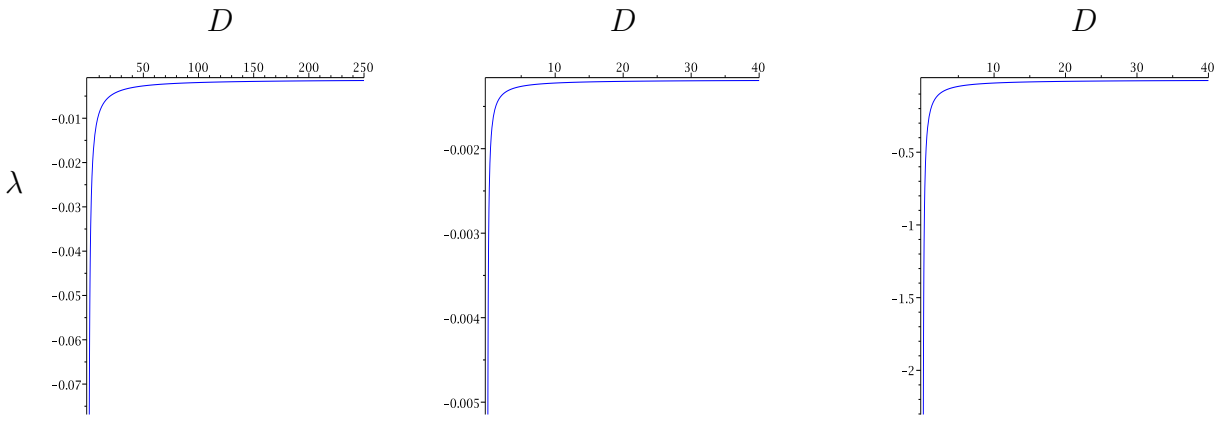

(a) (b) (c)

Figure 3.3: For the cubic model with $h(x) = 1 + \alpha\cos(2\pi x)$, with $\alpha = 0.1$, $\beta = 0.4$, $\varepsilon = 0.05$ and $L = 1$, plots of (a) λ_{odd} (b) $\lambda^{-}_{\pi/2}$ (c) $\lambda^{+}_{\pi/2}$ vs. D

Experiment 3.2: Two Mesas. Case (a)

Consider a two mesa solution on $[-1, 3]$. For the cubic model, let $h(x) = 1 + \alpha\cos(2\pi x)$ with $\alpha = 0.1$, $\beta = 0.4$, $\varepsilon = 0.05$ and $L = 1$. Note that $h(x)$ is symmetric about $x = 0$ on $[-1, 1]$ and is periodic on $[-1, 3]$. For this $h(x)$ and the given parameter values, $l = 0.7155$ and $G'(l) = 0.4743 > 0$. As well, $F^{-}(0) < 0$, therefore, these parameters give us case (a) in Principal Result 3.4.1. Plotting λ_{odd}, $\lambda^{-}_{\pi/2}$ and $\lambda^{+}_{\pi/2}$, from equations (3.97) and (3.106), in Figure 3.3, as we vary D, we observe that the eigenvalues are always negative. Thus, the $K = 2$ mesa pattern is always stable for these parameter values as predicted by Principal Result 3.4.1.

Experiment 3.3: Two Mesas. Case (b)

Again, for a two mesa solution and for the cubic model, let $h(x) = 1 + \alpha\cos(2\pi x)$ with $\alpha = 0.85$, $\beta = 0.05$, $\varepsilon = 0.05$ and $L = 1$. Then $l = 0.6135$ and $G'(l) = -24.6543 < 0$. As well, $F^{+}(\pi) = 0.02416 > 0$, therefore, these parameters give us case (b) in Principal Result 3.4.1. Plotting λ_{odd}, $\lambda^{-}_{\pi/2}$ and $\lambda^{+}_{\pi/2}$, in Figure 3.4, as we vary D, the eigenvalues are always positive. Thus, the $K = 2$ mesa pattern is always unstable for these parameter values. This agrees with the predicted behaviour of case (b).

Experiment 3.4: Two Mesas. Case (c)

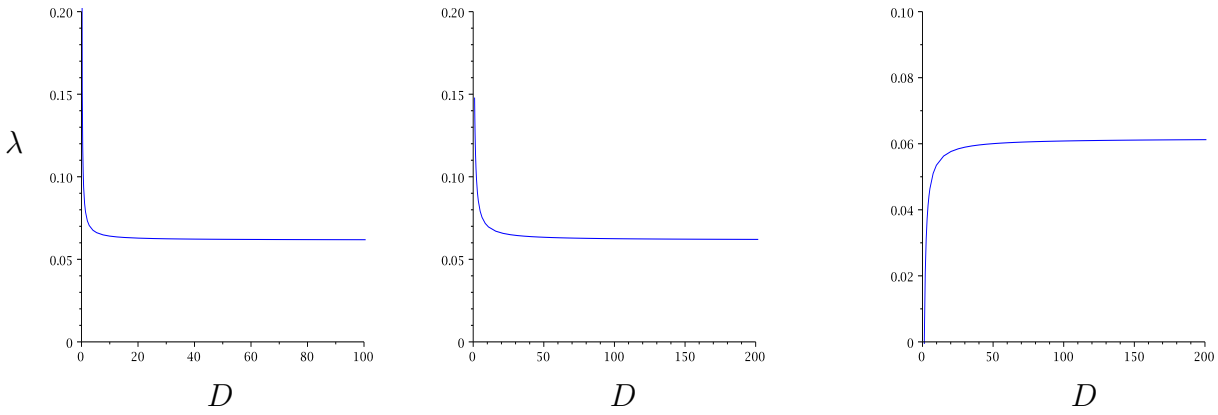

Figure 3.4: For the cubic model with $h(x) = 1 + \alpha\cos(2\pi x)$, with $\alpha = 0.1$, $\beta = 0.3$, $\varepsilon = 0.05$ and $L = 1$, plots of D vs. (a) λ_{odd} (b) $\lambda^{-}_{\pi/2}$ (c) $\lambda^{+}_{\pi/2}$

For the cubic model with $h(x) = 1 + \alpha\cos(2\pi x)$ with $\alpha = -0.95$, $\beta = 0.2$, $\varepsilon = 0.04$ and $L = 1$, we have $l = 0.5517$. We obtain $G'(l) = -19.7092 < 0$ and $F^{+}(\pi) = -0.3561 < 0$, and therefore these parameters, again, give us case (c) in Principal Result 3.4.1 with $D_2 = 6.30$. Plotting λ_{odd}, $\lambda^{-}_{\pi/2}$ and $\lambda^{+}_{\pi/2}$, in Figure 3.5, as we vary D, the eigenvalues are cross the axis. Thus, the $K = 2$ mesa pattern becomes unstable as D is increased. Simulations of the system 3.104 for these parameters are given in Figure 3.6 for $D = 3$ and $D = 9$ where we have shown the contour plot of the solution u. We see that for $D = 3 < D_2$, the solution moves towards the symmetric steady state and for $D = 9 > D_2$, the solution is unstable and one of the interfaces moves to the boundary.

Experiment 3.5: Three Mesas. Case (a)

For the same parameters as in Experiment 3.2, we consider initial conditions of six interfaces, that is, a three mesa solution, given by

$$u(x,0) = \tanh\left(\frac{x+0.5369}{\varepsilon}\right) - \tanh\left(\frac{x-0.5369}{\varepsilon}\right) + \tanh\left(\frac{x-1.4631}{\varepsilon}\right) - \tanh\left(\frac{x-2.5369}{\varepsilon}\right) + \tanh\left(\frac{x-3.4631}{\varepsilon}\right) - \tanh\left(\frac{x-4.5369}{\varepsilon}\right) - 1$$

In this case, all the eigenvalues are negative for all D. In Figure 3.7, we can see that,

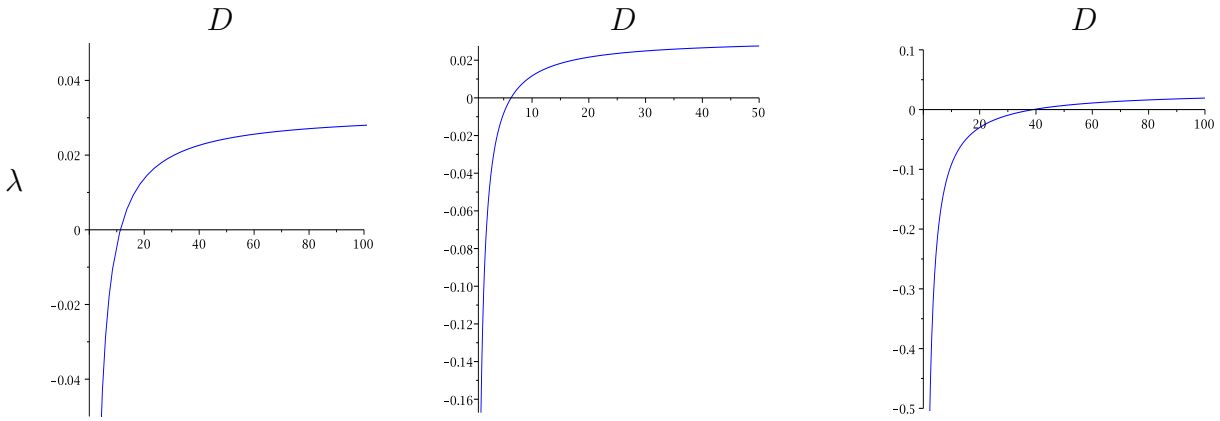

(a) (b) (c)

Figure 3.5: For the cubic model with $h(x) = 1+\alpha\cos(2\pi x)$, with $\alpha = -0.95$, $\beta = 0.2$, $\varepsilon = 0.04$ and $L = 1$, plots of D vs. (a) λ_{odd} (b) $\lambda^{-}_{\pi/2}$ (c) $\lambda^{+}_{\pi/2}$. We see that $\lambda^{-}_{\pi/2} > 0$ for $D \approx 6$.

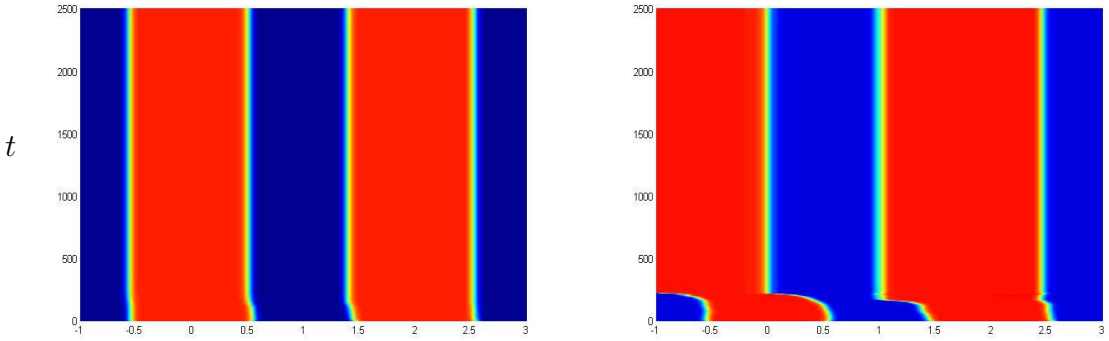

(a) (b)

Figure 3.6: For the cubic model with $h(x) = 1+\alpha\cos(2\pi x)$, with $\alpha = -0.95$, $\beta = 0.2$, $\varepsilon = 0.04$ and $L = 1$, a contour plot of the solution u for (a) $D = 3$ and (b) $D = 9$.

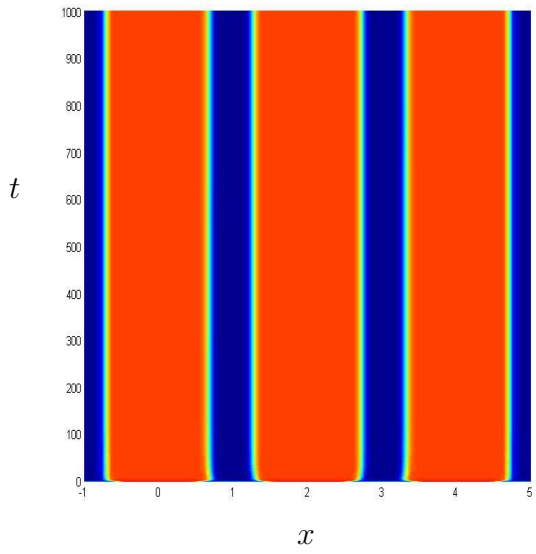

Figure 3.7: For the cubic model with $h(x) = 1 + \alpha\cos(2\pi x)$, with $\alpha = 0.1$, $\beta = 0.4$, $\varepsilon = 0.05$ and $L = 1$, the contour plot of u with initial condition of 6 interfaces for $D = 1500$.

as was predicted by Principal Result 3.4.1, this solution is stable, even for D large.

3.6 Discussion

In this chapter, we have considered a two-dimensional reaction-diffusion system. By assuming the spatial domain is a thin domain, we have approximated the problem with a one-dimensional reaction-diffusion system, with a dependence on the width of the domain. This is a well-known lubrication theory approach [24, 76]. After reducing the problem to one dimension, we consider mesa patterns, as considered in Chapter 2, except we assume that the interaction with the boundary and the interaction between interfaces are sufficiently small that they are negligible. For a symmetric K mesa pattern, we determine the stability of these patterns from the eigenvalues of the linearized problem. The stability depends on the sign of the term $G'(l)$ where

$$G'(l) = \frac{h''(l)}{h(l)} - \left(\frac{h'(l)}{h(l)}\right)^2$$

as well as integrals involving $h(x)$ and thus the stability in dependent on the function $h(x)$. For a particular $h(x)$, an instability threshold, D_K, exists, where $D < D_K$ implies that a K mesa pattern is stable and $D > D_K$ implies it is unstable.

There are many avenues to further this work. In this chapter, we have only considered the case were $h(x)$ is a symmetric function on the domain $[-L, L]$. It remains to determine the stability of the case where $h(x)$ is not symmetric or where $h(x)$ is not extended periodically to the whole domain $[-L, (2K-1)L]$. Since the condition that $h(x)$ is symmetric has been used throughout the calculation to simplify the analysis, it remains to be seen what could be said about the non-symmetric case.

Although we have considered a two-dimensional domain, the results are obtained by making the assumption that the two-dimensional domain is a thin domain, thus reducing the problem to one dimension. For the two-dimensional problem on a domain that is not thin, instabilities arise due to the curvature of the domain. It remains an open problem to calculate instability thresholds for the general two-dimensional problem.

Chapter 4

Oscillations of Mesa Patterns

In this chapter we again consider mesa pattern solutions to the system (1.1) with Neumann boundary conditions. In Chapter 2 we studied what occurs when $\tau = 0$ or τ is small, but now we consider τ large. As discussed in the introduction, as τ is increased beyond a certain critical threshold τ_h, these interface solutions can be destabilized due to a Hopf bifurcation. Under the assumption that D is large, we study the dynamics of these oscillatory fronts. We show, in this chapter, that there exists a second threshold, denoted τ_c, exists such that when $\tau_h < \tau < \tau_c$, a solution consisting of periodically oscillating interfaces with constant amplitude exists. As τ is increased further, that is when $\tau > \tau_c$, the oscillation eventually exceeds the spatial domain. Note that τ_c may be infinite. First, we consider the case of a solution for u with one interface, that is, a half-mesa pattern. We start by making a series of approximations of the PDE system (1.1) leading to a second-order ODE. Then, using multiple scales analysis, an equation for the amplitude of the oscillations of the interface is determined. From this amplitude equation we obtain the value of τ, namely τ_h, at which the Hopf bifurcation occurs. Next, we consider a single mesa pattern, as constructed in §2.1. In this case, we are concerned about the location of the mesa within the spatial domain, as well as the amplitude. We determine a similar result to what was obtained for a half-mesa. To verify these asymptotic results, we compare them to numerically computed solutions. Because of the nature of the solutions (there exist multiple spatial and temporal scales), the numerical computation of these solutions is not straightforward and we use numerical software that features adaptive error control in both space and time.

4.1 Oscillation of a Single Interface

In this section we consider the solution to (1.1) consisting of a single interface. We derive an equation for the amplitude of its oscillations. This allows us to obtain the Hopf bifurcation threshold, τ_h, as well as to describe in detail the behaviour of solutions when τ is well beyond the Hopf bifurcation. This is accomplished by first approximating (1.1) to a system consisting of a PDE and an ODE which describes the dynamics of the interface, then approximating this system to a system of ODEs. This system of ODEs can be written as a second-order ODE, on which a multiple scales analysis is performed to determine the amplitude equation [2, 58].

First, note that we will use much of the notation defined in 2.1. Define u_+, u_- and w_0 so that the conditions (2.4) are satisfied. Define $g_\pm$ as given in (2.5). Also assume that conditions (2.6) are satisfied. Then a single interface steady state solution, on the interval $[0,1]$, is given by

$$u(x) \sim U(y) = U\left(\frac{x-l_0}{\varepsilon}\right)\ ,\ w \sim w_0 \tag{4.1}$$

where $U(y)$ is the heteroclinic connection between u_+ and u_- satisfying

$$U_{yy} + f(U, w_0) = 0,\ f(U(0), w_0) = 0 \tag{4.2}$$

$$U \to u_\pm \text{ as } y \to \mp\infty \tag{4.3}$$

and l_0 is the equilibrium location of the interface given by(2.9) so that

$$u \sim \begin{cases} u_+, & 0 < x < l_0, \\ u_-, & l_0 < x < 1 \end{cases}. \tag{4.4}$$

Now we state the main result, describing the oscillation of the single interface.

Principal Result 4.1.1. *Consider a single interface solution u of (1.1) in the limit (2.3) on the interval $[0,1]$ with Neumann boundary conditions. Let*

$$\tau_0 = \frac{\varepsilon}{D}\tau. \tag{4.5}$$

Assume that

$$0 < l_0 < 1; \qquad (g_- - g_+)\int_{u_-}^{u_+} f_w du > 0; \qquad \left(g_w - \frac{f_w}{f_u}g_u\right)\Big|_{u=u_\pm, w=w_0} < 0, \tag{4.6}$$

where $w_0, u_\pm, g_\pm$ and l_0 are as defined by (2.4),(2.5), (2.9) Then the location of the interface l evolves according to

$$l(t) = l_0 + A(\hat{t}) \cos\left\{ \left(\frac{(g_- - g_+)\int_{u_-}^{u_+} f_w du}{\tau_0 \int_{-\infty}^{\infty} U_y^2 dy} \right)^{1/2} \phi + \phi_0 \right\} \tag{4.7}$$

where

$$\hat{t} = \frac{\varepsilon}{D} t; \qquad \phi = \frac{\varepsilon}{\sqrt{D}} t; \tag{4.8}$$

ϕ_0 is given below by initial conditions, l_0 is given by (2.9) and where $A(\hat{t})$ is the amplitude of the oscillation of the interface; $A(\hat{t})$ is the solution of the ODE

$$\begin{aligned} \frac{dA}{d\hat{t}} =& \frac{1}{2} \frac{\int_{u_-}^{u_+} f_w du}{\int_{-\infty}^{\infty} U_y^2 dy} \left\{ \hat{\sigma}_-(1 - l_0) + \hat{\sigma}_+ l_0 - \frac{g_-^2 (6l_0^2 - 6l_0 + 1)}{3l_0^2 (g_- - g_+)} \right\} A \\ & - \frac{(g_- - g_+)\int_{u_-}^{u_+} f_w du}{4 \int_{-\infty}^{\infty} U_y^2 dy} A^3 \end{aligned} \tag{4.9}$$

where

$$\hat{\sigma}_\pm := \frac{1}{\tau_0} \frac{\int_{-\infty}^{\infty} U_y^2 dy}{\int_{u_-}^{u_+} f_w du} \left(g_w - \frac{f_w}{f_u} g_u \right) \Big|_{u=u_\pm, w=w_0}. \tag{4.10}$$

The initial conditions are

$$\begin{cases} A(0)\cos\phi_0 = l(0) - l_0 \\ -\sqrt{g_- - g_+} A(0) \sin\phi_0 = \sqrt{\tau_0 D} \left(\frac{\int_{u_-}^{u_+} f_w du}{\int_{-\infty}^{\infty} U_y^2 dy} \right)^{1/2} (w(0) - w_0) \end{cases}. \tag{4.11}$$

Suppose that

$$\left| l_0 - \frac{1}{2} \right| < \frac{\sqrt{3}}{6}. \tag{4.12}$$

Then there exists a supercritical Hopf bifurcation which occurs as τ_0 is increased past τ_{0h} where

$$\tau_{0h} = \frac{3 \int_{-\infty}^{\infty} U_y^2 dy}{(g_- - g_+)\int_{u_-}^{u_+} f_w du} \frac{l_0 \left(g_w - \frac{f_w}{f_u} g_u \right)\Big|_{u=u_+} + (1 - l_0) \left(g_w - \frac{f_w}{f_u} g_u \right)\Big|_{u=u_-}}{(6l_0^2 - 6l_0 + 1)}, \tag{4.13}$$

Otherwise there is no Hopf bifurcation and $A \to 0$ as $\hat{t} \to \infty$ for any $\tau_0 > 0$.

Derivation of Principal Result 4.1.1. The derivation consists of a series of approximations, whereby the original system (1.1) is first reduced to a coupled ODE-PDE system, then to a system of ODE, then to a weakly forced harmonic oscillator on which the method of multiple scales is applied to obtain the amplitude equations.

First, we will reduce (1.1) to an ODE-PDE system. We scale τ as in (4.5) where τ_0 is $\mathcal{O}(1)$. Since we have assumed $D \gg 1$, we expand

$$u = u_0 + \frac{1}{D}u_1 + \dots, \quad w = w_0 + \frac{1}{D}w_1 + \dots \ .$$

For w, we have

$$w_{0xx} = 0 \tag{4.14}$$

therefore, to leading order, $w \sim w_0(t)$ is a constant in space. Expanding in terms of $\frac{1}{D}$, from the equation for u in (1.1), we obtain

$$0 = \varepsilon^2 u_{0_{xx}} + f(u_0, w_0), \tag{4.15}$$

$$Du_{0t} = \varepsilon^2 u_{1xx} + f_u(u_0, w_0)u_1 + f_w(u_0, w_0)w_1, \tag{4.16}$$

where $u_{0t} = \mathcal{O}\left(\frac{1}{D}\right)$ which will become evident with the scaling below. Consider a single interface located at $x = l$ in the domain $[0, 1]$. Let $l = l(t)$ and

$$u_0(x, t) = U\left(\frac{x - l}{\varepsilon}\right) = U(y) \tag{4.17}$$

where U is defined (4.1). Multiplying (4.16) by u_{0_x}, using (4.17), and integrating by parts over the domain, we obtain

$$-l'(t)\int_0^1 u_{0x}^2 dx = \frac{1}{D}\int_0^1 f_w w_1 u_{0x} dx. \tag{4.18}$$

Note that the boundary terms from integration are negligible because u_0 decays exponentially at the boundary. In the inner variables, we approximate $w_1 \sim w_1(l)$. Rearranging, we now have an equation for the dynamics of the interface

$$l_t = \frac{\varepsilon}{D}\frac{\int_{u_-}^{u_+} f_w du}{\int_{-\infty}^{\infty} U_y^2 dy} w_1(l).$$

Expanding in $\frac{1}{D}$, from the equation for w in (1.1), we obtain

$$\frac{\tau_0}{\varepsilon}w_{1t} = w_{1xx} + g(u_0, w_0) + \frac{1}{D}g_u(u_0, w_0)u_1 + \frac{1}{D}g_w(u_0, w_0)w_1 \tag{4.19}$$

Away from the interface, we can neglect the diffusion term, $u_{1_{xx}}$, so that

$$u_1 \sim -\frac{f_w(u_0, w_0)}{f_u(u_0, w_0)}w_1.$$

Then we have

$$\frac{\tau_0}{\varepsilon}w_{1t} = w_{1xx} + g(u_0, w_0) + \frac{1}{D}\left(g_w - \frac{f_w}{f_u}g_u\right)\Big|_{u=u_\pm, w=w_0} w_1.$$

Therefore, we obtain the following ODE-PDE system of $l(t)$ and $w_1(x,t)$

$$l_t = \frac{\varepsilon}{D}\frac{\int_{u_-}^{u_+} f_w du}{\int_{-\infty}^{\infty} U_y^2 dy} w_1(l), \tag{4.20}$$

$$\frac{\tau_0}{\varepsilon}w_{1t} = w_{1xx} + g(u_0, w_0) + \sigma w_1 \tag{4.21}$$

where

$$\sigma = \begin{cases} \sigma_+, & 0 < x < l \\ \sigma_-, & l < x < 1 \end{cases}, \tag{4.22}$$

with

$$\sigma_\pm = \frac{1}{D}\left(g_w - \frac{f_w}{f_u}g_u\right)\Big|_{u=u_\pm, w=w_0}. \tag{4.23}$$

Scaling the time variable and w_1 allows us to clearly see that the ordering given for u_{0_t} is consistent. Let this scaling be

$$s = \frac{\varepsilon}{\tau_0}\hat{\varepsilon}t; \quad \mathcal{W} = \hat{\varepsilon}w_1 \tag{4.24}$$

where

$$\hat{\varepsilon} = \sqrt{\frac{1}{D}}\left(\tau_0 \frac{\int_{u_-}^{u_+} f_w du}{\int_{-\infty}^{\infty} U_y^2 dy}\right)^{1/2}. \tag{4.25}$$

Then the scaled system is

$$l_s = \mathcal{W}(l), \tag{4.26}$$

$$\mathcal{W}_{xx} = \hat{\varepsilon}\mathcal{W}_s - \hat{\varepsilon}g(u_0, w_0) - \hat{\varepsilon}^2\hat{\sigma}\mathcal{W}, \tag{4.27}$$

where

$$\hat{\sigma} = \begin{cases} \hat{\sigma}_+, & 0 < x < l \\ \hat{\sigma}_-, & l < x < 1 \end{cases} \tag{4.28}$$

with $\hat{\sigma}_\pm$ as given by (4.10).

Next, we reduce the ODE-PDE system (4.26)- (4.27) to a system of three ODEs. Expanding $\mathcal{W}$ in terms $\hat{\varepsilon}$,

$$\mathcal{W} = \mathcal{W}_0(s) + \hat{\varepsilon}\mathcal{W}_1(x,s) + \hat{\varepsilon}^2\mathcal{W}_2(x,s) + \ldots, \tag{4.29}$$

we obtain

$$l_s = \mathcal{W}_0(s) + \hat{\varepsilon}\mathcal{W}_1(l,s), \tag{4.30}$$

$$\mathcal{W}_{0xx} = 0, \tag{4.31}$$

$$\mathcal{W}_{0s} = \mathcal{W}_{1xx} + g_0, \tag{4.32}$$

$$\mathcal{W}_{1s} = \hat{\sigma}\mathcal{W}_0 + \mathcal{W}_{2xx}. \tag{4.33}$$

where

$$g_0 = \begin{cases} g_+, & x < l, \\ g_-, & x > l \end{cases} \tag{4.34}$$

with $g_\pm$ as in (2.5). Equation (4.31) implies that $\mathcal{W}_0 = \mathcal{W}_0(s)$. From (4.32), we have the solvability condition

$$\int_0^1 \mathcal{W}_{1xx} dx = \int_0^1 (\mathcal{W}_{0s} - g_0) dx$$

so that

$$\mathcal{W}_{0s} = \int_0^1 g_0 dx. = (g_+ - g_-)l - g_-. \tag{4.35}$$

Also, from (4.32),

$$\mathcal{W}_{1xx} = \begin{cases} \mathcal{W}_{0s} - g_+, & x < l, \\ \mathcal{W}_{0s} - g_-, & x > l. \end{cases} \tag{4.36}$$

Substituting (4.35) into (4.36), integrating and imposing continuity of $\mathcal{W}_1$ at $x = l$, we obtain

$$\mathcal{W}_1 = \begin{cases} (g_+ - g_-)(l-1)\left(\frac{x^2}{2} - \frac{l^2}{2}\right) + K(s), & x < l \\ (g_+ - g_-)l\left(\frac{x^2}{2} - x - \frac{l^2}{2} + l\right) + K(s), & x > l \end{cases} \tag{4.37}$$

where $K(s)$ is to be determined as follows. From (4.33), we have the solvability condition

$$\int_0^1 \mathcal{W}_{1s} dx = \int_0^1 \hat{\sigma}\mathcal{W}_0 dx.$$

Substituting (4.37) into this, we solve for K_s to obtain

$$K_s = (g_+ - g_-)l_s \left\{ 2l^2 - 2l + \frac{1}{3} \right\} + (\hat{\sigma}_+ - \hat{\sigma}_-)\mathcal{W}_0 l + \hat{\sigma}_- \mathcal{W}_0.$$

We then obtain a system of three ODE's that capture the motion of the interface,

$$l_s = \mathcal{W}_0(s) + \hat{\varepsilon}K(s), \tag{4.38}$$

$$\mathcal{W}_{0s} = (g_+ - g_-)l + g_-, \tag{4.39}$$

$$K_s = \mathcal{W}_0 \left\{ (g_+ - g_-)\left(2l^2 - 2l + \frac{1}{3}\right) + (\hat{\sigma}_+ - \hat{\sigma}_-)l + \hat{\sigma}_- \right\}. \tag{4.40}$$

Next, we now approximate the system (4.38) – (4.40) by a weakly linear oscillator. We start by changing the variables

$$l = l_0 + y = \frac{g_-}{g_- - g_+} + y \tag{4.41}$$

to shift the equilibrium of (4.39) to zero. Then

$$y_s = \mathcal{W}_0 + \hat{\varepsilon}K, \tag{4.42}$$

$$\mathcal{W}_{0s} = (g_+ - g_-)y, \tag{4.43}$$

$$\begin{aligned} K_s = \mathcal{W}_0 \Big\{ & 2(g_+ - g_-)y^2 + (\hat{\sigma}_+ - \hat{\sigma}_-)y - 2(g_+ + g_-)y \\ & + \hat{\sigma}_-(1 - l_0) + \hat{\sigma}_+ l_0 - \frac{g_-^2\,(6l_0^2 - 6l_0 + 1)}{3l^2(g_- - g_+)} \Big\}. \end{aligned} \tag{4.44}$$

Differentiating (4.42) and substituting (4.43) and (4.44), we obtain

$$y_{ss} = \mathcal{W}_{0s} + \hat{\varepsilon}K_s \tag{4.45}$$

$$\begin{aligned} = (g_+ - g_-)y + \hat{\varepsilon}\mathcal{W}_0 \Big\{ & 2(g_+ - g_-)y^2 + (\hat{\sigma}_+ - \hat{\sigma}_-)y - 2(g_+ + g_-)y \\ & \hat{\sigma}_-(1 - l_0) + \hat{\sigma}_+ l_0 - \frac{g_-^2\,(6l_0^2 - 6l_0 + 1)}{3l^2(g_- - g_+)} \Big\}. \end{aligned} \tag{4.46}$$

From (4.42) we have $\mathcal{W}_0 = y_s + \mathcal{O}(\hat{\varepsilon})$. Keeping only $\mathcal{O}(1)$ and $\mathcal{O}(\hat{\varepsilon})$ terms we then obtain

$$\begin{aligned} y_{ss} = & (g_+ - g_-)y + \hat{\varepsilon}y_s \Big\{ 2(g_+ - g_-)y^2 + (\hat{\sigma}_+ - \hat{\sigma}_-)y - 2(g_+ + g_-)y \\ & \hat{\sigma}_-(1 - l_0) + \hat{\sigma}_+ l_0 - \frac{g_-^2\,(6l^2 - 6l + 1)}{3l^2(g_- - g_+)} \Big\} + \mathcal{O}(\hat{\varepsilon}^2). \end{aligned} \tag{4.47}$$

Now, we perform a multiple scales analysis on (4.47), see for example [2, 58]. We expand $y(s) = y_0(s, \hat{\tau}) + \hat{\varepsilon}y_1(s, \hat{\tau}) + \ldots$, where $\hat{\tau} = \hat{\varepsilon}s$ is the slow variable. We then

obtain, to two orders,

$$y_{0ss} + \omega^2 y_0 = 0, \tag{4.48}$$

$$\begin{aligned} y_{1ss} + \omega^2 y_1 = &-2y_{0s\hat{\tau}} + (\hat{\sigma}_+ - \hat{\sigma}_-)\, y_0 y_{0s} - 2(g_+ + g_-) y_0 y_{0s} + 2(g_+ - g_-) y_0^2 y_{0s} \\ &+ \left\{ \hat{\sigma}_-(1 - l_0) + \hat{\sigma}_+ l_0 - \frac{g_-^2\,(6l_0^2 - 6l_0 + 1)}{3l^2(g_- - g_+)} \right\} y_{0s} \end{aligned} \tag{4.49}$$

where we defined

$$\omega := \sqrt{g_- - g_+}.$$

From (4.48) we obtain

$$y_0 = A(\hat{\tau}) \cos\left(\omega s + \phi(\hat{\tau})\right). \tag{4.50}$$

Substituting into (4.49), we obtain

$$\begin{aligned} y_{1ss} + \omega^2 y_1 = &\Big\{ -2\omega(g_+ - g_-)A^3 - \omega A \left(\hat{\sigma}_-(1 - l_0) + \hat{\sigma}_+ l_0 \right. \\ &\left. - \frac{g_-^2(6l_0^2 - 6l_0 + 1)}{3l_0^2(g_- - g_+)} \right) \Big\} \sin(\omega s + \phi) + 2\omega A \phi_{\hat{\tau}} \cos(\omega s + \phi) \\ &- 2\omega(g_+ - g_-)A^3 \sin^3(\omega s + \phi) \\ &- \omega \left\{ (\hat{\sigma}_+ - \hat{\sigma}_-) - 2(g_+ + g_-) \right\} A^2 \cos(\omega s + \phi) \sin(\omega s + \phi). \end{aligned}$$

Eliminating the resonance terms (that is, the cosine and sine terms) , we obtain the system of equations

$$2A\frac{d\phi}{d\hat{\tau}} = 0 \tag{4.51}$$

$$2\frac{dA}{d\hat{\tau}} = -\left(\frac{g_- - g_+}{2} \right) A^3 + \left\{ \hat{\sigma}_-(1 - l_0) + \hat{\sigma}_+ l_0 - \frac{g_-^2\,(6l_0^2 - 6l_0 + 1)}{3l^2(g_- - g_+)} \right\} A \tag{4.52}$$

Equation (4.51) implies $\phi = \phi_0$ where ϕ_0 is a constant. Rewriting in terms of the original time variable t, the equation for the amplitude of the motion of the interface (4.52) yields

$$\begin{aligned} \frac{dA}{dt} = \frac{\varepsilon}{D} \frac{\int_{u_-}^{u_+} f_w du}{\int_{-\infty}^{\infty} U_y^2 dy} \Bigg\{ &\frac{-(g_- - g_+)}{4} A^3 + \frac{1}{2} \left\{ \hat{\sigma}_-(1 - l_0) + \hat{\sigma}_+ l_0 \right. \\ &\left. - \frac{g_-^2\,(6l_0^2 - 6l_0 + 1)}{3l_0^2(g_- - g_+)} \right\} A \Bigg\} \end{aligned} \tag{4.53}$$

The initial condition $A(0)$ and the constant ϕ_0 are determined from the initial conditions of the original problem (1.1). From (4.50),

$$\begin{aligned} y_0(0) =& A(0) \cos\phi_0, \\ y_{0s}(0) =& -\omega A(0) \sin\phi_0. \end{aligned}$$

From (4.41), we also have

$$y_0(0) = l(0) - l_0.$$

Beginning with (4.42) and tracing backwards,

$$y_{0s}(0) \sim \mathcal{W}_0(0) \sim \hat{\varepsilon} w_1(0) \sim \varepsilon D(w(0) - w_0) \tag{4.54}$$

which yields the equations (4.11).

From (4.9), the bifurcation of τ_0 occurs when the coefficient of A changes from positive to negative. Setting to zero and solving for τ_0 yields (4.13). Assuming $\tau_{0h} > 0$, we can see that the term inside the curly brackets in (4.9) is negative for $\tau < \tau_{0h}$ provided that the assumptions (4.6) hold. This implies that the bifurcation is supercritical. From (4.13) (and the assumptions is (4.6)), τ_{0h} is positive when $6l_0^2 - 6l_0 + 1 < 0$. This is true when

$$\frac{1}{2} - \frac{\sqrt{3}}{6} < l_0 < \frac{1}{2} + \frac{\sqrt{3}}{6} \tag{4.55}$$

which gives condition (4.12).

We note that the oscillation of the interface must be contained in the domain $[0, 1]$. To satisfy this, we must have

$$l_0 + A < 1, \;\; l_0 - A > 0.$$

This may impose additional thresholds on the parameters. We will discuss this further in the context of the cubic model (1.12) in §4.3

4.2 Oscillations of a Single Mesa

Now we consider a solution consisting of one mesa, that is, two interfaces, for the general system (1.1). We state a similar result to that obtained in §4.1 for one interface.

Principal Result 4.2.1. *Consider a single mesa solution u of (1.1) in the limit (2.3) on the interval $[-1, 1]$, with Neumann boundary conditions, having the general form*

$$u \sim \begin{cases} u_+, & x \in (x_l, x_r) \\ u_-, & x \in [-1, 1] \backslash (x_l, x_r). \end{cases}$$

and assume that the conditions (4.6) hold with $w_0, u_\pm, g_\pm, l_0$ *as defined in Principal Result 4.1.1. Here,* $x_l = x_l(t), x_r = x_r(t)$ *are time-dependent locations of the left and right interface, respectively, with* $-1 < x_l < x_r < 1$. *Define*

$$x_0 := \frac{x_r + x_l}{2} \tag{4.56}$$

and

$$l := \frac{x_r - x_l}{2}. \tag{4.57}$$

Then l *evolves according to (4.7) where* $\hat{t}, \phi, \omega$ *are as given in Principal Result 4.1.1, and* A *and* x_0 *satisfy a coupled ODE system*

$$\frac{dx_0}{d\hat{t}} = -\frac{(g_- - g_+)\int_{u_-}^{u_+} f_w du}{\int_{-\infty}^{\infty} U_y^2 dy} x_0 \left(\frac{A^2}{2} + l_0^2\right) \tag{4.58}$$

$$\begin{aligned}\frac{dA}{d\hat{t}} =& \frac{\int_{u_-}^{u_+} f_w du}{2\int_{-\infty}^{\infty} U_y^2 dy}\left\{\hat{\sigma}_-(1-l_0) + \hat{\sigma}_+ l_0 - \frac{g_-^2\,(6l_0^2 - 6l_0 + 1)}{3l_0^2(g_- - g_+)} - (g_- - g_+)x_0^2\right\} A \\ & - \frac{(g_- - g_+)\int_{u_-}^{u_+} f_w du}{4\int_{-\infty}^{\infty} U_y^2 dy} A^3 \end{aligned} \tag{4.59}$$

where $\hat{\sigma}_\pm$ *is defined as in (4.10). A supercritical Hopf bifurcation occurs when* $\tau_0 = \tau_{0h}$ *where* τ_{0h} *is given by (4.13).*

Before deriving this result, we consider how this result differs from our previous result. From (4.58), as $\hat{t} \to \infty$, $x_0 \to 0$ so that (4.59) becomes (4.9). Thus, the Hopf bifurcation occurs at the same critical τ_0 value as for the one interface case, as given in (4.13). Since $x_0 \to 0$, the mesa solution exhibits *in-phase* oscillations, that is, the oscillation is in the distance between interfaces. In [26], *out-of-phase* oscillations are also shown (see Figures 1.7, 1.10 and 1.11). Since we have assumed that the interaction between the interfaces and the boundary is negligible, there are no out-of-phase oscillations and these are not examined here. Further discussion of this is found in §4.4 .

Derivation of Principal Result 4.2.1. The derivation is similar to Principal Result 4.1.1. As before, we scale τ as (4.5) and we expand

$$u = u_0 + \frac{1}{D}u_1 + \dots \text{ and } w = w_0 + \frac{1}{D}w_1 + \dots \tag{4.60}$$

we then obtain the reduced ODE-PDE system,

$$\begin{aligned} x_{rt} =& \frac{\varepsilon}{D}\frac{\int_{u_-}^{u_+} f_w du}{\int_{-\infty}^{\infty} U_y^2 dy} w_1(x_r), \\ x_{lt} =& -\frac{\varepsilon}{D}\frac{\int_{u_-}^{u_+} f_w du}{\int_{-\infty}^{\infty} U_y^2 dy} w_1(x_r), \\ & \frac{\tau_0}{\varepsilon} w_{1t} = w_{1xx} + g(u_0, w_0) + \sigma w_1 \end{aligned}$$

where σ and u_0 is given by

$$\sigma = \begin{cases} \sigma_+, & x \in (x_l, x_r) \\ \sigma_-, & x \in (-1, x_l) \bigcup (x_r, 1) \end{cases}; \qquad u_0 = \begin{cases} u_+, & x \in (x_l, x_r) \\ u_-, & x \in (-1, x_l) \bigcup (x_r, 1) \end{cases} \tag{4.61}$$

with $\sigma_\pm$ given by (4.23). We scale t and w_1 as before, in (4.24) where $\hat{\varepsilon}$ is given by (4.25). Then

$$\begin{aligned} \mathcal{W}_{xx} &= \hat{\varepsilon}\mathcal{W}_s - \hat{\varepsilon} g(u_0, w_0) - \hat{\varepsilon}^2 \hat{\sigma} \mathcal{W}, \\ x_{rs} &= \mathcal{W}(x_r), \\ x_{ls} &= -\mathcal{W}(x_l) \end{aligned}$$

where $\hat{\sigma}$ is

$$\hat{\sigma} = \begin{cases} \hat{\sigma}_+, & x \in (x_l, x_r) \\ \hat{\sigma}_-, & x \in (-1, x_l) \bigcup (x_r, 1) \end{cases} \tag{4.62}$$

with $\hat{\sigma}_\pm$ given in (4.10). Expanding $\mathcal{W} = \mathcal{W}_0(x,s) + \hat{\varepsilon}\mathcal{W}_1(x,s) + \hat{\varepsilon}^2\mathcal{W}_2(x,s) + \ldots$, similar to (4.30) – (4.33), we now have the system

$$x_{rs} = \mathcal{W}_0(s) + \hat{\varepsilon}\mathcal{W}_1(x_r, s), \tag{4.63}$$

$$x_{ls} = -\mathcal{W}_0(s) - \hat{\varepsilon}\mathcal{W}_1(x_l, s), \tag{4.64}$$

$$\mathcal{W}_{0s} = \mathcal{W}_{1xx} + g(u_0, w_0), \tag{4.65}$$

$$\mathcal{W}_{1s} = \hat{\sigma}\mathcal{W}_0 + \mathcal{W}_{2xx}. \tag{4.66}$$

We integrate (4.65) over the domain to obtain

$$\mathcal{W}_{0s} = (g_+ - g_-)\left(\frac{x_r - x_l}{2}\right) + g_-. \tag{4.67}$$

We rewrite x_l, x_r in terms of x_0, l as defined in (4.56, 4.57) so that

$$x_l = x_0 - l \quad \text{and} \quad x_r = x_0 + l.$$

Then, in terms of l and x_0, we obtain

$$x_{0s} = \mathcal{W}_0 + \hat{\varepsilon}\mathcal{W}_1(x_0 + l, s) - l_s \tag{4.68}$$

$$l_s = \mathcal{W}_0 + \hat{\varepsilon}\mathcal{W}_0 + \hat{\varepsilon}(x_0 - l, s) - x_{0s} \tag{4.69}$$

$$\mathcal{W}_{0s} = (g_+ - g_-)l + g_- \tag{4.70}$$

$$\mathcal{W}_{1s} = \hat{\sigma}\mathcal{W}_0 + \mathcal{W}_{2xx} \tag{4.71}$$

As before, we integrate (4.65), impose continuity of $\mathcal{W}_1$ at the interfaces x_l and x_r, and substitute (4.67) to obtain

$$\mathcal{W}_1 = \begin{cases} (g_+ - g_-)l\left(\frac{x^2}{2} + x\right) + (g_+ - g_-)\frac{(x_0-l)^2}{2} + K(s), & -1 < x < x_0 - l \\ (g_+ - g_-)(l-1)\left(\frac{x^2}{2}\right) + (g_+ - g_-)x_0 x + K(s), & x_0 - l < x < x_0 + l \\ (g_+ - g_-)l\left(\frac{x^2}{2} - x\right) + (g_+ - g_-)\frac{(x_0+l)^2}{2} + K(s), & x_0 + l < x < 1 \end{cases}$$

Integrating (4.71) over the domain, we have the solvability condition

$$\int_{-1}^{1} (\mathcal{W}_{1s} - \hat{\sigma}\mathcal{W}_0)\, dx = 0.$$

Solving this, we have the following equation for K_s

$$K_s = -\frac{1}{2}(g_+ - g_-)l_s\left(-x_0^2 - l^2 + 2l - \frac{2}{3}\right) - (g_+ - g_-)x_0 x_{0s}(1-l) - \mathcal{W}_0(\hat{\sigma}_+ l + \hat{\sigma}_-(l-1)).$$

Then, as for one interface, we obtain the following ODE system

$$x_{0s} = \hat{\varepsilon}(g_+ - g_-)x_0 l^2, \tag{4.72}$$

$$l_s = \mathcal{W}_0 + \hat{\varepsilon}\frac{1}{2}(g_+ - g_-)(x_0^2(l+1) + l^3 - l^2) + \hat{\varepsilon}K(s), \tag{4.73}$$

$$\mathcal{W}_{0s} = (g_+ - g_-)l + g_-, \tag{4.74}$$

$$K_s = \frac{1}{2}(g_- - g_+)l_s\left(-\frac{2}{3} - x_0^2 - l^2 + 2l\right) - (g_- - g_+)x_0 x_{0s}(l+1) - \mathcal{W}_0(\hat{\sigma}_+ l + \hat{\sigma}_-(l-1)). \tag{4.75}$$

As before, we let $l = l_0 + y$ to shift the equilibrium of (4.74) and eliminate the K and $\mathcal{W}_0$ equations to obtain the approximate system

$$x_{0s} = \hat{\varepsilon}(g_+ - g_-)x_0\left(l_0 + y\right)^2, \tag{4.76}$$

$$y_{ss} = (g_+ - g_-)y + \hat{\varepsilon}y_s\left\{2(g_+ - g_-)y^2 + (\hat{\sigma}_+ - \hat{\sigma}_-)y - 2(g_+ + g_-)y - (g_- - g_+)x_0^2 + \hat{\sigma}_-(1 - l_0) + \hat{\sigma}_+ l_0 - \frac{g_-^2\left(6l_0^2 - 6l_0 + 1\right)}{3l_0^2(g_- - g_+)}\right\}. \tag{4.77}$$

We again follow with a multiple scales analysis. Let $y \sim y_0(s,\hat{\tau}) + \hat{\varepsilon} y_1(s,\hat{\tau})$ where $\hat{\tau} = \hat{\varepsilon} s$. Also, expand $x_0 = x_{00}(s,\hat{\tau}) + \hat{\varepsilon} x_{01}(s,\hat{\tau})$. This expansion gives

$$x_{00s} = 0, \tag{4.78}$$

$$x_{01s} = -x_{00\hat{\tau}} - \omega^2 x_{00}\left(y_0 + l_0\right)^2, \tag{4.79}$$

$$y_{0ss} + \omega^2 y_0 = 0, \tag{4.80}$$

$$\begin{aligned} y_{1ss} + \omega^2 y_1 = & -2y_{0s\hat{\tau}} + 2(g_+ - g_-)y_0^2 y_{0s} + ((\hat{\sigma}_+ - \hat{\sigma}_-) - 2(g_+ + g_-))y_0 y_{0s} \\ & + \left(\hat{\sigma}_-(1-l_0) + \hat{\sigma}_+ l_0 - (g_- - g_+)x_0^2 - \frac{g_-^2\left(6l_0^2 - 6l_0 + 1\right)}{3l_0^2(g_- - g_+)}\right) y_{0s} \end{aligned} \tag{4.81}$$

where

$$\omega = \sqrt{g_- - g_+}.$$

From (4.80), $y_0 = A(\hat{\tau})\cos(\omega s + \phi(\hat{\tau}))$ and (4.78) implies that $x_{00}(s,\hat{\tau}) = x_{00}(\hat{\tau})$. Eliminating the resonance terms for x_{01} then yields

$$\frac{dx_{00}}{d\hat{\tau}} = -\omega^2 x_{00}\left(\frac{A^2}{2} + l_0^2\right). \tag{4.82}$$

Eliminating the resonance terms in (4.80), we obtain

$$2\frac{dA}{d\hat{\tau}} = -\left(\frac{g_- - g_+}{2}\right)A^3 + \left(\hat{\sigma}_-(1-l_0) + \hat{\sigma}_+ l_0 - (g_- - g_+)x_0^2 - \frac{g_-^2\left(6l_0^2 - 6l_0 + 1\right)}{3l_0^2(g_- - g_+)}\right)A \tag{4.83}$$

Rescaling, we obtain (4.59). As $t \to \infty$, $x_0 \to 0$ so that (4.59) becomes (4.9). Thus, the Hopf bifurcation occurs at the same critical τ_0 value as for the one interface case, as given in (4.13). This completes the derivation of the Principal Result 4.2.1.

4.3 Numerical Simulations

It is important to be able to verify the asymptotic results we have derived, thus, it is important to numerically simulate the system (1.1). In this section, we first consider the cubic model (1.12):

$$\begin{cases} u_t = \varepsilon^2 u_{xx} + 2(u - u^3) + w \\ \tau w_t = D w_{xx} - u + \beta \end{cases}.$$

We apply the principal results of §4.1 and §4.2. Then we discuss the numerical software used in computing the solution to the PDE system. Finally, we compare numerically the solution of the PDE system with that of the asymptotic amplitude equations.

4.3.1 Applying Principal Results (4.2.1) and (4.2.1) to the Cubic Model

We illustrate our results for the cubic model (1.12). We consider the initial conditions consisting of a single interface on $x \in [0,1]$ for the solution u, such as shown in Figure 4.1(a). For the system (1.12), such a solution has the leading-order profile $u(x,t) \sim \tanh((l(t)-x)/\varepsilon)$, $w \sim 0$, where $l(t)$ represents the interface position that changes slowly with time as given in (4.7).

For the system (1.12):

$$f(u,w) = 2(u-u^3)+w; \quad g(u,w) = \beta - u. \tag{4.84}$$

From (2.4) we obtain

$$w_0 = 0; \quad u_- = -1,\ u_+ = +1; \quad U(y) = -\tanh(y); \tag{4.85}$$

$$g_+ = \beta - 1, \quad g_- = \beta + 1; \quad l_0 = \frac{1+\beta}{2}, \tag{4.86}$$

and then

$$\int_{-\infty}^{\infty} U_y^2 dy = \frac{4}{3}; \quad \int_{u_-}^{u_+} f_w du = 2; \tag{4.87}$$

$$\left(g_w - \frac{f_w}{f_u} g_u\right)\Big|_{u=u_\pm, w=w_0} = -\frac{1}{4}, \tag{4.88}$$

so that the necessary conditions (4.6) hold, provided that $|\beta| < 1$.

The interface position is given by $l(t) \sim l_0 + A\left(\hat{t}\right)\cos(\sqrt{3/\tau_0}\phi(t)+\phi_0)$. Here, l_0 is the position of the interface at the equilibrium given by $l_0 = (1+\beta)/2$. The initial conditions $A(0)$ and ϕ_0 are determined by the initial positions of $l(0)$ and $w(l(0),0)$, as given by (4.11).

Applying Principal Result 4.1.1 to the cubic model, we obtain that the oscillation envelope A satisfies the ODE

$$\frac{dA}{d\hat{t}} = \left(\frac{1}{4}(1-3\beta^2) - \frac{1}{8\tau_0}\right)A - \frac{3}{4}A^3. \tag{4.89}$$

The Hopf bifurcation threshold for τ can then be easily determined by looking at the sign of the expression in brackets in (4.89). It is clearly negative for small (but positive) τ_0 but crosses zero when $\tau = \tau_h = \frac{D}{\varepsilon}\tau_{0h}$ with τ_{0h} given by

$$\tau_{0h} = \begin{cases} \frac{1}{2(1-3\beta^2)} & \text{if} \quad |\beta| < \frac{1}{\sqrt{3}}; \\ \infty & \text{otherwise} \end{cases}.$$

For $\tau_0 < \tau_{0h}$, the interface settles at the position $l \sim l_0$ whereas for $\tau_0 > \tau_{0h}$, the interface exhibits a periodic motion that converges to $l \sim l_0 + A_\infty \cos(\sqrt{3/\tau_0}\phi + \phi_0)$ where A_∞ is given below by (4.93). The periodic motion of the interface converges as above provided that l remains within the domain; that is $l_0 + A_\infty < 1$ and $l_0 - A_\infty > 0$. Otherwise, the interface will eventually merge with the boundary. Note that, since $\tau_0 > 0$, if $|\beta| > 3^{-1/2}$ then there is no Hopf bifurcation. These behaviours are described, for the cubic model, in Proposition 4.3.1.

For the cubic model, for a single mesa, the Principal Result 4.2.1 yields the system

$$\frac{dx_0}{d\hat{t}} = -\frac{3}{2}x_0\left(\frac{A^2}{2} + l_0^2\right), \tag{4.90}$$

$$\frac{dA}{d\hat{t}} = \left(\frac{1}{4}(1-3\beta^2) - \frac{1}{8\tau_0} - \frac{3}{2}x_0^2\right)A - \frac{3}{4}A^3. \tag{4.91}$$

Recall that x_0 decays as $\hat{t} \to \infty$, thus, (4.91) approaches (4.89) as $\hat{t} \to \infty$.

As mentioned above, depending on the values of τ_0 and β, the solution u can exhibit several different behaviours. For the cubic model (1.12) we summarize this as follows.

Proposition 4.3.1. *Consider a single interface solution of the form (4.1) for the cubic system (1.12). Define*

$$\beta_1 := \frac{3}{15} + \frac{2\sqrt{6}}{15} \approx 0.52659 \quad \textit{and} \quad \beta_2 := \frac{1}{\sqrt{3}} \approx 0.57735$$

The system (1.12) exhibits the following three distinct regimes:

1. *If $|\beta| < \beta_1$ then define*

$$\tau_{0h} := \frac{1}{2-6\beta^2}; \quad \tau_{0c} := \frac{1}{\frac{1}{2} + 3|\beta| - \frac{15}{2}\beta^2}. \tag{4.92}$$

   (a) *If $\tau_0 < \tau_{0h}$ then $l \to l_0$ in the limit $\hat{t} \gg 1$.*

   (b) *If $\tau_0 \in (\tau_{0h}, \tau_{0c})$ then, in the limit $\hat{t} \gg 1$, the interface exhibits periodic oscillations of the form*

$$l(t) \sim l_0 + A_\infty \cos(\sqrt{3/\tau_0}\varepsilon D^{-1/2}t + \phi_0)$$

   where

$$A_\infty = \sqrt{\frac{1}{3}(1-3\beta^2) - \frac{1}{6\tau_0}}. \tag{4.93}$$

(c) *If $\tau_0 > \tau_{0c}$, then eventually the interface merges with the boundary and the periodic oscillations cease.*

2. *If $|\beta| \in (\beta_1, \beta_2)$, then define τ_{0h} as in (4.92) and $\tau_{0c} = \infty$. Cases 1(a) and (b) above hold.*

3. *If $|\beta| > \beta_2$, then $l \to l_0$ in the limit $\hat{t} \gg 1$, for all $\tau_0 > 0$. Case 1(a) above holds.*

Similar results as in Proposition 4.3.1 hold for two interfaces.

4.3.2 BACOL

The numerical software that we use for the treatment of the cubic model is a recently developed package called BACOL (see [83, 82, 81]). This software uses B-spline collocation for the discretization of the spatial domain. The PDE system together with the boundary conditions is approximated by a system of differential algebraic equations which is solved using DASSL [3]. DASSL uses adapative methods to estimate and control the temporal error. A key feature of BACOL is the adaptive spatial error control which allows the software to efficiently compute numerical solutions that have sharp interfaces to a desired accuracy. We will apply the results given in the previous sections and then compare them to the numerically computed solutions obtained using BACOL.

4.3.3 Numerical Simulations of the Cubic Model

We now examine our results and compare them with numerically computed solutions. First, we consider the half mesa solution (a single interface), then the single mesa solution (two interfaces).

Experiment 4.1: Single Interface, $\beta = 0$. We choose $\beta = 0$, $\varepsilon = 0.01, D = 150$ from which it follows that $l_0 = 1/2$. Proposition 4.3.1 yields $\tau_{0h} = 0.5$, $\tau_{0c} = 2$, so that for $0.5 < \tau_0 < 2$, the interface oscillates and approaches an amplitude of $A_\infty = \sqrt{\frac{1}{3} - \frac{1}{6\tau_0}}$. We then computed a numerical solution of the cubic model (1.12) using BACOL, starting with the initial conditions given by

$$u(x,0) = -\tanh\left(\frac{x - l_0 - 0.1}{\varepsilon}\right), \; w(x,0) = 0.01. \tag{4.94}$$

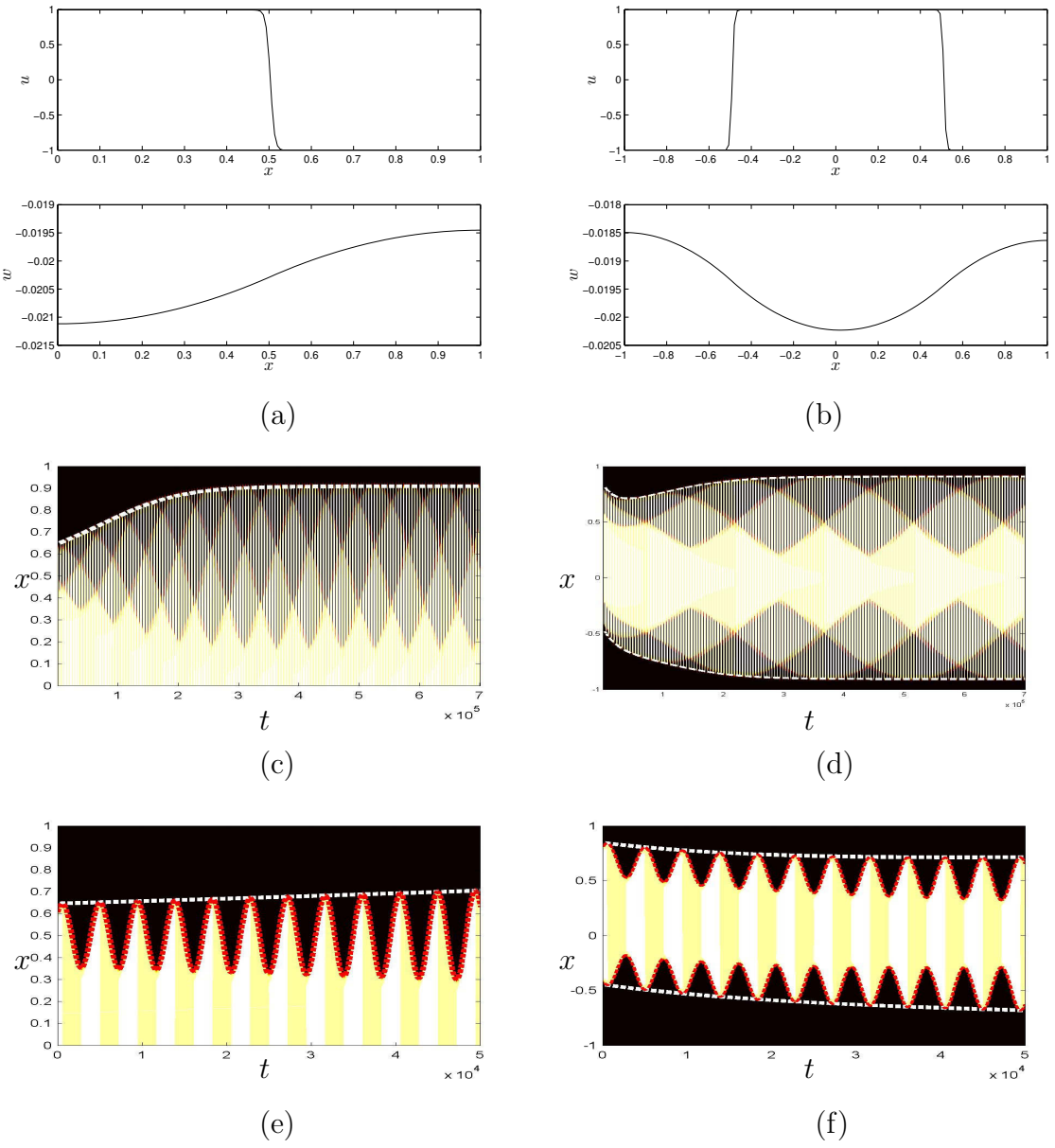

Figure 4.1: Simulations of the cubic model (1.12) with $\beta = 0$, $\varepsilon = 0.01$, $D = 150$ and $\tau = D/\varepsilon$, that is, $\tau_0 = 1.0$. Left column shows the solution consisting of a single interface on the domain $[0, 1]$. Right column shows a two-interface solution on the domain $[-1, 1]$. (a) The profile of u and w at time $t = 55001$. The initial condition for u consisted of a single interface located at $l(0) = 0.6$, given by (4.94). (c) The contour plot of u showing the oscillation of the interface in time. Dark colour corresponds to $u \approx -1$ and light to $u \approx +1$. The dashed white line denotes the amplitude of the oscillation as determined from our asymptotic results. (e) Zoom of (c) where $l(t)$, the location of the interface, is denoted by the dashed red line. (b,d,f): similar to (a,c,d) but for two-interface solution on the domain $[-1, 1]$. Initial conditions consisted of two interfaces located at -0.4 and 0.8, given by (4.96).

The numerical solution is shown as a contour plot in Figure 4.1(c,e) along with the amplitude A as given by (4.89) and the location of the interface l as given by (4.7).

The white dashed line in Figure 4.1(c,e) shows the oscillation envelope which was derived in Principal Result 4.1.1 for the general system (1.1). The dashed red line is the location of $l(t)$ as determined by (4.7). It is observed that the results from the asymptotic formulas for A and l agree very well with the numerical solution of (1.12).

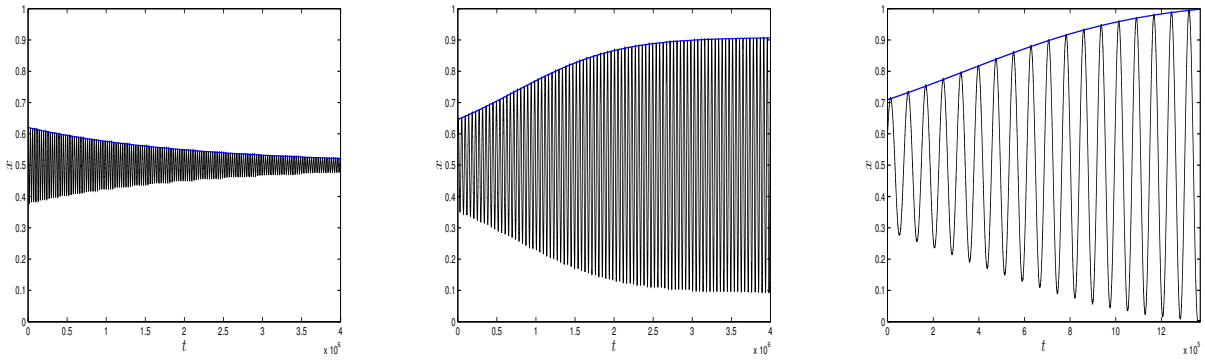

(a) (b) (c)

Figure 4.2: Comparison of numerical simulations of (1.12) with asymptotics. Parameter values are $\beta = 0$, $D = 100$, $\varepsilon = 0.001$; initial conditions are given by (4.95). Dashed line indicates the oscillation envelope $A(t)$. Solid line indicates the location of the interface of the computed solution $u(x,t)$. (a) $\tau_0 = 0.4$ (b) $\tau_0 = 1$ (c) $\tau_0 = 3$. (See Experiment 4.1)

We next choose $\beta = 0$, $\varepsilon = 0.001$ and $D = 150$ and, again, $l_0 = 0.5$. For $\tau_0 < \tau_{0h} = 0.5$, the oscillations eventually die out leading to a stable interface located at l_0, whereas for $\tau_0 > \tau_{0c}2$, the interface eventually hits the boundary. These three possible behaviours are illustrated in Figure 4.2. The dashed line indicates the oscillation envelope $A(t)$ and the solid line indicates the location of the interface of the computed solution $u(x,t)$In Figure 4.2(a) we took $\tau_0 = 0.4 < \tau_{0h}$. As expected, the oscillations damp out leading to a stable interface located at $l_0 = 0.5$. In Figure 4.2(b) we took $\tau_0 = 1$ so that $\tau_{0h} < \tau_0 < \tau_{0c}$. After a long transient, the solution converges to a periodically oscillating interface whose amplitude approaches $A_\infty \approx 0.3958$. Finally in Figure 4.2(c), we have taken $\tau_0 = 3 > \tau_{0c}$. As expected, the interface eventually

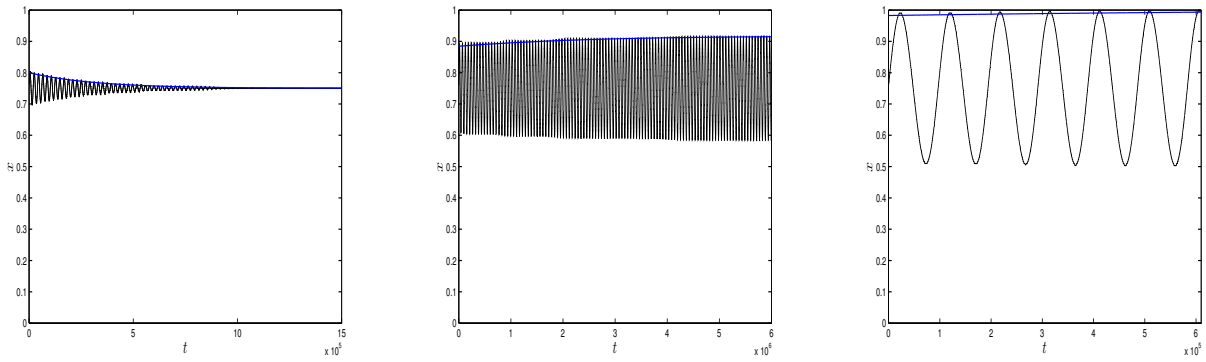

(a) (b) (c)

Figure 4.3: Comparison of numerical simulations of (1.12) with asymptotics. Parameter values are $\beta = 0.5$, $D = 80$, $\varepsilon = 0.001$; initial conditions are given by (4.95). Dashed line indicates the oscillation envelope $A(t)$. Solid line indicates the location of the interface of the computed solution $u(x,t)$. (a) $\tau_0 = 0.4$ (b) $\tau_0 = 3$ (c) $\tau_0 = 9$. (See Experiment 4.2)

merges with the boundary and disappears.

Experiment 4.2: Single Interface, $\beta = 0.5$. Next, we take β a little further from zero. We took $\beta = 0.5$, $\varepsilon = 0.001$ and $D = 80$ giving $l_0 = 0.75$. Here, we have taken the initial conditions as

$$u(x,0) = -\tanh\left(\frac{x - l_0 - 0.01}{\varepsilon}\right), \; w(x,0) = 0.01. \tag{4.95}$$

(Note that we have taken $l(0) = l_0 + 0.01$). Proposition 4.3.1 yields $\tau_{0h} = 2$, $\tau_{0c} = 8$, so that for $2 < \tau_0 < 8$, the interface oscillates and approaches an amplitude of $A_\infty = \sqrt{0.0833 - \frac{1}{6\tau_0}}$. In Figure 4.3, for these parameters, the location of the interface of the computer solution is plotted for three different values of τ_0. Figure 4.3 demonstrates similar three behaviours as given in Figure 4.2. Note in Figure 4.3(c) the numerical solution merges with the boundary at $t = 6 \times 10^5$.

Experiment 4.3: Single Interface, Hopf Bifurcation Structure. In this experiment, we compare the predicted value of A_∞ given by (4.93) with the value obtained from numerical simulations. We take $\beta = 0, \varepsilon = 0.01$, and vary τ_0 from 0.2 to 0.75 (recall $\tau_{0h} = 0.5$ for these parameters). For each fixed value of τ_0 in that range, we numerically solve the system (1.12) until time $t = 10^6$ and then read off

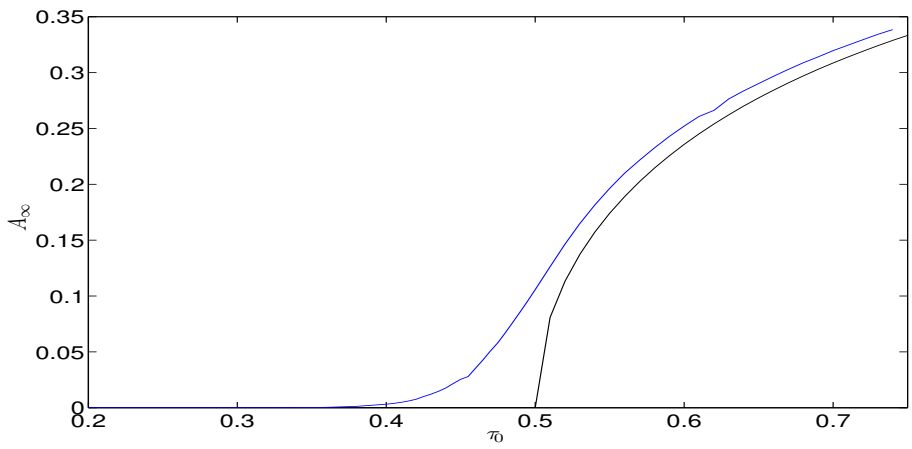

Figure 4.4: Comparison of A_∞ for the model (1.12) using parameter values $\beta = 0$, $\varepsilon = 0.01$, $D = 150$, with τ_0 as indicated on the horizontal axis. Solid curve is given by (4.93). Dashed curve is obtained by numerically integrating (1.12) up to $t = 10^6$ starting with initial conditions (4.94). (See Experiment 4.3)

the amplitude at that time. The resulting bifurcation diagram is shown in Figure 4.4. As expected, a good agreement is observed. Also as expected, the agreement with the numerical results is poor very close to the bifurcation point $\tau_0 = 0.5$: near the bifurcation, the amplitude changes very slowly. If we were to continue the numerical computation, in this case, for larger t values, we would see better agreement near $\tau_0 = 0.5$ in Figure 4.4.

Experiment 4.4: Two Interfaces, $\beta = 0$. Here, we consider the two-interface solution on the domain $[-1, 1]$. We take $\varepsilon = 0.01,\ D = 150,\ \beta = 0$, and $\tau_0 = 1$. For initial conditions, we take

$$u(x,0) = \tanh\left(\frac{x-(-0.4)}{\varepsilon}\right) - \tanh\left(\frac{x-0.8}{\varepsilon}\right) - 1,\ w(x,0) = 0.01. \tag{4.96}$$

so that the initial conditions correspond to two interfaces located at -0.4 and $+0.8$. Figure 4.1(d,f) shows the numerical computations as well as the theoretical prediction given by (4.90), (4.91) and l given by (4.7). Very good agreement is observed.

Experiment 4.5: Two Interfaces, $\beta = 0.1$. We took $\beta = 0.1$, $\varepsilon = 0.01$ and $D = 150$. As before, the value of τ_0 is varied and the location of the interfaces of the computed solution $u(x,t)$ is plotted in Figure 4.5. We obtain similar results to those in Experiment 4.2.

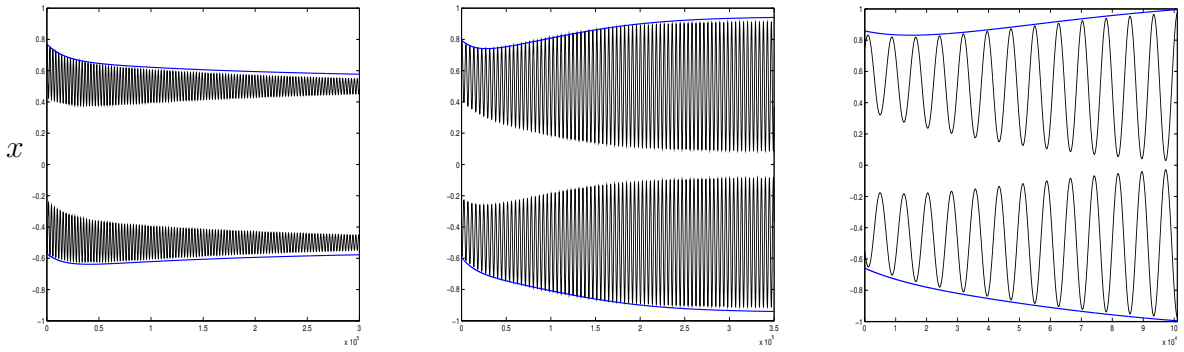

(a) (b) (c)

Figure 4.5: Comparison of numerical simulations of (1.12) with asymptotics. Parameter values are $\beta = 0.1$, $D = 150$, $\varepsilon = 0.01$. Dashed line indicates the oscillation envelope $A(t)$. Solid line indicates the location of the interfaces of the computed solution $u(x,t)$. (a) $\tau_0 = 0.4$ (b) $\tau_0 = 1$ (c) $\tau_0 = 3$. (See Experiment 4.5)

4.3.4 Turing Instability

From our numerical simulations of the cubic model, we have observed that when the interface merges with the boundary, as in Figures 4.2(c), 4.3(c) and 4.4(c), the interface disappears. We consider whether Turing instability (as discussed in the Introduction) can arise here to lead to chaos. For a detailed discussion of Turing instability, please see [54].

Suppose that (u_0, w_0) is a stable steady state of

$$\begin{cases} u_t = f(u,w) \\ \tau w_t = g(u,w) \end{cases} \tag{4.97}$$

Linearizing with $u(t) = u_0 + e^{\lambda t}\eta$, $w(t) = w_0 + e^{\lambda t}\xi$, we obtain

$$\lambda \begin{bmatrix} \eta \\ \xi \end{bmatrix} = \begin{bmatrix} f_u(u_0,w_0) & f_w(u_0,w_0) \\ \frac{1}{\tau}g_u(u_0,w_0) & \frac{1}{\tau}g_w(u_0,w_0) \end{bmatrix} \begin{bmatrix} \eta \\ \xi \end{bmatrix} \tag{4.98}$$

Here, (u_0, w_0) is a stable steady state if the trace of the matrix on the right-hand side

is negative and the determinant is positive, that is,

$$f_u(u_0, w_0)g_w(u_0, w_0) - f_w(u_0, w_0)g_u(u_0, w_0) > 0 \tag{4.99}$$

$$f_u(u_0, w_0) + \frac{1}{\tau}g_w(u_0, w_0) < 0. \tag{4.100}$$

Now consider (1.1). Linearize $u \sim u_0 + \cos(mx)e^{\lambda t}\eta$, $w \sim w_0 + \cos(mx)e^{\lambda t}\xi$. We now obtain

$$\lambda \begin{bmatrix} \eta \\ \xi \end{bmatrix} = \mathbf{M} \begin{bmatrix} \eta \\ \xi \end{bmatrix} \tag{4.101}$$

where

$$\mathbf{M} = \begin{bmatrix} -m^2\varepsilon^2 + f_u(u_0, w_0) & f_w(u_0, w_0) \\ \frac{1}{\tau}g_u(u_0, w_0) & -m^2\frac{1}{\tau}D + \frac{1}{\tau}g_w(u_0, w_0) \end{bmatrix}. \tag{4.102}$$

For stability, we must have $\mathrm{tr}\mathbf{M} < 0$ and $\det\mathbf{M} > 0$, that is,

$$(\varepsilon^2 g_w + Df_u)^2 - 4(\varepsilon^2 D)(f_u g_w - f_w g_u) \geq 0 \tag{4.103}$$

$$\varepsilon^2 g_w + Df_u \geq 0 \tag{4.104}$$

Let $r = \frac{D}{\varepsilon^2}$, then we have

$$r^2 f_u^2 + r(4f_w g_u - 2f_u g_w) + g_w^2 \geq 0 \tag{4.105}$$

$$g_w + rf_u \geq 0. \tag{4.106}$$

Thus, there will be an instability that develops if r is sufficiently large and $f_u(u_0, w_0) > 0$. We note that we have $r = \frac{D}{\varepsilon^2}$ is very large, so instability develops for our system if

$$f_u(u_0, w_0) > 0. \tag{4.107}$$

For the cubic model (1.12), the steady state $(u_0, w_0) = (\beta, -2\beta(1-\beta^2))$ is a stable steady state if

$$f_u(u_0, w_0) < 0 \implies 2 - 6\beta^2 < 0, \tag{4.108}$$

that is,

$$\beta < -\sqrt{\frac{1}{3}}, \quad \beta > \sqrt{\frac{1}{3}}. \tag{4.109}$$

To have mesa pattern solutions, we have assumed that $|\beta| < \sqrt{\frac{1}{3}}$ and thus, the condition above is never satisfied. Therefore for the cubic model, we can never have Turing instability in the regime where mesas oscillate beyond the boundary.

4.4 Discussion

In this chapter, we have examined how a one or two interface solution of (1.1) can have oscillatory behaviour for particular values of τ. We also found that the oscillations correspond to a supercritical Hopf bifurcation, provided that the conditions (4.6) hold. These conditions are the same ones that are needed to guarantee the existence and stability of a single interface when $\tau = 0$ (shown in Chapter 2). The determination of this supercritical Hopf bifurcation was done by studying the ODE that describes the amplitude of the oscillations. This was accomplished by approximating the original PDE system to a system consisting of an ODE and a PDE, and then approximating this system to a system of ODEs. Finally, reducing the system of ODEs to a second order ODE, we performed a multiple scales analysis to determine an equation for the amplitude of the oscillations of the sharp interfaces of the solution of u. When comparing these asymptotic results with numerical simulation of the cubic model (1.12), excellent agreement was observed.

We found that no oscillations exist when $\tau < O(\varepsilon/D)$, either for one or two-interface solutions. For a solution that consists of two interfaces (a single mesa solution), it was shown in Chapter 2 that even when $\tau = 0$, a two-interface solution is stable provided that $1 \ll \ln(D) \ll 1/\varepsilon$ but is destabilized when D becomes exponentially large in ε. Such instability is due to a positive (but real) small eigenvalue that arises due to translation invariance; it induces a monotonic motion of the mesa towards one of the boundaries. On the other hand, we have implicitly assumed in this chapter that $\ln(D) \ll 1/\varepsilon$, so that the boundary terms in (4.18) arising from the integration were negligible. It is an open question to examine how the results in this paper would change if $\ln(D)$ becomes sufficiently big, or equivalently, when the distance between interfaces, $2l_0$, becomes sufficiently small.

For some parameter regimes, oscillations can eventually exceed domain size (see for example Proposition 4.3.1, subcase (c) and the accompanying Figures 4.2(c), and 4.3(c)). Numerically, when the interface collides with the boundary, it typically disappears and the system gets "reset" to a nearly-uniform steady state. A natural question is whether this can lead to "chaos" via a subsequent destabilization of the homogeneous steady state through a Turing instability. We have found that this is not the case for the variety of models we tried. For example, it is easy to show that

no Turing instability is possible when $g(u, w) = g(u)$, as is case of the cubic model (1.12). For the general system, it is possible that chaos could develop, but we could not determine this.

We have shown that an unstable two interface solution exhibits *in-phase* oscillations, whereby the two interfaces eventually oscillate in opposite directions about the center of the domain (also so-called breather instability). On the other hand, numerical simulations in [26] show that a different mode of instability is also possible when the two interfaces are close together; namely the two interfaces can exhibit *out-of-phase* oscillations, whereby they oscillate in the same direction. We think that this effectively corresponds to the regime where the two interfaces interact sufficiently strongly or where the interfaces interact with the boundary, and this interaction must be taken into account. It is remains an open question to study this regime using methods of formal asymptotics.

Numerically, tracking the interface oscillations is a challenging problem. This is because there are two different temporal scales as well as two spatial scales. The software that we employ for the computation of the numerical solutions features adaptive error control in time and space and is therefore able to efficiently and accurately compute a numerical solution even when it exhibits rapid changes.

It would be interesting to extend this work to study solutions consisting of more than two interfaces. Indeed, as we have seen earlier in the thesis, the symmetrical oscillations of a single interface on the domain of size 1 can be trivially extended by reflections to a K interface solution on the domain of size K. However there are other oscillatory modes that could potentially lead to an instability (there are as many modes as there are interfaces). Which mode dominates for K interfaces is an open question. Finally, the analogous oscillations in two or higher dimensions remain unexplored.

Chapter 5

Conclusion

In this thesis, we have examined three different mechanisms in which solutions of reaction diffusion equations consisting of sharp interfaces, so-called *mesa patterns*, become unstable. We began by considering K mesa pattern solutions for(1.1) with Neumann boundary conditions on a finite interval with τ sufficiently small. For D of $\mathcal{O}(1)$, under certain additional conditions on f and g, a K mesa pattern is stable and for the shadow system, $D \to \infty$, it is unstable. These two regimes have been previously studied (see [59, 55, 26, 31]). The instability arises from the exponentially small interaction between the interfaces or from the interaction of an interface with the boundary. For the Brusselator model (1.4), in [34], the authors showed that, for D not exponentially large, a K mesa pattern is stable. By constructing asymmetric patterns, the authors determine instability thresholds for K mesa patterns of the Brusselator model, without actually computing the eigenvalues. Unlike previous works, we explicitly computed the eigenvalues of the linearized system corresponding to the general system (1.1) to determine instability thresholds. These eigenvalues were found by extending the result on the linearized problem with periodic boundary conditions to the linearized problem with Neumann boundary conditions. The threshold for D for which K mesas transition from a stable pattern to an unstable pattern was obtained. As well, we studied the dynamics of the interfaces when D is in this regime; that is, where D is exponentially large, allowing us to examine the mechanism leading to the instability.

Next, we considered the two-dimensional analogue of (1.1) with τ sufficiently small. On a thin domain, this problem can be approximated by (1.7) with Neumann boundary conditions. For equations similar to those making up the system (1.7),

the stability of a front solution and a single spike solution has been studied where the function $h(x)$ was perturbed with an exponentially small term from $h(x) = 1$ [73, 27]. In this thesis, we considered the stability of a K mesa solution (as opposed to a solution with just one interface) for $h(x)$ of a more general form. We assume that the height of the domain is represented by $h(x)$ which is positive, differentiable and symmetric on $[-L, L]$ about $x = 0$ as well as periodic on the entire domain $[-L, (2K-1)L]$. Here the instability arises from the effects of a heterogenous domain. Instability thresholds were determined which have a dependence on $h(x)$.

As mentioned in §1.1, oscillatory behaviour of (1.1) has been studied extensively. As τ is increased past a critical threshold, the interfaces oscillate in-phase with a constant amplitude. This instability occurs through a supercritical Hopf bifurcation. For τ near τ_h, the structure [20] and the normal form [19] of the Hopf bifurcation have been determined, however, the constants in this normal form are not easily determined analytically. Unlike these previous works, we have examined the dynamics of the oscillating mesa pattern, even away from the bifurcation and the equation for the amplitude of the oscillation of the interface is explicitly computed. The amplitude equation is determined through a careful set of approximations followed by multiple scale analysis.

It is important to note that throughout this work, we have used methods of formal asymptotics to derive our results as opposed to rigorous proofs. There are techniques available to provide formal justification such as the renormalization group method [68, 9] or a method based on Liapunov-Schmidt reduction [85]. It is an open problem to apply these rigorous methods to the problems studied in this thesis.

There are many directions for further work. Although in Chapter 3 we considered a two-dimensional analogue of (1.1), since we made the assumption of considering the problem on a thin spatial domain, in this work, all of our analysis has been in one spatial dimension. In two dimensions, another instability occurs for radially symmetric spot solutions, see for example [36], [52], [51]. However the instability computed there is initiated because of the curvature of the spot and the instability thresholds occur when $D = D_c = O(1/\varepsilon)$, with the spot being *stable* if $D > D_c$ and *unstable* if $D < D_c$. Such instability leads to the deformation of the spot into a peanut-like shape and has no analogy to the one dimensional instabilities studied in

this thesis. Yet, as is the case in one dimension, it is expected that an interior two-dimensional spot is unstable for the shadow system. This suggests that there exists in two dimensions a number $D_{c'} > D_c$ such that one spot is stable when $D \in (D_c, D_{c'})$ and is unstable otherwise. We anticipate that as in one dimension, $D_{c'}$ would be exponentially large. The computation of this threshold remains an open problem. A similar calculation has been performed for a spike in the Gierer-Meinhardt model [39].

It is an open problem to extend the method of determining the amplitude equation for breather behaviour, as studied in Chapter 4, to the two-dimensional problem. Another possible extension of this work is to add delay into the reaction terms of (1.1).

The analytical techniques in this thesis can be applied to systems that describe various ecological and physical phenomena [49, 14, 71] that exhibit solutions that consist of patterns as discussed. One possible avenue of research is to extend the previous techniques to models that involve non-local interaction, such as a model for animal group formation and movement [14, 12, 13] or a model for cell aggregation and cancer invasion [71].

Bibliography

[1] Malay Banerjee and Sergei Petrovski. Self-organised spatial patterns and chaos in a ratio-dependent predator-prey system. *Theor Ecol*, 4:37–53, 2010.

[2] Carl M. Bender and Steven A. Orszag. *Advanced mathematical methods for scientists and engineers. I.* Springer-Verlag, New York, 1999. Asymptotic methods and perturbation theory, Reprint of the 1978 original.

[3] K. E. Brenan, S. L. Campbell, and L. R. Petzold. *Numerical solution of initial-value problems in differential-algebraic equations*, volume 14 of *Classics in Applied Mathematics*. Society for Industrial and Applied Mathematics (SIAM), Philadelphia, PA, 1996. Revised and corrected reprint of the 1989 original.

[4] V. Castets, E. Dulos, J. Boissonade, and P. De Kepper. Experimental evidence of a sustained standing turing-type nonequilibrium chemical pattern. *Phys. Rev. Lett.*, 64(24):2953–2956, Jun 1990.

[5] Guillemette Chapuisat and Emmanuel Grenier. Existence and nonexistence of traveling wave solutions for a bistable reaction-diffusion equation in an infinite cylinger whose diameter is suddenly increased. *Comm. in Partial Diff. Eq.*, 30:1805–1816, 2005.

[6] Wan Chen and Michael J. Ward. Oscillatory instabilities and dynamics of multi-spike patterns for the one-dimensional Gray-Scott model. *European J. Appl. Math.*, 20(2):187–214, 2009.

[7] Rustum Choksi and Xiaofeng Ren. On the derivation of a density functional theory for microphase separation of diblock copolymers. *J. Statist. Phys.*, 113(1-2):151–176, 2003.

[8] M. C. Cross and P. C. Hohenberg. Pattern formation outside of equilibrium. *Rev. Mod. Phys.*, 65(3):851, Jul 1993.

[9] Arjen Doelman, Tasso J. Kaper, and Keith Promislow. Nonlinear asymptotic stability of the semistrong pulse dynamics in a regularized Gierer-Meinhardt model. *SIAM J. Math. Anal.*, 38(6):1760–1787 (electronic), 2007.

[10] Arjen Doelman, Björn Sandstede, Arnd Scheel, and Guido Schneider. The dynamics of modulated wave trains. *Mem. Amer. Math. Soc.*, 199(934):viii+105, 2009.

[11] Arjen Doelman, Peter van Heijster, and Tasso J. Kaper. Pulse dynamics in a three-component system: existence analysis. *J. Dynam. Differential Equations*, 21(1):73–115, 2009.

[12] R. Eftimie, G. de Vries, and M. A. Lewis. Complex spatial group patterns result from different animal communication mechanisms. *Proc. Natl. Acad. Sci. USA*, 104(17):6974–6979 (electronic), 2007.

[13] R. Eftimie, G. de Vries, and M. A. Lewis. Weakly nonlinear analysis of a hyperbolic model for animal group formation. *J. Math. Biol.*, 59(1):37–74, 2009.

[14] R. Eftimie, G. de Vries, M. A. Lewis, and F. Lutscher. Modeling group formation and activity patterns in self-organizing collectives of individuals. *Bull. Math. Biol.*, 69(5):1537–1565, 2007.

[15] Shin-Ichiro Ei, Hideo Ikeda, and Takeyuki Kawana. Dynamics of front solutions in a specific reaction-diffusion system in one dimension. *Japan J. Indust. Appl. Math.*, 25(1):117–147, 2008.

[16] K. B. Glasner and T. P. Witelski. Collision versus collapse of droplets in coarsening of dewetting thin films. *Phys. D*, 209(1-4):80–104, 2005.

[17] Raymond E. Goldstein, David J. Muraki, and Dean M. Petrich. Interface proliferation and the growth of labyrinths in a reaction-diffusion system. *Phys. Rev. E (3)*, 53(4, part B):3933–3957, 1996.

[18] R. Grimshaw. *Nonlinear ordinary differential equations*. Applied Mathematics and Engineering Science Texts. CRC Press, Boca Raton, FL, 1993.

[19] S. V. Gurevich, Sh. Amiranashvili, and H.-G. Purwins. Breathing dissipative solitons in three-component reaction-diffusion system. *Phys. Rev. E (3)*, 74(6):066201, 7, 2006.

[20] Aric Hagberg and Ehud Meron. Pattern formation in nongradient reaction-diffusion systems: the effects of front bifurcations. *Nonlinearity*, 7(3):805–835, 1994.

[21] D. Haim, G. Li, Q. Ouyang, W.D. McCormick, H.L. Swinney, A. Hagberg, and E. Meron. Breathing spots in a reaction-diffusion system. *Phys. Rev. Lett.*, 77:190–193, 1996.

[22] Heather Hardway and Yue-Xian Li. Stationary and oscillatory fronts in a two-component genetic regulatory network model. *Phys. D*, 239(17):1650–1661, 2010.

[23] T. Hillen and K. J. Painter. A user's guide to PDE models for chemotaxis. *J. Math. Biol.*, 58(1-2):183–217, 2009.

[24] Sam Howison. *Practical applied mathematics*. Cambridge Texts in Applied Mathematics. Cambridge University Press, Cambridge, 2005. Modelling, analysis, approximation.

[25] Hideo Ikeda and Tsutomu Ikeda. Bifurcation phenomena from standing pulse solutions in some reaction-diffusion systems. *J. Dynam. Differential Equations*, 12(1):117–167, 2000.

[26] Tsutomu Ikeda and Yasumasa Nishiura. Pattern selection for two breathers. *SIAM J. Appl. Math.*, 54(1):195–230, 1994.

[27] David Iron, Michael J. Ward, and Juncheng Wei. The stability of spike solutions to the one-dimensional Gierer-Meinhardt model. *Phys. D*, 150(1-2):25–62, 2001.

[28] A. Kaminaga, V.K. Vanag, and I.R. Epstein. Black spots in a surfactant-rich belousov-zhabotinsky reaction dispersed in a water-in-oil microemulsion system. *J. Chem. Phys.*, 122, 2005.

[29] Akiko Kaminaga, Vladimir K. Vanag, and Irving R. Epstein. A reaction-diffusion memory device. *Angewandte Chemie*, 45(3):037110, 11, 2006.

[30] R. Kapral and K. Showalter. *Chemical waves and patterns*, volume 14 of *Classics in Applied Mathematics*. Kluwer, Dordrecht, 1995. Revised and corrected reprint of the 1989 original.

[31] B. S. Kerner and V. V. Osipov. *Autosolitons*, volume 61 of *Fundamental Theories of Physics*. Kluwer Academic Publishers Group, Dordrecht, 1994. A new approach to problems of self-organization and turbulence, With the collaboration of A. Dubitsky [A. L. Dubitskiĭ] (Appendix 1) and E. Kuznetsova (Appendix 2), Translated from the Russian by A. S. Dobroslavsky [A. S. Dobroslavskiĭ].

[32] A.J. Koch and H. Meinhardt. Biological patterns formation: from basic mechanisms to complex structures. *Rev. Modern Physics*, 66(4):1481–1507, 1994.

[33] S. Koga and Y. Kuramoto. Localized patterns in reaction-diffusion systems. *Progress of Theoretical Physics*, 63(1):106–121, 1980.

[34] T. Kolokolnikov, T. Erneux, and J. Wei. Mesa-type patterns in the one-dimensional Brusselator and their stability. *Phys. D*, 214(1):63–77, 2006.

[35] T. Kolokolnikov and M. Tlidi. Spot deformation and replication in the two-dimensional belousov-zhabotinki reaction-diffusion system. *Phys. Rev. Letters*, 98(18), 2007.

[36] T. Kolokolnikov and M. Tlidi. Spot deformation and replication in the two-dimensional belousov-zhabotinski reaction in a water-in-oil microemulsion system. *Phys. Rev. Letter*, 98, 2007.

[37] T. Kolokolnikov, M. Ward, and J. Wei. Self-replication of mesa patterns in reaction-diffusion models. *Phys. D*, 236(2):104–122, 2007.

[38] Theodore Kolokolnikov, Wentao Sun, Michael Ward, and Juncheng Wei. The stability of a stripe for the Gierer-Meinhardt model and the effect of saturation. *SIAM J. Appl. Dyn. Syst.*, 5(2):313–363 (electronic), 2006.

[39] Theodore Kolokolnikov and Michael J. Ward. Bifurcation of spike equilibria in the near-shadow Gierer-Meinhardt model. *Discrete Contin. Dyn. Syst. Ser. B*, 4(4):1033–1064, 2004.

[40] Theodore Kolokolnikov, Michael J. Ward, and Juncheng Wei. The existence and stability of spike equilibria in the one-dimensional gray-scott model: The pulse-splitting regime. *Physica D: Nonlinear Phenomena*, 202(3-4):258 – 293, 2005.

[41] K.J. Lee, W.D. McCormick, J.E. Pearson, and H.L. Swinney. Experimental observations of self-replicating spots in a reaction-diffusion system. *Nature*, 369:215–218, 1994.

[42] Kyoung J. Lee, W. D. McCormick, Qi Ouyang, and Harry L. Swinney. Pattern formation by interacting chemical fronts. *Science*, 261(5118):192–194, 1993.

[43] I. Lengyel and I.R. Epstein. Modeling of turing structures in the chlorite-iodide-malonic acid-starch reaction system. *Interfaces Free Bound.*, 251:650–652, 1991.

[44] R. C. McKay and T. Kolokolnikov. Stability transitions and dynamics of mesa patterns near the shadow limit of reaction-diffusion systems in one space dimension, (accepted). *Discrete and Continuous Dynamical Systems - B*, 2011.

[45] R. C. McKay, T. Kolokolnikov, and P. Muir. Interface oscillations in reaction-diffusion systems beyond the hopf bifurcation (submitted). *Journal of Dynamics and Differential Equations*, 2011.

[46] H. Meinhardt. *Models of biological pattern formation*. Academic Press, London, 1982.

[47] Hans Meinhardt. *The algorithmic beauty of sea shells*. The Virtual Laboratory. Springer-Verlag, Berlin, 1995. With contributions and images by Przemysław Prusinkiewicz and Deborah R. Fowler, With 1 IBM-PC floppy disk (3.5 inch; HD).

[48] E. Meron, H. Yizhaq, and E. Gilad. Localized structures in dryland vegetation: forms and functions. *Chaos*, 17, 2007.

[49] Masayasu Mimura, Yasumasa Nishiura, Alberto Tesei, and Tohru Tsujikawa. Coexistence problem for two competing species models with density-dependent diffusion. *Hiroshima Math. J.*, 14(2):425–449, 1984.

[50] Alberto P. Muñuzuri, Vicente Pérez-Villar, and Mario Markus. Splitting of autowaves in an active medium. *Phys. Rev. Lett.*, 79(10):1941–1944, Sep 1997.

[51] C. B. Muratov. Theory of domain patterns in systems with long-range interactions of Coulomb type. *Phys. Rev. E (3)*, 66(6):066108, 25, 2002.

[52] C. B. Muratov and V. V. Osipov. General theory of instabilities for patterns with sharp interfaces in reaction-diffusion systems. *Phys. Rev. E (3)*, 53(4, part A):3101–3116, 1996.

[53] C.B. Muratov and V.V. Osipov. Scenarios of domain pattern formation in a reaction-diffusion system. *Phys. Rev. E*, 54:4860–4879, 1996.

[54] J. D. Murray. *Mathematical biology*, volume 19 of *Biomathematics*. Springer-Verlag, Berlin, 1989.

[55] Wei-Ming Ni, Peter Poláčik, and Eiji Yanagida. Monotonicity of stable solutions in shadow systems. *Trans. Amer. Math. Soc.*, 353(12):5057–5069 (electronic), 2001.

[56] Wei-Ming Ni and Moxun Tang. Turing patterns in the Lengyel-Epstein system for the CIMA reaction. *Trans. Amer. Math. Soc.*, 357(10):3953–3969 (electronic), 2005.

[57] G. Nicolis and I. Prigogine. *Self-organization in nonequilibrium systems*. Wiley-Interscience [John Wiley & Sons], New York, 1977. From dissipative structures to order through fluctuations.

[58] Yasumasa Nishiura. *Far-from-equilibrium dynamics*, volume 209 of *Translations of Mathematical Monographs*. American Mathematical Society, Providence, RI, 2002. Translated from the 1999 Japanese original by Kunimochi Sakamoto, Iwanami Series in Modern Mathematics.

[59] Yasumasa Nishiura and Hiroshi Fujii. Stability of singularly perturbed solutions to systems of reaction-diffusion equations. *SIAM J. Math. Anal.*, 18(6):1726–1770, 1987. Translated in J. Soviet Math. **4**5 (1989), no. 3, 1205–1218.

[60] Yasumasa Nishiura and Masayasu Mimura. Layer oscillations in reaction-diffusion systems. *SIAM J. Appl. Math.*, 49(2):481–514, 1989.

[61] Yasumasa Nishiura and Daishin Ueyama. Spatio-temporal chaos for the gray-scott model. *Physica D: Nonlinear Phenomena*, 150(3-4):137 – 162, 2001.

[62] Felix Otto, Tobias Rump, and Dejan Slepčev. Coarsening rates for a droplet model: rigorous upper bounds. *SIAM J. Math. Anal.*, 38(2):503–529 (electronic), 2006.

[63] Q. Ouyang, V. Castets, J. Boissonade, J. C. Roux, P. de Kepper, and H. L. Swinney. Sustained patterns in chlorite-iodide reactions in a one-dimensional reactor. *J. Chem. Phys.*, 95:351–360, July 1991.

[64] Q. Ouyang and H. L. Swinney. Transition from a uniform state to hexagonal and striped Turing patterns. *Nature*, 352:610–612, August 1991.

[65] J.E. Pearson. Complex patterns in a simple system. *Science*, 261(5118):189–192, 1993.

[66] S. Petrovskii and V. Volpert. Reaction-diffusion waves in biology. *Physics of Lire Reviews*, 6:267–310, 2009.

[67] I. Progogine and R. Lefever. Symmetry breaking instabilities in dissipative systems. ii. *Journal of Chemical Physics*, 48(4), 1968.

[68] Keith Promislow. A renormalization method for modulational stability of quasi-steady patterns in dispersive systems. *SIAM J. Math. Anal.*, 33(6):1455–1482 (electronic), 2002.

[69] William N. Reynolds, Silvina Ponce-Dawson, and John E. Pearson. Self-replicating spots in reaction-diffusion systems. *Phys. Rev. E (3)*, 56(1, part A):185–198, 1997.

[70] Jacob Rubinstein, Peter Sternberg, and Joseph B. Keller. Fast reaction, slow diffusion, and curve shortening. *SIAM J. Appl. Math.*, 49(1):116–133, 1989.

[71] Jonathan A. Sherratt, Stephen A. Gourley, Nicola J. Armstrong, and Kevin J. Painter. Boundedness of solutions of a non-local reaction-diffusion model for adhesion in cell aggregation and cancer invasion. *European J. Appl. Math.*, 20(1):123–144, 2009.

[72] PDE Solutions. Flexpde software.

[73] Xiaodi Sun and Michael J. Ward. Metastability and pinning for convection-diffusion-reaction equations in thin domains. *Methods Appl. Anal.*, 6(4):451–475, 1999.

[74] Mami Suzuki, Takao Ohta, Masayasu Mimura, and Hideo Sakaguchi. Breathing and wiggling motions in three-species laterally inhibitory systems. *Phys. Rev. E (3)*, 52(4, part A):3645–3655, 1995.

[75] M. Taki, M. Tlidi, and T. Kolokolnikov. Dissipative localized structures in extended systems. *Chaos*, 17, 2007.

[76] A. B. Tayler. *Mathematical models in applied mechanics*. Oxford Applied Mathematics and Computing Science Series. The Clarendon Press Oxford University Press, New York, 1986.

[77] Alan M. Turing. The chemical basis of morphogenesis. *Phil. Trans. Royal Soc. London*, 237(641), 1952.

[78] Harmen van der Ploeg and Arjen Doelman. Stability of spatially periodic pulse patterns in a class of singularly perturbed reaction-diffusion equations. *Indiana Univ. Math. J.*, 54(5):1219–1301, 2005.

[79] Peter van Heijster, Arjen Doelman, and Tasso J. Kaper. Pulse dynamics in a three-component system: stability and bifurcations. *Phys. D*, 237(24):3335–3368, 2008.

[80] Vladimir K. Vanag and Irving R. Epstein. Localized patterns in reaction-diffusion systems. *Chaos*, 17(3):037110, 11, 2007.

[81] R. Wang, P. Keast, and P. Muir. BACOL: B-spline Adaptive COLlocation software for 1-D parabolic PDEs. *ACM Trans. Math. Software*, 30(4):454–470, 2004.

[82] R. Wang, P. Keast, and P. Muir. A high-order global spatially adaptive collocation method for 1-D parabolic PDEs. *Appl. Numer. Math.*, 50(2):239–260, 2004.

[83] Rong Wang, Patrick Keast, and Paul Muir. A comparison of adaptive software for 1D parabolic PDEs. *J. Comput. Appl. Math.*, 169(1):127–150, 2004.

[84] M. J. Ward and J. Wei. Hopf bifurcations and oscillatory instabilities of spike solutions for the one-dimensional Gierer-Meinhardt model. *J. Nonlinear Sci.*, 13(2):209–264, 2003.

[85] Juncheng Wei and Matthias Winter. Multi-peak solutions for a wide class of singular perturbation problems. *J. London Math. Soc. (2)*, 59(2):585–606, 1999.